TECHNICAL REPORT 2073
April 2014

Capture Matrices Handbook

P. A. Boss
M. D. Putnam

SSC Pacific
San Diego, CA 92152-5001

SSC Pacific
San Diego, California 92152-5001

K. J. Rothenhaus, CAPT, USN
Commanding Officer

C. A. Keeney
Executive Director

ADMINISTRATIVE INFORMATION

The work described in this report was performed by the Advanced Concepts & Applied Research Branch (Code 71730) and the Environmental Sciences Branch (Code 71750), Space and Naval Warfare Systems Center Pacific (SSC Pacific), San Diego, CA. The Naval Innovative Science and Engineering (NISE) Program at SSC Pacific funded this effort as a Basic Research project.

Released by
M. De Andrade, Acting Head
Advanced Concepts &
Applied Research Branch

Under authority of
A. D. Ramirez. Head
Advanced Systems &
Applied Sciences Division

The citation of trade names and names of manufacturers in this report is not to be construed as official government endorsement or approval of commercial products or services referenced in this report.

SB

EXECUTIVE SUMMARY

OBJECTIVE

This report describes the fabrication and use of capture matrices for the enhanced detection of harmful chemicals. Capture matrices are composed of affinity ligands grafted onto magnetic microparticles. These capture matrices are essentially preconcentrators/transducers that can be used with either field-deployable sensors or microelectromechanical systems (MEMS) devices. For MEMS, these capture matrices address integrating the device with "real-world" sampling. Depending on the chemical nature of the affinity ligands, capture matrices can be used to enhance the detection of toxic industrial chemicals (TICs), explosive materials, and chemical warfare agents.

The technology developed has relevancy in information dominance. Capture matrices, when used with either MEMs or current field-deployable detectors, will provide the warfighter with information on what chemical species are present in the environment. This will provide the warfighter with enhanced situational awareness and understanding as well as force protection. This technology can also be used for long-term monitoring (LTM) of contaminated U.S. Navy and Department of Defense (DoD) sites. More than 2000 DoD sites have undergone remediation. Long-term monitoring of these sites is required. This LTM cannot be deferred and is a significant part of remediation life-cycle costs for the DoD. The capture matrices technology will benefit the fleet by reducing the costs of LTM. The savings can then be used to procure equipment, vessels, etc. that will directly benefit the warfighter.

RESULTS

Perchlorate, hexavalent chromium, RDX (Research Department explosive), naphthalene, and heavy metals are contaminants that were identified by DoD Environment, Safety and Occupational Health Network and Information Exchange (DENIX) as emerging chemical and material risks. Affinity ligands for these contaminants were identified and strategies to immobilize the ligands onto magnetic microparticles were developed. Capture matrices were fabricated specifically for chromate, perchlorate, polycyclic aromatic hydrocarbons (PAHs), RDX, and heavy metals. Capture matrices were evaluated specifically for chromate, perchlorate, and PAHs. RDX-specific capture matrices were untested as we were unable to procure RDX. We were also unable to test heavy metal capture matrices, as the portable potentiostat arrived a month before the program ended. We assembled a prototype in-line mixer to increase capture efficiency. This mixer is composed of two syringe pumps (one for sample and one for the capture matrices), an in-line binary HyperShear mixer for folded flow mixing of the capture matrices with the sample, and a flow-through cell with a magnet that concentrates the capture matrices onto a flat optical surface.

RECOMMENDATIONS

The U.S. Navy needs to characterize EDTA-derivatized capture matrices to detect heavy metals. Likewise, to detect RDX selectively, the ligands need evaluation. We must optimize the prototype mixer.

While the focus of these efforts is detecting perchlorate, hexavalent chromium, PAHs, and explosive materials (all of which are on the DoD's Materials of Evolving Regulatory Interest Team, MERIT list), by simply changing the affinity ligand, we can use capture matrices to detect other chemicals such as chlorinated solvents, nerve and blister agents, pesticides, pharmaceuticals, etc. Enhanced detection of these chemicals has wide applicability in both the private and government sectors. To detect these materials, the affinity ligand would need identification, as well as chemistries that graft the affinity ligand onto the surface of magnetic microparticles.

CONTENTS

Figures

Tables

ABBREVIATIONS

a	equation parameter
A_1	symmetry type of a vibration mode
ACN	acetonitrile
Ag	silver
AgCl	silver chloride
Au	gold
b	equation parameter
BPh_4	tetraphenylborate
c	equation parameter
C	carbon
°C	degrees Celsius
C_{18}	octadecyltrimethoxysilane
CCD	charge coupled device
Cd^{2+}	cadmium ion
CE	counter electrode
Cl	chlorine
Cl^-	chloride
ClO_4^-	perchlorate
C.M.	capture matrices
cm^{-1}	wavenumber
CN^-	cyanide
Cr	chromium
Cr(III)	trivalent chromium
Cr(VI)	hexavalent chromium
CRADA	Cooperative Research and Development Agreement
$CrO_4^=$	chromate
CPME	conducting polymer modified electrode
Cu	copper
Cu^{2+}	copper ion
DAPI	4',6-diamidino-2-phenylindole
DENIX	DoD Environment, Safety and Occupational Health Network and Information Exchange
DMA	dimethylaminoethanethiol
$DMAH^+$	protonated dimethylaminoethanethiol
DMF	dimethylformamide
DMSO	dimethylsulfoxide
DNT	dinitrotoluene
DoD	Department of Defense
ESI	electrospray ionization
EDTA	ethylenediaminetetraacetic acid
EM	emission
EtOH	ethanol
EX	excitation
exp	exponent, base 10

FID	flame ionization detector
g	Frumkin parameter
g	gram
GC	gas chromatography
GCE	glassy carbon electrode
h	hour
H	hydrogen
Hg	mercury
Hg^{2+}	mercury cation
H_2O	water
H_2O_2	hydrogen peroxide
$HPO_4^{=}$	monohydrogen phosphate
$H_2PO_4^{-}$	dihydrogen phosphate
H_2SO_4	sulfuric acid
HCl	hydrochloric acid
HMX	octogen
HPLC	high performance liquid chromatography
K	ion pair constant
L	liter
LC	liquid chromatography
LED	light emitting diode
LP	long pass
m	medium
M	molarity
mA	milliampere
MACS	magnetically assisted chemical separation
MEMS	microelectromechanical systems
MEP	4-(2-mercaptoethyl)pyridinium hydrochloride
mg	milligram
min	minute
mL	milliliter
MS	mass spectrometry
mW	milliwatt
$NaBH_4$	sodium borohydride
$NaBPh_4$	sodium tetraphenylborate
NdFeB	neodynium iron boron
nm	nanometer
nM	nanomolarity
NMR	nuclear magnetic resonance
NO_3^{-}	nitrate
O	oxygen
OH	hydroxide
oop	out of plane
PAHs	polyaromatic hydrocarbons
PAR	4-(2- pyridylazo) resorcinol

Pb	lead
Pb^{2+}	lead cation
PE	polyethylene
PETN	pentaerythritol tetranitrate
pH	$-\log[H^+]$
PMT	photomultiplier tube
ppb	parts per billion
ppm	parts per million
pptr	parts per trillion
Pt	platinum
R^2	coefficient of determination
RE	reference electrode
RDX	cyclotrimethylenetrinitramine
s	second
s	strong
SAM	self-assembled monolayer
SERS	surface enhanced Raman scattering
Si	silicon
SMA	SubMiniature version A
$SO_4^=$	sulfate
SPE	solid phase extraction
SWV	square wave voltammetry
t-BuS-	tertiary butyl sulfide
THF	tetrahydrofuran
TICs	toxic industrial chemicals
TMEDA	tetramethylethylenediamine
TMEDA-$Zn(Ac)_2$	tetramethylethylenediamine- zinc acridine complex
TMEDA-$Zn(HAc^+)_2$	tetramethylethylenediamine- zinc monohydrogen acridine complex
TMEDA-$Zn(H_2Ac)_2$	tetramethylethylenediamine- zinc dihydrogen acridine complex
TNT	2,4,6-trinitrotoluene
UV	ultraviolet
vw	very weak
w	weak
WE	working electrode
x	abscissa
y	ordinate
$Zn(NO_3)_2$	zinc nitrate
λ	wavelength
µA	microampere
µg	microgram
µL	microliter
µm	micron
µM	micromolarity

~	approximately
°	degree
°C	degrees Celsius
%	percent
®	trademark
et al.	Latin for ‘and others’
vide infra	Latin for ‘see below’
vide supra	Latin for ‘see above’

1. CAPTURE MATRICES FOR ENHANCED CHEMICAL DETECTION

1.1 INTRODUCTION

Capture matrices are composed of affinity ligands grafted onto magnetic microparticles. These capture matrices are essentially preconcentrators/transducers that can be used with either field deployable sensors or microelectromechanical systems (MEMS) devices. For MEMS, these capture matrices address the issue of integrating the device with "real-world" sampling. They also address issues of selectivity, sensitivity, and reversibility. Depending on the chemical nature of the affinity ligands, capture matrices can enhance the detection of toxic industrial chemicals (TICs), explosive materials, and chemical warfare agents. The result is an enhanced sensing capability for the war-fighter. Figure 1.1-1 shows conceptually how these capture matrices are used.

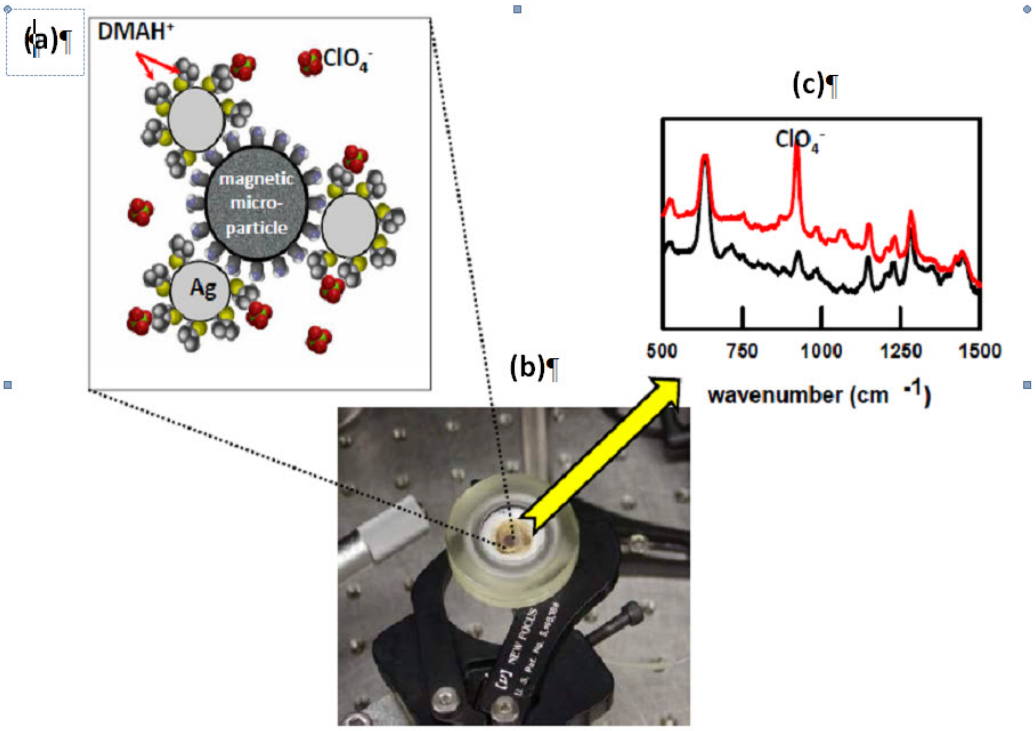

Figure 1.1-1. The use of capture matrices for enhanced chemical detection: (a) schematic of perchlorate interacting with a Ag/DMA capture matrice, (b) NdFeB magnets concentrate capture matrices onto the optical surface, and (c) SERS spectra obtained in the absence (black) and presence (red) of perchlorate.

1.2 BACKGROUND

In the past, preconcentration methods include liquid-liquid extraction, precipitation, and solid phase extraction. Use of these methods to separate and preconcentrate an analyte from large volumes of solution is time consuming. These methods also require significant chemical additives and complex equipment, generate a large secondary waste stream, and are difficult to automate. Magnetically assisted chemical separation (MACS), which uses capture matrices composed of affinity ligands grafted onto magnetic nano or microparticles, combines the selective and efficient separation offered by chemical extraction with magnetic recovery of extractant for selective separation of a given analyte. The greatest advantage of this method is that the desired materials are separated from solution by a simple and compact process that produces minimal secondary wastes.

Other advantages are a large active surface area for a given mass of particles; the ability to process a solution that contains suspended solids (since the majority of accompanying impurities in a suspension are diamagnetic, they do not interfere with magnetic particles during the magnetic separation step); avoidance of channeling effects that are common in packed beds; the ability to manipulate the capture matrices by application of an external magnetic field; and suitability for automation. In fact, the use of derivatized magnetic microparticles in trace chemical analysis is growing.[1] The main difference in our use of capture matrices versus those of others[1-3] is that we do not require elution of the analyte off the magnetic particles prior to detection. While the ultimate goal is to use these magnetic microparticles as preconcentrators for MEMs devices, they can also be used with current hand-held, field-deployable detection systems to increase sensitivity.

1.3 TARGET ANALYTES AND AFFINITY LIGANDS

Table 1.3-1 summaries the target analytes, affinity ligands, and analytical techniques for detection. The target analytes are on the Department of Defense (DoD) Environment, Safety and Occupational Health Network and Information Exchange (DENIX) as emerging chemical and material risks.

Table 1.3-1 Summary of target analytes, affinity ligands, and analytical techniques.

Target Analyte	Affinity Ligand	Analytical Technique[a]
Perchlorate	Dimethylaminoethanethiol hydrochloride (DMA)[4]	SERS
Hexavalent Chromium	4-(2-mercaptoethyl)pyridinium hydrochloride (MEP)[5]	SERS
RDX, TNT, DNT	Bare Au colloid[6,7]	SERS
RDX	2-(4-pyridylethyl)trimethoxysilane[8]	Fluorescence
Naphthalene, PAHs	Octadecyltrimethoxysilane (C_{18})[9]	Fluorescence
Heavy Metals	Ethylenediaminetetraacetic acid (EDTA)[10]	SWV

a. SERS = surface-enhanced Raman spectroscopy
SWV = square wave voltammetry

1.4 REFERENCES

1. M. Šafařikova and I. Šafařik. 2002. "Magnetic Solid-phase Extraction of Target Analytes from Large Volumes of Urine," *European Cells and Materials 3*:192–195.

2. I. Šafařik and M. Šafařikova.2002. "Detection of Low Concentrations of Malachite Green and Crystal Violet in Water," *Water Research 36*:196–200.

3. M.R. Shishehbore, A. Afkhami, and H. Bagheri. 2011. "Salicylic Acid Functionalized Silica-coated Magnetite Nanoparticles for Solid Phase Extraction and Preconcentration of Some Heavy Metal Ions from Various Real Samples," *Chemistry Central Journal 5*:41–50.

4. B. Gu, C, Ruan, and W. Wang. 2009. "Perchlorate Detection at Nanomolar Concentrations by Surface-Enhanced Raman Scattering," *Applied Spectroscopy Reviews 63*:98–102.

5. I. Turyan and D. Mandler. 1997. "Selective Determination of Chromium by a Self-Assembled Monolayer Based Electrode," *Analytical Chemistry 69*:894–897.

6. N. H. Hatab, G. Eres, P. B. Hatzinger, and B. Gu. 2010. Detection and Analysis of Cyclotrimethylenetriamine (RDX) in Environmental Samples by Surface–enhanced Raman Spectroscopy," *Journal of Raman Spectroscopy 41*:1131–1136.

7. J. I. Jerez-Rozo, O. M. Primera-Pedrozo, M. A. Barreto-Cabán, and S. P. Hernández-Rivera. 2008. "Enhanced Raman Scattering of 2,4,6-TNT Using Metallic Colloids," *IEEE Sensors Journal 8*:974–982.

8. G. L. Anspach, W. E. Jones, and J. F, Kitchens. 1982. "Evaluation of Solid Sorbents for Sampling and Analysis pf Explosives from Water." USATHAMA Report DRXTH-TE-CR-82142. Aberdeen Proving Ground, MD.

9. J. J. Kirkland and J. J. Stefano. 1970. "Controlled Surface Porosity Supports with Chemically-bonded Organic Stationary Phases for Gas and Liquid Chromatography," *Journal of Chromatographic Science 8*:309–314.

10. A. Rahman, M. -S. Won, and Y.-B. Shim. 2003. "Characterization of an EDTA Bonded Conducting Polymer Modified Electrode: Its Application for the Simultaneous Determination of Heavy Metal Ions," *Analytical Chemistry 75*:1123–1129.

2. Au/MEP CAPTURE MATRICES FOR THE DETECTION OF CHROMATE BY SERS

2.1 INTRODUCTION

Turyan and Mandler[1] used 4-(2-mercaptoethyl) pyridinium (MEP) hydrochloride to detect hexavalent chromium by square wave voltammetry (SWV). MEP binds to the Au surface through its sulfhydryl group to form a self-assembled monolayer (SAM). This Au/MEP electrode was used to preconcentrate chromate on the electrode surface prior to detection/quantification by cathodic SWV. Turyan and Mandler showed that the analysis of 0.1-ppb Cr(VI) was unaffected by the presence of a 1000-fold excess of Cr(III). They also showed that the anions chloride, nitrate, phosphate, acetate, and perchlorate did not interfere in the detection of chromate.

The use of conventional Au/MEP substrates to detect chromate by SERS has also been demonstrated.[2] Mosier-Boss and Lieberman showed that, when the chromate concentration is in M, the concentration response is described by a Frumkin isotherm. The shape of the Frumkin isotherm is determined by two parameters: (1) K, the ion-pair constant between the anion and the coating, and (2) g, the Frumkin parameter that takes into account interactions between adsorbed species. The researchers also measured other anions.[2] The selectivity for MEP for anions, as measured by SERS, was (ion pair constants are indicated):

$$CrO_4^{=}\ (K = 142700) \gg CN^{-}\ (K = 1090) > Cl^{-}\ (K = 92) > ClO_4^{-}\ (K = 38) > SO_4^{=},$$
$$NO_3^{-},\ H_2PO_4^{-}\ (K = 0).$$

Molecular modeling of the SAM showed the presence of microcavities between adjacent MEP moieties on the SERS surface, with a three-dimensional structure complementary in both shape and chemical functionality to that of the chromate anion.[3] This complementary three-dimensional structure is responsible for the high selectivity of the MEP SAM for chromate.

In this section, we describe how to synthesize the Au/MEP capture matrices and show how calibration curves can be generated that determine the amount of chromate present in a sample. Subsection 2.1.1 discusses the use of capture matrices to pre-concentrate chromate to achieve lower detection limits.

2.1.1 Brief Description of Detection Scheme

A suspension of Au/MEP capture matrices and the sample for analysis are injected into a mixer with folded flow mixing to increase capture efficiency (Section 9 discusses mixers). Once mixed, the sample/capture matrices suspension goes into a flow-through cell where a magnet pulls the capture matrices down onto an optical surface. A Raman spectrometer, operating at 785-nm excitation, measures the SERS response of both the MEP coating on the capture matrices, as well as the hexavalent chromium bound to the coating. The advantage of this detection method is that the hexavalent chromium does not need elution off the capture matrices prior to detection.

2.2 SYNTHESIS OF Au/MEP CAPTURE MATRICES

2.2.1 Reagents

The SSC Pacific team used hydrogen tetrachloroaurate (III) trihydrate (Aldrich), sodium citrate (Aldrich), 4-(2-mercaptoethyl) pyridinium (MEP) hydrochloride (Toronto Research Chemicals), water (HPLC grade, Aldrich), and ethanol (HPLC grade, Aldrich) as received.

We washed a 0.5-mL aliquot of 5-μm-diameter, amine-terminated, silica-coated iron oxide microparticles (Bioclone, part no. FA-104) 10 times with 1-mL aliquots of HPLC water to remove surfactant. Between washes, we used a NdFeB magnet to separate the magnetic microparticles from the water. After the washes, we adjusted the volume of the amine-terminated, magnetic microparticles to 1.0 mL with water.

2.2.2 Preparation of Gold Cooloid

An aqueous solution of 100 mL of 0.01% (g/mL) of hydrogen tetrachloroaurate (III) trihydrate, in a 250-mL round bottom flask equipped with a condenser, was brought to a vigorous boil. Once boiling, we added 0.85 mL of 1 % sodium citrate. After 40 min of refluxing, the solution had changed from a light yellow color to red-violet. We removed the flask from the heat and allowed to cool to room temperature. The colloidal suspension was then concentrated, by centrifugation, to a final volume of ~ 2 mL.

2.2.3 Preparation of Au/MEP Capture Matrices

A 100-μL aliquot of the washed, amine-terminated, magnetic microparticles was pippetted into a glass vial containing 1 ml of water (HPLC grade, Aldrich). A 200-μL aliquot of the concentrated gold colloidal suspension was added to the glass vial and the vial was placed on a roller. The amine groups of the magnetic microparticles bind to the gold colloidal particles. After rolling for 2 h, a NdFeB magnet was used to separate the microparticles from the liquid. If the liquid was clear, half the volume was removed and another 200-μL aliquot of the concentrated gold colloidal suspension was added to the glass vial and placed on the roller. The process was repeated until the surface of the magnetic microparticles was completely covered with colloidal gold particles as indicated when the liquid remained red-violet in color.

The Au-covered, magnetic microparticles were then washed three times with water (HPLC grade, Aldrich) and then three times with ethanol (HPLC grade, Aldrich). Between washings, a NdFeB magnet is used to separate the Au-covered magnetic microparticles. Afterwards, we added a dilute ethanolic solution of MEP to the glass vial. The MEP was allowed to react with the immobilized gold colloidal particles for ~ 24 h to form a SAM. The Au/MEP capture matrices were then washed three times in ethanol, as described above. The volume of the Au/MEP capture matrices were adjusted to 1 mL using ethanol. We refrigerated the capture matrices between uses.

2.3 CONVENTIONAL Au/MEP SERS SUBSTRATE

A discussion on conventional Au/MEP SERS substrates is included to demonstate how spectral data is handled. In the appendix, relevent papers are included that describe how the conventional SERS substrate is fabricated and how the spectral data are acquired. Here we describe data manipulation to generate a calibration curve that is used to determine the amount of analyte present in a sample.

The SERS spectra obtained for the conventional SERS substate are acquired at a fixed spot on the substrate. A reference spectrum is obtained with the flow-through cell filled with water. We then sequentially replaced the water with solutions of varying concentration of chromate, going from the lowest chromate concentration to the highest. The response of the MEP coating to chromate was instantaneous. Figure 2.3-1a shows examples of SERS spectra obtained for the Au/MEP coating in the absence and presence of chromate. When chromate is added, a new peak grows in at ~ 835 cm^{-1}. This new peak is due to the symmetric and asymmetric Cr-O stretching modes of chromate. It can also be seen that this chromate peak significantly overlaps with peaks due to the MEP coating. To determine the chromate peak area, the spectral contributions of the coating need to be subtracted out,

As shown in Figure 2.3-1a, the spectra exhibit similar baselines and the spectral peaks lineup. Under these circumstances, the spectral contributions of the reference spectrum (0-ppm chromate) can be subtracted out resulting in the difference spectra shown in Figure 2.3-1b. The broad band due to chromate in the difference spectra is indicated The difference spectra also show increased intensity of the MEP peaks at 1196, 1558, and 1600 cm-1, respectively. These peaks are primarily assigned to the pyridine ring vibrational modes.[3] The intensity changes indicate that the chromate anion is interacting with the pyridine ring of MEP.

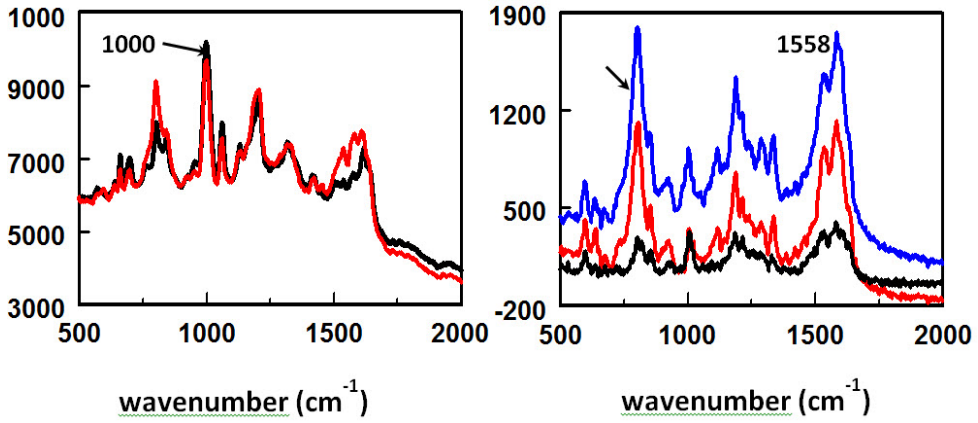

Figure 2.3.1. (a) SERS spectra of a conventional AuMEP SERS substrate obtained at chromate concentrations of 0 (black) and 2500 (red) ppm. Spectra were obtained using 785-nm excitation at 30 mW and averaging 10 2-s spectra, (b) difference spectra obtained by subtracting the 0-ppm spectrum from the 1-ppm (black), 100-ppm (red), and 500-ppm (blue) chromate AuMEP spectra. The chromate peak is indicated.

To generate a calibration curve, the chromate peak area is plotted as a function of chromate concentration (Figure 2.3-2). At low chromate concentration, the chromate peak area increases with concentration. At higher chromate solution concentrations, the response levels off as the adsorption sites on the MEP SAM become fully occupied. Table 2.3-1 lists the equation that describes this curve. Determining the equation that describes the curve was an iterative process. In a Microsoft® Excel® spreadsheet, we modeled the curves using various combinations of linear and exponential features. When a given combination looked promising, we used a Marquardt[4] nonlinear least squares fitting routine to obtain the values of the parameters and their uncertainties.

2.4 Au/MEP SERS-ACTIVE CAPTURE MATRICES

To evaluate the chromate response of the Au/MEP capture matrices, an aliquot of known volume of the capture matrices are pipetted into a glass vial. We used a NdFeB magnet to separate the capture matrices from the ethanol and washed the capture matrices three times with 0.5 mL of water. A NdFeB magnet was used to separate the capture matrices from the liquid between washes. Afterwards, we added a 1-mL aliquot of an aqueous chromate solution of known concentration to the vial. The sample was allowed to equilibrate overnight. Afterwards, a pipette was used to transfer the capture matrices and solution to a cell with an Au foil optical surface. A NdFeB magnet on the other side of the Au foil was used to concentrate the capture matrices in a single spot. Examples of SERS spectra obtained are shown in Figure 2.4-1. The figure shows that the intensities of the peaks caused by MEP and chromate vary, as do the baselines. Because of these variabilities between the spectra obtained for the individual samples, it is impossible to do spectral subtractions to obtain the chromate peak area. However, Crane et al.[5] showed that it was possible to use SERS to obtain adsorption

isotherms for 4-(2- pyridylazo) resorcinol (PAR) with Pb^{2+}, Cu^{2+}, and Cd^{2+} metal ions that do not exhibit Raman active bands by ratioing the intensities of a PAR Raman peak that varied upon complexation to one that did not.

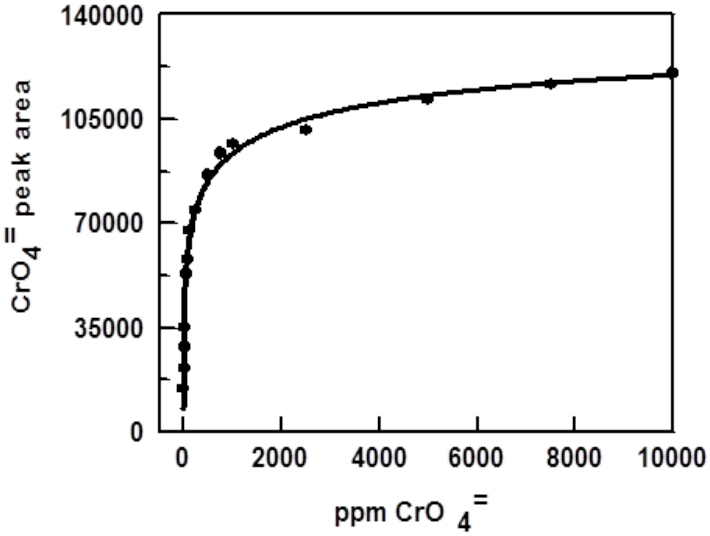

Figure 2.3-2. Plot of chromate peak area as a function of chromate concentration obtained for a conventional Au/MEP SERS substrate.

Table 2.3-1. Summary of equations that describe the observed calibration curves.

Curve (Figure No.)	Equation Describing Curve[a]	R^2	Values of Parameters
2.3-2	$y = c + a(1-\exp(-bx^{0.2}))$	0.9879	a = 188000 ± 6000 b = 0.346 ± 0.047 c = -47100 ± 9400
2.4-2	$y = c + a(1-\exp(-bx^{0.3}))$	0.9894	a = 0.546 ± 0.029 b = 0.143 ± 0.021 c = 0.360 ± 0.017
2.4-3	$y = c + a(1-\exp(-bx^{0.5}))$	0.9923	a = 0.547 ± 0.036 b = 0.176 ± 0.024 c = 0.269 ± 0.024

a. In the equations, y is either the chromate peak area or the ratio of peak intensities and x is the ppm chromate.

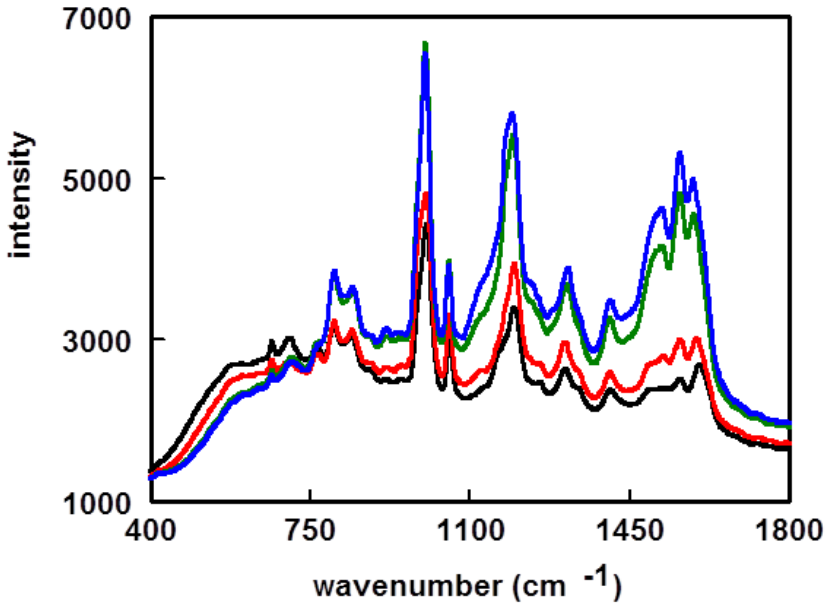

Figure 2.4-1. SERS spectra of Au/MEP capture matrices immersed in solutions of (bottom to top) 0-, 5-, 50-, and 1000-ppm chromate.

As shown in Figure 2.3-1a, the MEP peak at 1000 cm^{-1} minimally varies as a function of chromate concentration. However, the MEP peak at 1558 cm^{-1} increases in intensity with increasing chromate concentration. The results of ratioing the 1558 cm^{-1} peak to the 1000 cm^{-1} peak for the conventional Au/MEP substrate are shown in Figure 2.4-2, where Figure 2.4-2a covers the chromate concentration range 1 to 10000 ppm and Figure 2.4-2b covers the chromate concentration range 1 to 100 ppm. The equation that describes this curve is summarized in Table 2.3-1. Like the plot of chromate peak area as a function of chromate concentration shown in Figure 2.4-2, the ratio increases with increasing chromate concentration at low chromate concentrations. At higher chromate concentrations (≥ 100-ppm chromate), the ratio levels off as chromate fully occupies the sites on the MEP coating. The results summarized in Figure 2.4-2 show that reasonable calibration curves can be obtained by ratioing MEP peaks that change upon complexation to one that does not.

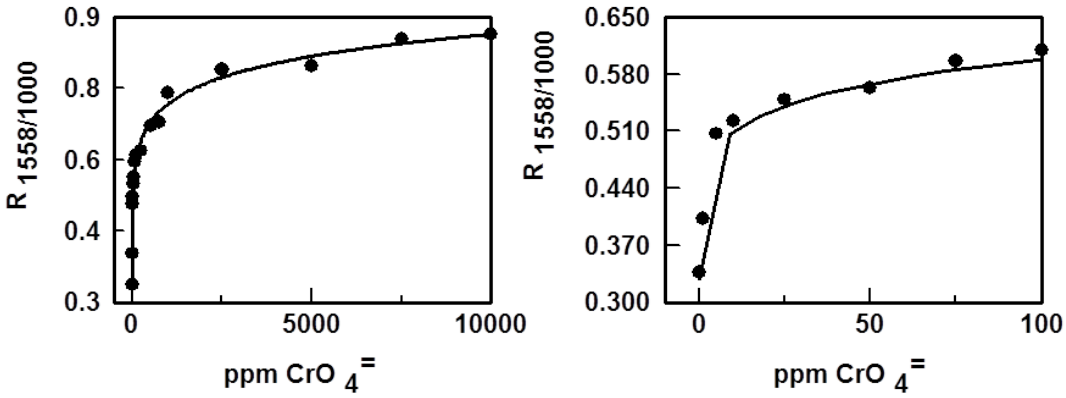

Figure 2.4-2. Plots of the MEP peak intensity at 1558 cm^{-1} ratioed to the 1000 cm^{-1} peak as a function of chromate concentration. for the conventional Au/MEP SERS substrate. Chromate concentration ranges are (a) 0 to 10 000 ppm and (b) 0 to100 ppm. Equation describing the curves is summarized in Table 2.3-1.

The ratioing approach to generate calibration curves was then applied to the Au/MEP capture matrices. Figure 2.4-3 summarizes the results obtained by ratioing the 1558 cm^{-1} MEP peak to the 1000 cm^{-1} peak where Figure 2.4-3a covers the 0 to 1000 ppm chromate concentration range and Figure 2.4-3b covers the 0 to 50 ppm chromate concentration range. The equation that describes this curve is summarized in Table 2.3-1. It can be seen that the results in Figure 2.4-3 obtained for the Au/MEP capture matrices are very similar to what was observed for the Au/MEP conventional SERS substrate, Figure 2.4-2, and shows that the ratioing method can be used to obtain reasonable calibration curves for the capture matrices.

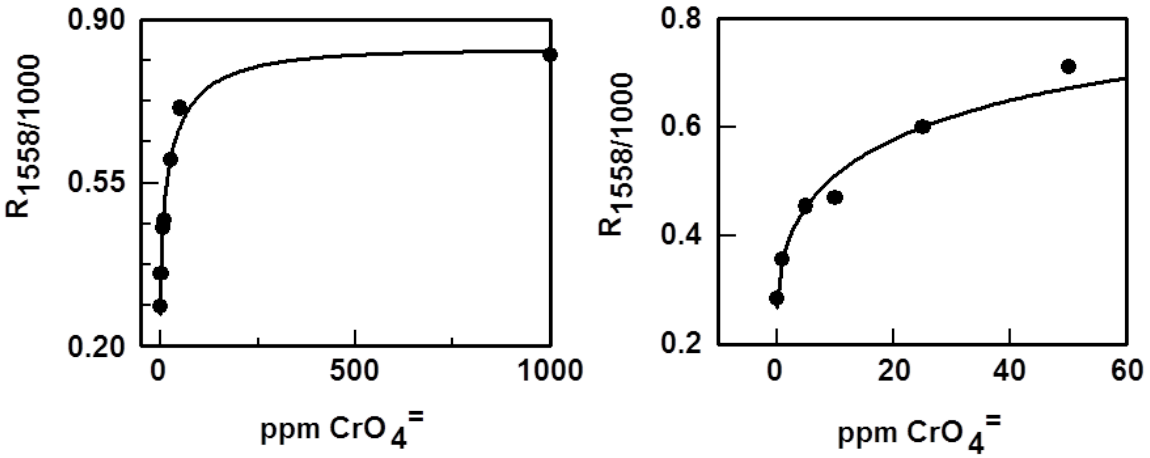

Figure 2.4-3. Plots of MEP peak intensity at 1558 cm^{-1} ratioed to the 1000- cm^{-1} peak as a function of chromate concentration for Au/MEP SERS active capture matrices. Chromate concentration ranges are (a) 0 to 1000 ppm and (b) 0 to 50 ppm. Equation describing the curves is summarized in Table 3.2-1.

2.5 REFERENCES

1. I. Turyan and D. Mandler. 1997. "Selective Determination of Chromium by a Self-Assembled Monolayer Based Electrode," *Analytical Chemistry 69*:894–897.

2. P. A. Mosier-Boss and S. H. Lieberman. 2003. "Detection of Anions by Normal Raman Spectroscopy and Surface-enhanced Raman Spectroscopy of Dationic-coated Substrates," *Applied Spectroscopy 57*:1129–1137.

3. P. A. Mosier-Boss and S. H. Lieberman. 2003. "Surface-Enhanced Raman Spectroscopy (SERS) and Molecular Modeling of the Chromate Interaction with 4-(2-Mercaptoethyl)Pyridinium," *Langmuir 19*:6826–6836.

4. D. W. Marquardt. 1963. "An Algorithm for Least-squares Estimation of Nonlinear Parameters," *Journal of the Society for Industrial and Applied Mathematics 11*:431–441.

5. L. G. Crane, D. X. Wang, L. M. Sears, B. Heyns, and K. Carron. 1995. "SERS Surfaces Modified with a 4-(2-Pyridylazo)resorcinol Disulfide Derivative: Detection of Copper, Lead, and Cadmium," *Analytical Chemistry 67*:360–364.

3. Ag/DMA CAPTURE MATRICES FOR THE DETECTION OF PERCHLORATE BY SERS

3.1 INTRODUCTION

Gu et al.[1] demonstrated the use of 2-dimethylaminoethanethiol hydrochloride (DMA) modified gold nanoparticles to detect perchlorate by SERS in both simulated and contaminated groundwater samples. Using these DMA derivatized-Au nanoparticles, they detected concentrations of perchlorate as low as 0.1 μg/L (or 0.1 ppb). They reported that the presence of higher concentrations of background ionic species (nitrate, sulfate, phosphate, and chloride) did not impact the quantitative analysis of perchlorate. The perchlorate analysis cartridges developed by OndaVia use dimethylaminoethanethiol hydrochloride as the perchlorate selective coating. These cartridges worked pretty well, at least to ~ 100 ppb, in pH-adjusted (2.5) northern California groundwater samples that have (at least) nitrate and sulfate.[2] The interaction of anions with conventional Ag/DMA SERS substrates was reported.[3] They showed that when the anion concentration is in M, the measured response of the anion with the DMA coating was described by a Frumkin isotherm. The shape of the Frumkin isotherm is described by two parameters - (1) K, the ion-pair constant between the anion and the coating, and (2) g, the Frumkin parameter that takes into account interactions between adsorbed species. The selectivity for DMA for anions, as measured by SERS, was (ion pair constants are indicated):

$$SO_4^{=}\ (972) > ClO_4^{-}\ (404) > Cl^{-}\ (310) > NO_3^{-}\ (301) >> HPO_4^{=},\ H_2PO_4^{-}\ (0).$$

In this section, we describe how to synthesize Ag/DMA capture matrices and show how calibration curves can be generated to determine the amount of perchlorate present in a sample. The use of capture matrices to pre-concentrate perchlorate to achieve lower detection limits is discussed in Section 9.

3.1.1 Brief Description of Detection Scheme

A suspension of Ag/DMA capture matrices and the sample to be analyzed are injected into a mixer that has folded flow mixing to increase capture efficiency (see Section 9). Once mixed, the sample/capture matrices suspension goes into a flow-through cell where a magnet pulls the capture matrices down onto an optical surface. A Raman spectrometer, operating at 785-nm excitation, measures the SERS response of the DMA coating on the capture matrices as well as the perchlorate bound to the coating. The advantage of this method of detection is that the perchlorate does not need elution off the capture matrices prior to detection. However, chloride ion was found to be significantly interferent, which requires some sample pretreatment to eliminate, as will be discussed.

3.2 SYNTHESIS OF Ag/DMA CAPTURE MATRICES

3.2.1 Reagents

Silver nitrate (Aldrich), sodium citrate (Aldrich), dimethylaminoethanethiol hydrochloride (Aldrich), water (HPLC grade, Aldrich), and ethanol (HPLC grade, Aldrich), were used as received.

We washed a 0.5-mL aliquot of 5 μm diameter, amine-terminated, silica-coated iron oxide microparticles (Bioclone, part no. FA-104) 10 times with 1-mL aliquots of HPLC water to remove surfactant. Between washes, a NdFeB magnet separates the magnetic microparticles from the water. After the washes, the volume of the amine-terminated, magnetic microparticles was adjusted to 1.0 mL with water.

3.2.2 Preparation of Silver Colloid

A 250-mL solution containing 45 mg of silver nitrate and a Teflon®-coated stirbar were placed in a two-neck 500-mL, round-bottom flask. A condenser with attached water line was placed on the center neck of the flask. A 25-mL addition funnel, containing 5 mL of 1% sodium citrate dihydrate in water, was placed on the second neck of the flask. Once the silver nitrate solution was brought to boil, the sodium citrate solution was added rapidly with constant stirring. After heating/stirring for 1 h, we removed the reaction flask from the heat and allowed it to cool to room temperature. The colloidal suspension was yellowish brown in appearance. The colloidal suspension was concentrated to a final volume of ~ 3 mL by centrifugation.

3.2.3 Preparation of Ag/DMA Capture Matrices

A 100-µL aliquot of the washed, amine terminated, magnetic microparticles was pippetted into a glass vial containing 1 ml of water (HPLC grade, Aldrich). A 200-µL aliquot of the concentrated silver colloidal suspension was added to the glass vial and the vial was placed on a roller. The amine groups of the magnetic microparticles bind to the silver colloidal particles. After rolling for 2 h, a NdFeB magnet was used to separate the microparticles from the liquid. If the liquid was clear, we removed half the volume and added another 200-µL aliquot of the concentrated silver colloidal suspension to the glass vial and placed it on the roller. The process was repeated until the surface of the magnetic microparticles was completely covered with colloidal silver particles as indicated when the liquid remained yellow-gray in color. The Ag-covered, magnetic microparticles were then washed three times with water (HPLC grade, Aldrich) and then three times with ethanol (HPLC grade, Aldrich). Between washings, a NdFeB magnet is used to separate the Ag-covered magnetic microparticles. Afterwards, a dilute ethanolic solution (~ 0.09 M) of DMA was added to the glass vial. The DMA was allowed to react with the immobilized silver colloidal particles for ~ 24 h to form a SAM. The Ag/DMA capture matrices were then washed three times in ethanol, as described above. The volume of the Ag/DMA capture matrices was adjusted to 1 mL using ethanol. We refrigerated capture matrices between uses.

3.3 CONVENTIONAL Ag/DMA SERS SUBSTRATE

A discussion on conventional Ag/DMA SERS substrates is included to demonstate how spectral data is handled. In the appendix, relevent papers are included that describe how the conventional SERS substrate is fabricated and how the spectral data are acquired. Here we describe data manipulation to generate a calibration curve that is used to determine the amount of analyte is present in a sample.

The SERS spectra obtained for the conventional SERS substate are acquired at a fixed spot on the substrate. A reference spectrum is obtained with the flow-through cell filled with water. The water was then sequentially replaced with solutions of varying concentration of perchlorate, going from the lowest perchlorate concentration to the highest. The response of the DMA coating to perchlorate was instantaneous. Figure 3.3-1a shows examples of SERS spectra obtained for the Ag/DMA coating in the absence and presence of perchlorate. When exposed to perchlorate, a peak due to the symmetric Cl-O stretching mode of perchlorate grows in at 923 cm^{-1}. As for the Au/MEP conventional SERS substrate results described in the previous chapter, a calibration curve can be generated by ratioing the perchlorate peak intensity to a DMA peak that does not change in the presence of perchlorate ion. Two DMA peaks that do not vary with perchlorate concentration are at 985 and 1149 cm^{-1}. The results of ratioing the perchlorate peak to the 985 and 1149 cm^{-1} DMA peaks are shown in Figure 3.3-2. At low perchlorate concentration, the perchlorate peak area increases with concentration. At

higher perchlorate solution concentrations, the response levels off as the adsorption sites on the DMA SAM become fully occupied. The equation that describes this curve is summarized in Table 3.3-1.

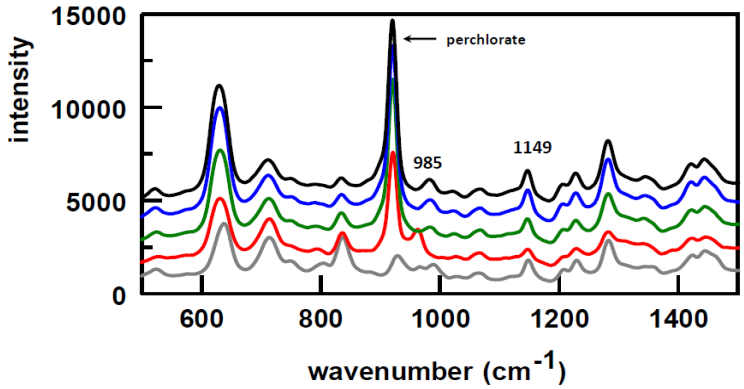

Figure 3.3-1. SERS spectra of a conventional Ag/DMA SERS substrate obtained at perchlorate concentrations of bottom to top) 0, 500, 1000, 5000, and 10000 ppm. Spectra were obtained using 785-nm excitation at 30 mW and averaging 10 1-s spectra. The perchlorate peak and DMA peaks at 985 and 1149 cm^{-1} are indicated.

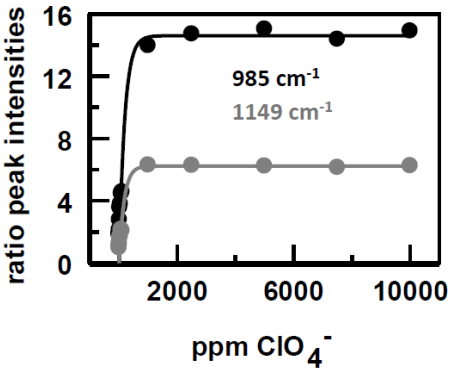

Figure 3.3-2. Plots of the perchlorate peak intensity at 920 cm^{-1} ratioed to the DMA peaks at 985 and 1149 cm^{-1} as a function of perchlorate concentration. Equations describing the curves are summarized in Table 3.3-1.

Table 3.3-1. Summary of equations that describe the observed calibration curves.

Curve	Equation Describing Curve[a]	R^2	Values of Parameters
Fig. 3.3-2 ratio to 985 cm^{-1} DMA peak	y = a (1-exp(-bx))	0.9904	a = 14.60 ± 0.61 b = 0.0051 ± 0.0010
Fig. 3.3-2 ratio to 1149 cm^{-1} DMA peak	y = a (1-exp(-bx))	0.9871	a = 6.23 ± 0.30 b = 0.0058 ± 0.0013
Fig. 3.4-2 ratio to 985 cm^{-1} DMA peak	y = a (1-exp(-bx))	0.9738	a = 7.12 ± 0.81 b = 0.00199 ± 0.00072
Fig. 3.4-2 ratio to 1149 cm^{-1} DMA peak	y = a (1-exp(-bx))	0.9723	a = 2.66 ± 0.30 b = 0.00201 ± 0.00072

a. In the equations, y is the ratio of peak intensities and x is the ppm perchlorate.

3.4 Ag/DMA SERS-ACTIVE CAPTURE MATRICES

To evaluate the perchlorate response of the Ag/DMA capture matrices, an aliquot of known volume of the capture matrices are pipetted into a glass vial. A NdFeB magnet was used to separate the capture matrices from the ethanol. The capture matrices were washed three times with 0.5 mL of water. A NdFeB magnet was used to separate the capture matrices from the liquid between washes. Afterwards, we added 1-mL aliquot of an aqueous perchlorate solution of known concentration to the vial. The sample was allowed to equilibrate overnight. Afterwards, a pipette was used to transfer the capture matrices and solution to a cell with an Au foil optical surface. A NdFeB magnet on the other side of the Au foil was used to concentrate the capture matrices in a single spot. Examples of SERS spectra obtained are shown in Figure 3.4-1. The figure shows that the intensities of the peaks caused by DMA and perchlorate vary, as do the baselines. Because of these variabilities between the spectra obtained for the individual samples, it is impossible to do spectral subtractions to obtain the perchlorate peak area. However, a calibration curve can be generated by ratioing the perchlorate peak intensity to a DMA peak that does not change in the presence of perchlorate ion. As was discussed *vide supra*, two DMA peaks that do not change in the presence of perchlorate ion occur at 985 and 1149 cm^{-1}, respectively. Figure 3.4-2 summarizes the results obtained by ratioing the perchlorate peak intensity to the intensities of the 985 and 1149 cm^{-1} DMA peaks. The equations that describe these curves are summarized in Table 3.3-1. This table shows that the results in Figure 3.4-2 obtained for the Ag/DMA capture matrices are very similar to what was observed for the Ag/DMA conventional SERS substrate in Figure 3.4-2, and shows that the ratioing method can be used to obtain reasonable calibration curves for the capture matrices.

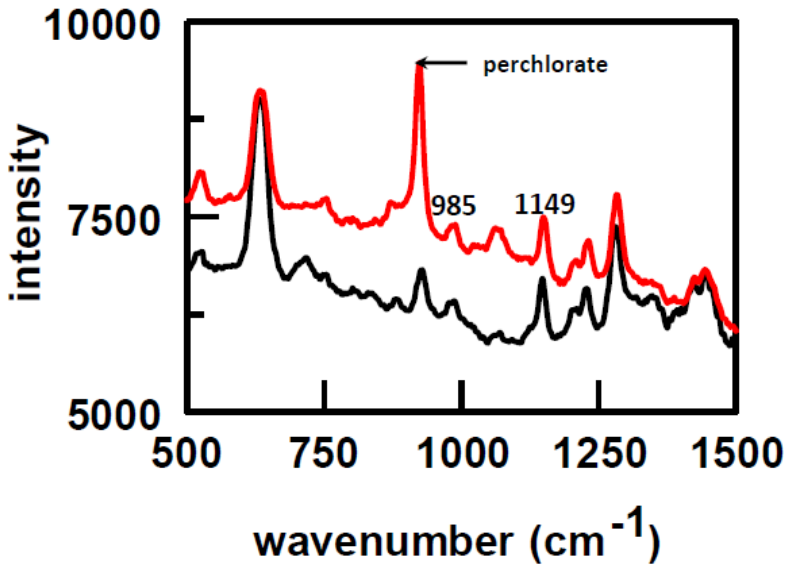

Figure 3.4-1. SERS spectra of Ag/ DMA capture matrices immersed in solutions of 0-ppm (bottom) and 10000-ppm (top) perchlorate.

3.5 THE USE OF SPE TO ELIMINATE CHLORIDE ION INTERFERENCE

Experiments were conducted using the Ag/DMA capture matrices to detect perchlorate in solutions containing nitrate, sulfate, and chloride anions. The purpose of these experiments was to determine the extent these other anions interfere in the detection of perchlorate. In these experiments, a 50-µL aliquot of Ag/DMA capture matrices was pipetted onto the gold surface of the flow-through cell

shown in Figure 3.5-1. Figure 3.5-2a shows spectra obtained when water, a solution containing 25-ppm perchlorate, and a solution containing 25-ppm perchlorate and 250 ppm each of nitrate and sulfate were flowed through the cell. When a solution of 25-ppm perchlorate is flowed through the cell, a new peak at 923 cm^{-1} appears in the spectrum of the Ag/DMA capture matrices. This new peak is caused by perchlorate. When a solution containing 25-ppm perchlorate and 250 ppm each of nitrate and sulfate is flowed through the cell, we observed a decrease in the intensity of the perchlorate peak. A new peak at 1047 cm^{-1} grows in. Nitrate causes this peak. We observed no sulfate peak at 982 cm^{-1}. These results indicate that sulfate does not interfere with the detection of perchlorate. Nitrate minimally interferes.

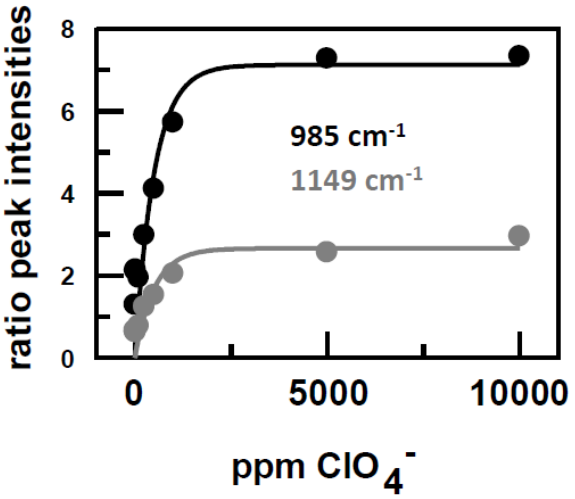

Figure 3.4-2. Plots of the perchlorate peak intensity at 923 cm^{-1} ratioed to the DMA peaks at 985 and 1149 cm^{-1} as a function of perchlorate concentration. Equations describing the curves are summarized in Table 3.3-1.

Figure 3.5-2b shows spectra obtained when water, a solution containing 25-ppm perchlorate, and a solution containing 25-ppm perchlorate and 250-ppm chloride are flowed through the cell. When a solution of 25-ppm perchlorate is flowed through the cell, a new peak at 923 cm^{-1} caused by perchlorate appears in the spectrum of the Ag/DMA capture matrices. When a solution containing 25-ppm perchlorate and 250-ppm chloride is flowed through the cell, the intensity of the perchlorate peak is significantly reduced, indicating that chloride is a significant interferent to the detection of perchlorate using SERS-active Ag/DMA capture matrices.

In ion chromatography of anions, chloride ion is removed from aqueous solutions using solid phase extraction (SPE).[4] A schematic of the SPE cartridge is shown in Figure 3.5-3a. Maxi-Clean™ IC-Ag Plus cartridges (Alltech) consist of 1.5 mL of polystyrene-based packing material sandwiched between 20-µm polyethylene frits in a medical-grade polypropylene housing that mounts on a syringe, Figure 3.5-3b. Each IC-Ag Plus cartridge contains 2 milliequivalents of silver ion. These cartridges remove excess halides through the formation of insoluble silver-halide salts. During the process, cations from the sample are taken up by the resin to replace the silver consumed in the precipitation of the silver halide.

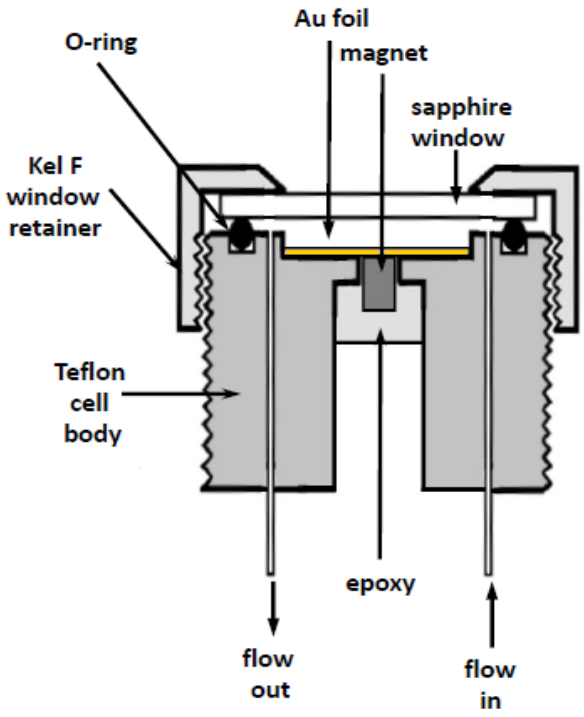

Figure 3.5-1. Schematic of the flow-through cell used to evaluate the SERS response of Ag/DMA capture matrices.

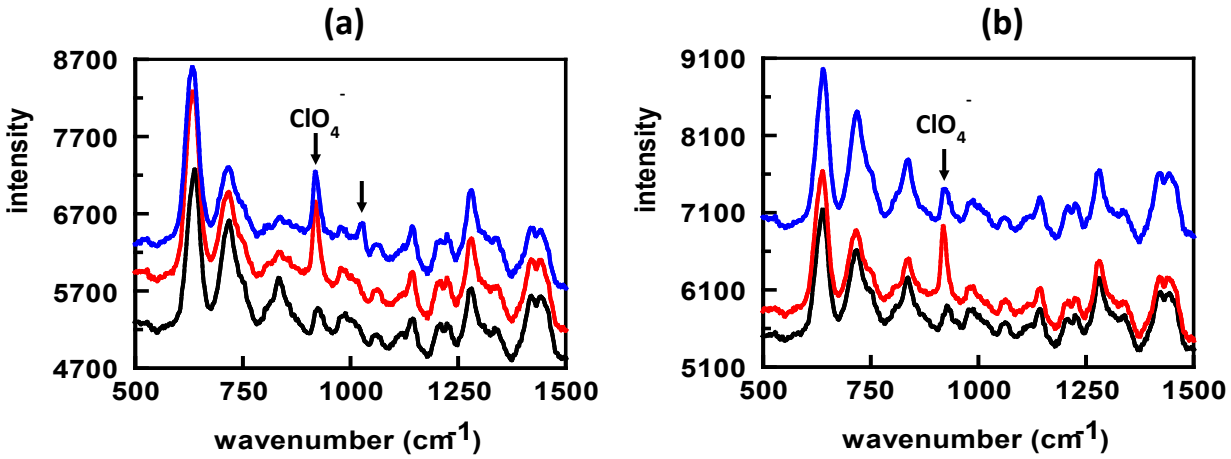

Figure 3.5-2. SERS spectra of Ag/DMA capture matrices obtained using the cell shown in Figure 3.5-1: (a) spectra obtained in water (black), 25-ppm perchlorate (red), and 25-ppm perchlorate and 250 ppm each nitrate and sulfate (blue); (b) spectra obtained in water (black), 25-ppm perchlorate (red), and 25-ppm perchlorate and 250-ppm chloride (blue). Perchlorate and nitrate peaks are indicated.

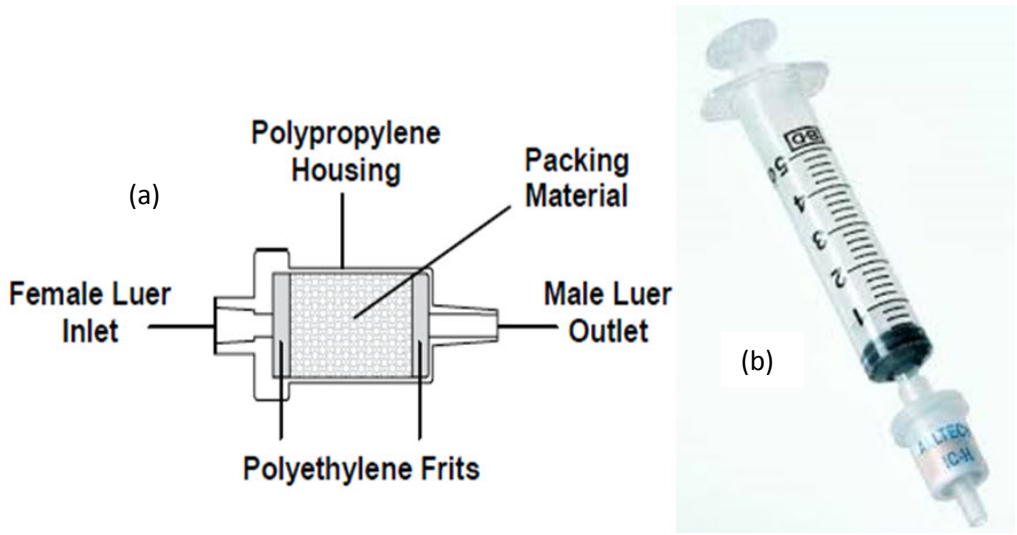

Figure 3.5-3. (a) Schematic of a SPE cartridge, (b) SPE cartridge mounted on a syringe.

As shown in Figure 3.5-3b, the SPE cartridge has a female Luer inlet that attaches to a syringe. Prior to using the IC-Ag cartridge to remove chloride ions in the sample, 10 mL of deionized water is passed through the cartridge to remove interstitial contaminants and to wet the packed bed. The sample is then loaded onto the cartridge at a flow rate of 1 mL/min. The first 1 mL of cartridge mobile phase is discarded and the remaining eluate is collected for further analysis.

Samples of 25- and 100-ppm perchlorate were prepared in the absence of other anions; in the presence of only 250-ppm chloride, and in the presence of 250 ppm each of nitrate, sulfate, and chloride, SPE of the chloride containing solutions was completed. A 50-µL aliquot of Ag/DMA capture matrices was pipetted onto the gold surface of the flow-through cell shown in Figure 3.5-1. Figure 3.5-4a summarizes the results obtained for 25-ppm perchlorate. When a solution of 25-ppm perchlorate was flowed over the Ag/DMA capture matrices, we observed a peak caused by perchlorate at 920 cm^{-1} in the spectrum (Figure 3.5-4a, red curve). The eluant obtained after SPE of the 25-ppm perchlorate and 250-ppm chloride solution was then flowed through the cell. The resultant spectrum (Figure 3.5-4a, blue curve) shows a slight increase of the perchlorate peak. This increase indicates that the IC-Ag cartridge has removed the chloride ion interference. When the eluant obtained after SPE of the 25-ppm perchlorate and 250 ppm each chloride, nitrate, and sulfate was flowed through the cell, the resultant spectrum (Figure 3.5-4a green curve) showed a decrease in the perchlorate peak and two new peaks at 832 and 954 cm^{-1}, respectively. We obtained similar results using a fresh 50-µL aliquot of Ag/DMA capture matrices and the 100-ppm perchlorate solutions, Figure 3.5-4b. Addition of sodium chloride to the perchlorate-nitrate-sulfate-chloride SPE eluants showed the presence of silver ions. An earlier Raman study showed that silver ions form ion pairs with nitrate and sulfate in aqueous solution but not with perchlorate.[5] Consequently, the new peaks observed at 832 and 954 cm^{-1} are attributed to these silver-nitrate and silver-sulfate complex ions.

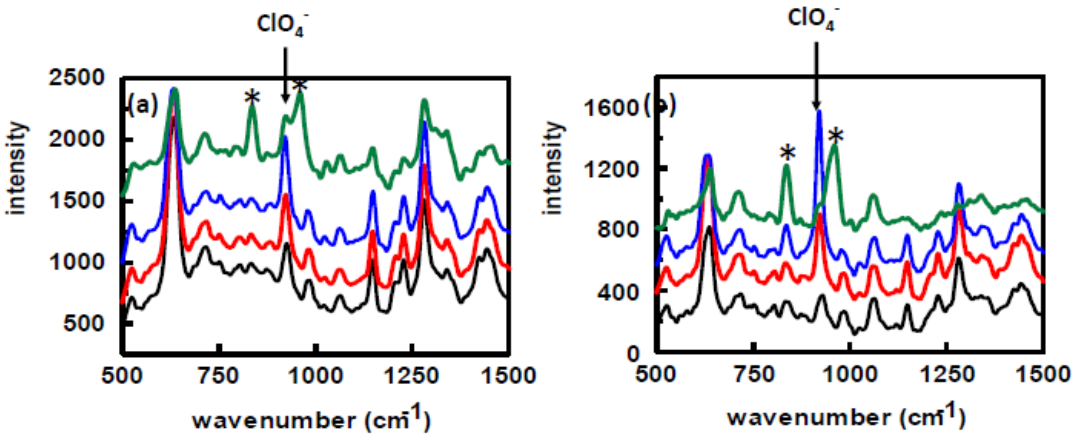

Figure 3.5-4. SERS spectra of Ag/DMA capture matrices obtained using the cell shown in Figure 3.5-1: (a) spectra obtained in water (black), 25-ppm perchlorate (red), 25-ppm perchlorate and 250 ppm each nitrate and sulfate (blue), and 25-ppm perchlorate and 250 ppm each nitrate and sulfate after SPE (green); (b) spectra obtained in water (black), 100-ppm perchlorate (red), 100-ppm perchlorate and 250-ppm chloride (blue), and 100-ppm perchlorate and 250 ppm each nitrate and sulfate after SPE (green). Perchlorate peaks are indicated. * indicates the peaks due to nitrate and sulfate complex ions with silver.

3.6 REFERENCES

1. B. Gu, C, Ruan, and W. Wang. 2009. "Perchlorate Detection at Nanomolar Concentrations by Surface-enhanced Raman Scattering," *Applied Spectroscopy Reviews* *63*:98–102.

2. Mark Peterman of OndaVia, personal communication.

3. P. A. Mosier-Boss and S.H. Lieberman. 2003. "Detection of Anions by Normal Raman Spectroscopy and Surface-enhanced Raman Spectroscopy of Cationic-coated Substrate," *Applied Spectroscopy Reviews* *57*:1129–1137.

4. I. K. Henderson, R. Sarri-Nordhaus, and J. M. Anderson Jr. 1991. "Sample Preparation for Ion Chromatography by Solid-phase Extraction," *Journal of Chromatography* *546*:61–71.

5. R. E. Hester and R. A. Plane. 1964. "A Raman Spectrophotometric Comparison of Interionic Association in Aqueous Solutions of Metal Nitrates, Sulfates, and Perchlorates," *Inorganic Chemistry* *3*:769–770.

4. C_{18} CAPTURE MATRICES FOR THE DETECTION OF PAHs BY FLUORESCENCE

4.1 INTRODUCTION

Methods for determining PAHs in the environment include gas chromatography with flame ionization detection (GC/FID) and high-performance liquid chromatography (HPLC) with ultraviolet or fluorescence detection.[1] While GC/FID is the more sensitive technique, it is subject to background interferences from other carbonaceous sources. Both chromatography methods are not practical for use in the field. As PAHs are fluorescent, fluorescence can be used to detect PAHs in the environment. However, preconcentration is required to achieve low detection limits. SPE using cartridges containing C_{18} resins have been used to achieve low detection limits.[2]

4.1.1 Brief Description of Detection Scheme

C_{18} capture matrices are extremely hydrophobic. They stick to plastic surfaces, so all mixing has to be done in glass vessels. Vortexing is used to increase capture efficiency between the capture matrices and the ≥ 5-mL volume of aqueous sample. Due to their extreme hydrophobicity, C_{18} capture matrices are difficult to manipulate. Consequently, the amount of PAHs taken up by the capture matrices cannot be directly measured. However, the PAHs can be eluted off the capture matrices into a 1-mL volume of acetonitrile. The fluorescence of the PAHs in acetonitrile is then measured. The standard addition method is then used to quantify the amount of PAHs in the sample.

4.2 SYNTHESIS OF C_{18} CAPTURE MATRICES

4.2.1 Reagents

Hydrochloric acid (Baker), sulfuric acid (Baker), hydrogen peroxide (Aldrich), toluene (Aldrich), water (HPLC grade, Aldrich), and ethanol (HPLC grade, Aldrich), were used as received.

A 0.5-mL aliquot of 5-μm-diameter, silica-modified magnetic microparticles (Bioclone, part no. FF-104) was washed 10 times with 1 mL aliquots of HPLC water to remove surfactant. Between washes, we used a NdFeB magnet to separate the magnetic microparticles from the water. After the washes, we adjusted the volume of the silica-modified magnetic microparticles to 1.0 mL with water.

4.2.2 Preparation of C_{18} Capture Matrices

A 250-μL aliquot of the washed silica-modified microparticles was pipetted into a microvial. A NdFeB magnet was used to separate the microparticles from the water. We soaked the microparticles in a 5% HCl solution overnight. This step removes impurities on the surfaces of the microparticles. A NdFeB magnet was used to separate the microparticles from the HCl solution and the microparticles are washed three times with water. We used a NdFeB magnet to separate the microparticles from the water and added a 1:1 solution composed of 50% H_2SO_4 and 30% H_2O_2. This step activates the microparticles by increasing the hydroxyl group concentration on their surfaces. After reacting for 40 min, we separated and washed the microparticles three times with water, three times with ethanol, then three times with toluene. Figure 4.2-1a shows a photograph of the activated microparticles in toluene. This photograph shows that the activated microparticles do not homogeneously disperse in the toluene. The increased number of hydroxyl groups makes the microparticles lipophobic. With the addition of 300 μL of octadecyltrimethoxysilane and 75-μL n-butylamine (a transesterification catalyst), the microparticles homogeneously disperse in toluene, Figure 4.2-1b. The structure of octadecyltrimethoxysilane is shown in Figure 4.2-1c. The fact that the microparticles homogeneously disperses upon the addition of octadecyltrimethoxysilane indicates that the

trimethoxysilane groups are interacting with the hydroxyl groups of the activated microparticles and the octadecyl group is interacting with the toluene to essentially form gigantic micelles. The suspension is then transferred, using toluene, to a 25-mL round-bottom flask and refluxed for ~ 2 h. Afterwards, the microparticles are transferred to a glass microvial and washed three times with ethanol. The volume of the C_{18} capture matrices was adjusted to 1 mL using ethanol. We refrigerated the capture matrices between uses. To test that the magnetic microparticles are indeed derivatized, a 50-µL sample of the C_{18} capture matrices was pipetted into a glass vial of water. As shown in Figure 4.2-1d, the C_{18} capture matrices reside at the air–water interface, indicating that the capture matrices are extremely hydrophobic.

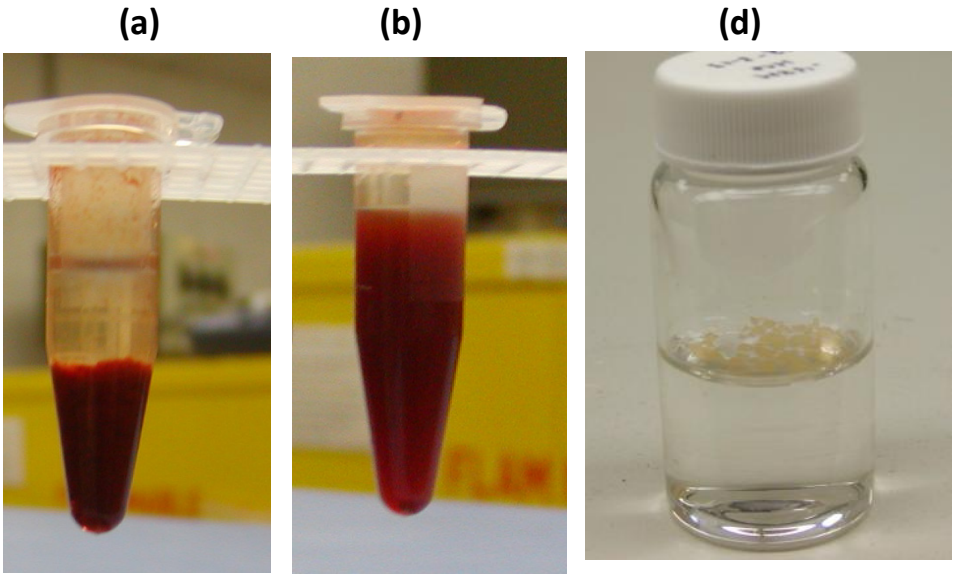

(c) $CH_3(CH_2)_{16}CH_2-Si(OCH_3)_3$ (with OCH_3 above and below Si)

Figure 4.2-1. Activated silica-modified magnetic microparticles in toluene: (a) before the addition of octadecyltrimethoxysilane and n-butylamine, (b) after the addition of octadecyl-trimethoxysilane and n-butylamine, (c) structure of octadecyltrimethoxysilane, (d) C_{18}-derivatized magnetic microparticles in water.

4.3 DETECTION OF PAHs

4.3.1 Methods of Extraction

For capture matrices, the efficiency of the analyte extraction depends on the contact time of the sample with the capture matrices. To improve the probability of contact between the analyte and the capture matrices, Shishehbore, Afkhami, and Bagheri[3] used ultrasonication for 10 min to disperse the capture matrices in aqueous samples. Šafařik and Šafařiková[4] stirred their aqueous samples for 4 h after adding their capture matrices. As shown in Figure 4.2-1d, C_{18} capture matrices cannot be dispersed directly in water because of the hydrophobicity of the C_{18} chains. Since mixing for 4 h is impractical, we explored using ultrasonication and vortexing to disperse the C_{18} capture matrices in

aqueous samples. Fluoranthene, whose structure is shown in Figure 4.3-1a, was used in these investigations. The concentration of fluoranthene is 265 µg/L (or 265 ppb) when saturated in water.

Into two glass vials, 10-mL aliquots of fluoranthene-saturated water were pipetted. To one glass vial, we added 25 µL of C_{18} capture matrices in ethanol. Both samples were then sonicated for 30 min. Sonication did cause the samples to warm up by 14 ^{o}C. Fluorescence measurements before and after sonication are summarized in Figures 4.3-1b and 4.3-1c. Figure 4.3-1b shows the results of sonication in the absence of the C_{18} capture matrices. For fluoranthene, there is no measureable difference in the fluorescence spectra before and after sonication, indicating that although sonication causes the sample to warm up, no loss of fluoranthene occurred because of volatilization. This may not be true of lighter PAHs such as naphthalene. Figure 4.3-1c shows the results of sonication in the presence of the C_{18} capture matrices. The fluorescence spectrum after sonication shows a decrease in intensity compared to the spectrum obtained before sonication. This decrease indicates that the C_{18} capture matrices have taken up some fluoranthene. The amount taken up was only ~ 20%.

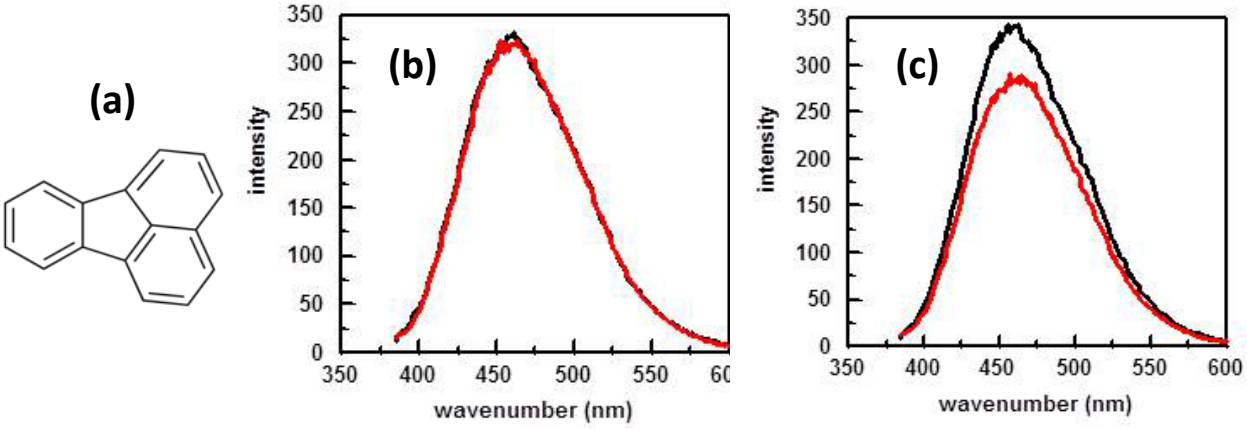

Figure 4.3-1. (a) Structure of fluoranthene, (b) fluorescence of fluoranthene before (black) and after (red) sonication in the absence of C_{18} capture matrices, (c) fluorescence of fluoranthene before (black) and after (red) sonication with C_{18} capture matrices. Fluorescence spectra were obtained using λ_{EX} = 350 nm; λ_{EM} = 385 to 600 nm; scan rate of 60 nm/min; and excitation and emission slits of 10 and 20 nm, respectively.

We used a vertical, high-speed 15-mL tube holder that mounts on top of the Vortex-Genie® 2 to vortex samples, Figure 4.3-2a. We then added 50 µL of C_{18} capture matrices in ethanol into a glass tube containing 5 mL of 132.5-ppb fluoranthene in water. The sample was then vortexed using a setting of 4.5. Periodically, we stopped vortexing and a took out a sample for measurement. Once the measurement was complete, the sample was returned to the glass tube and vortexing resumed. Figure 4.3-2b shows fluorescence spectra of fluoranthene obtained as a function of vortexing time. Figure 4.3-2c shows a plot of fluoranthene peak area as a function of vortexing time. This figure shows that with vortexing, the amount of fluoranthene remaining in solution decreases rapidly and then levels off. After 30 s of vortexing, ~ 50% of the fluoranthene had been extracted by the C_{18} capture matrices. We determined that 10 min of vortexing is sufficient for the C_{18} capture matrices to extract the PAHs. Unlike sonication, vortexing did not cause the sample to heat up. This is an important consideration for more volatile PAHs such as naphthalene. Also, the data summarized in Figures 4.3-2b and c clearly show that vortexing was more efficient than sonication in extracting PAHs from aqueous solutions. Vertical tube attachments are available for the Vortex Genie® that can hold 50-mL sample tubes.

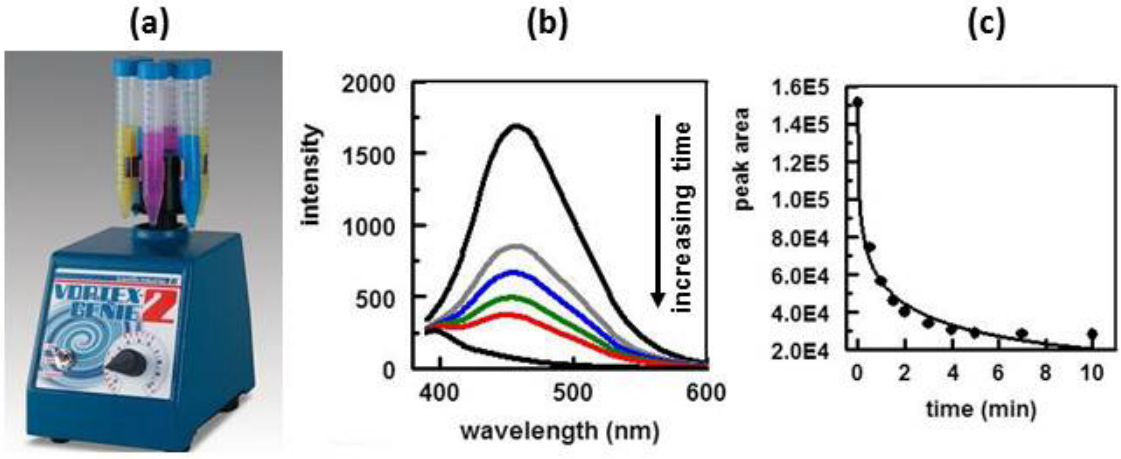

Figure 4.3-2. (a) Vortex Genie® 2 with vertical, high-speed 15-mL tube holder attachment, (b) fluorescence spectra of fluoranthene obtained as a function of vortexing time, (c) plot of fluoranthene peak area as a function of vortexing time.

4.3.2 Microscopic Imaging of C_{18} Capture Matrices

An Eclipse E600 (Nikon™) epifluorescence microscope equipped with a CoolSnap™ HQ CCD camera (Photometrics, Ltd.) was used to image the C_{18} capture matrices. Figure 4.3-3a shows the excitation and emission curves for fluoranthene.[5] As shown in Figure 4.3-3b, the spectral curves of the DAPI filter set[6] encompasses both the excitation and emission curves for fluoranthene. Using the DAPI filter set, the image of a fluoranthene crystal was obtained using the epifluorescent microscope.

To show that fluoranthene partitions in to the C_{18} capture matrices, a 10-mL sample of fluoranthene saturated water was added to a glass vial. To this sample, 50 µL of C_{18} capture matrices in ethanol was added. The sample was then sonicated for 30 min. When sonication was complete, the capture matrices were filtered onto a 0.02-µm Whatman™ Anodisc™ filter and imaged using the epifluorescence microscope. Figure 4.3-4a shows images taken of a clump of capture matrices. The top image was taken without filters and shows no fluorescence. The bottom image is an overlay of two images where one image was taken without filters and the other with the DAPI filter cube. This image shows that the capture matrices are fluorescing, indicating that fluoranthene has partitioned into the C_{18} coating. In another experiment, 50 µL of C_{18} capture matrices in ethanol was added to a 100-mL sample of fluoranthene-saturated water. After 4 days, the sample was filtered through a 0.1-µm Whatman™ Anodisc™ filter. Figure 4.3-4b shows the images obtained for clumps of the capture matrices. Crystals of fluoranthene can be seen in the bottom image. This shows that once fluoranthene partitions into the C_{18} coating, this fluoranthene can act as nucleation sites for crystal growth.

4.3.3 Detecting and Quantifying PAHs

As shown in Figure 4.3-4, one can directly detect PAHs that have partitioned inside the C_{18} coating. We then attempted to try to collect the beads on an optical surface to detect and quantify the amount of PAHs extracted by the C_{18} capture matrices. This was difficult because of the hydrophobic nature of the capture matrices. We could use a NdFeB magnet (K&J Magnetics, Inc. Part Number D22-N52) to concentrate the capture matrices onto the tip of a 5-mm-diameter NMR tube. The tube was then placed inside a quartz cuvette fitted with an Ace Glass Incorporated #7 Threaded Connector, Figure 4.3-5a. The cuvette was then placed inside the sample holder of a spectrofluorometer. The resultant spectra are shown in Figure 4.3-5b. The gray spectrum is that of C_{18} capture matrices on the tip of the NMR tube. These capture matrices had not been exposed to any PAHs, so this is the background spectrum of the capture matrices. The upper three black spectra were obtained for C_{18} capture matrices that had been exposed to fluoranthene. We rotated the NMR tube in three positions to obtain the three spectra. Figure 3.4-5 shows that fluorescence from the capture matrices can be directly measured off the capture matrices. However, the figure also shows that the fluorescence peak for the three spectra do not overlap, which is caused by the inhomogeneous distribution of the capture matrices on the tip of the glass tube. The amount of fluoranthene taken up in the capture matrices cannot be quantified. We began to explore the use of standard addition to quantify the PAHs taken up by the C_{18} capture matrices.

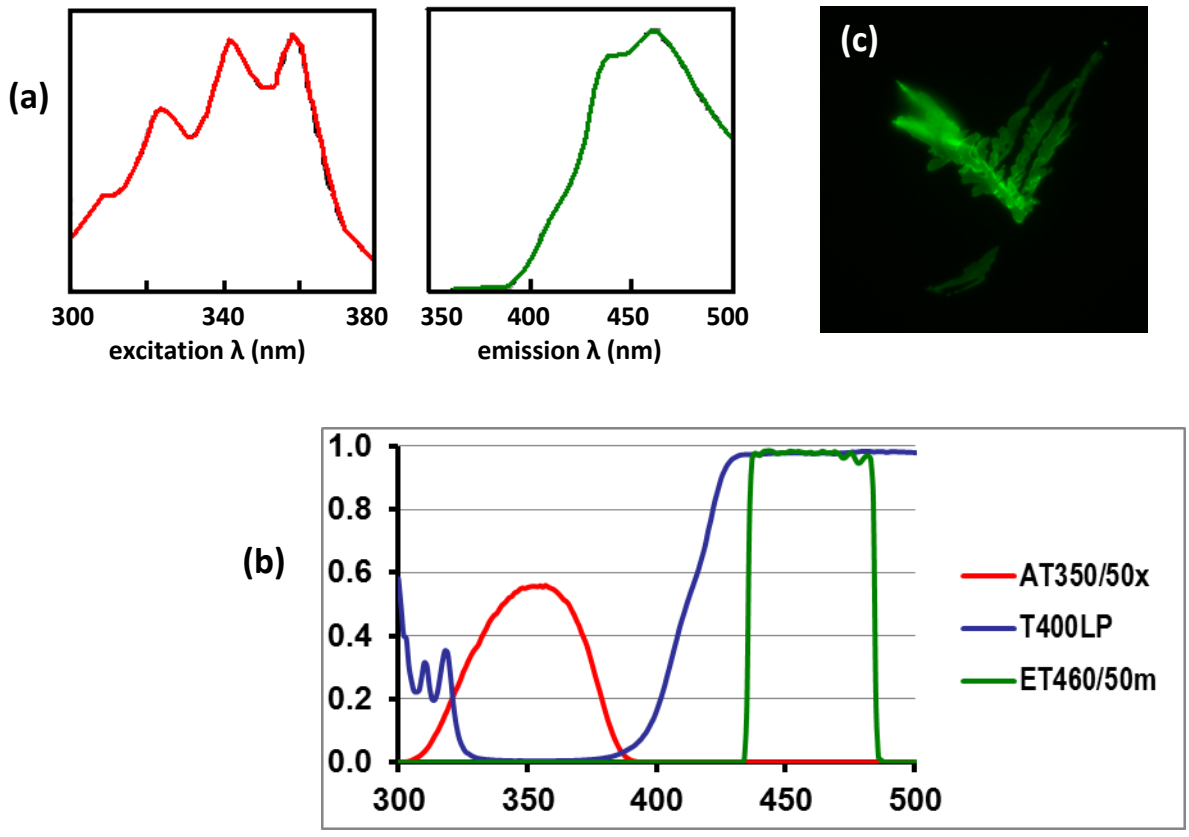

Figure 4.3-3. (a) Excitation and emission spectra for fluoranthene, (b) transmission spectra for a DAPI filter set, (c) fluorescence image of a fluoranthene crystal taken with the epifluorescence microscope using the DAPI filter set.

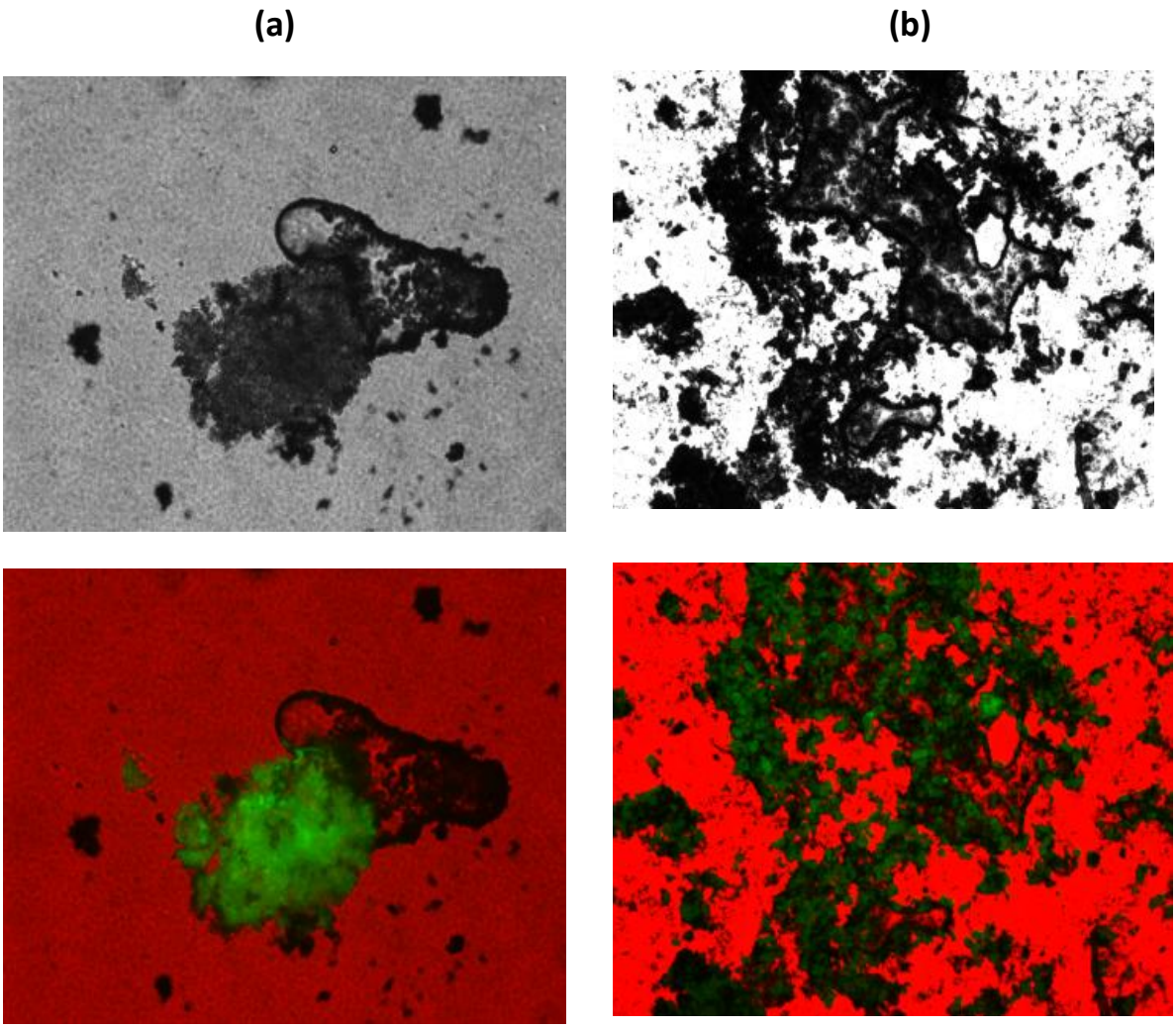

Figure 4.3-4. Photomicrographs taken of C_{18} capture matrices: (a) the capture matrices sonicated for 30 min in 10 mL of fluoranthene saturated water, (b) the capture matrices in a 100 mL of fluoranthene saturated water for 4 days. For both (a) and (b), the top images were taken without any filters. The bottom images are an overlay of two images, one taken without filters and another taken using the DAPI filter cube.

Figure 4.3-6 summarizes the steps involved in the method to quantify the amount of PAHs in an aqueous sample. We explored three cases. In case one, the aqueous fluoranthene solution exhibited a distinct fluorescence peak (5 mL of 50-ppb fluoranthene). In the second case, the baseline increases because of the presence of fluoranthene, but no distinct fluorescence peak (5 mL of 5-ppb fluoranthene in water) exists. In the third case, there is no difference in the spectra for neat water and the aqueous fluoranthene solution (5 mL of 500-pptr fluoranthene).

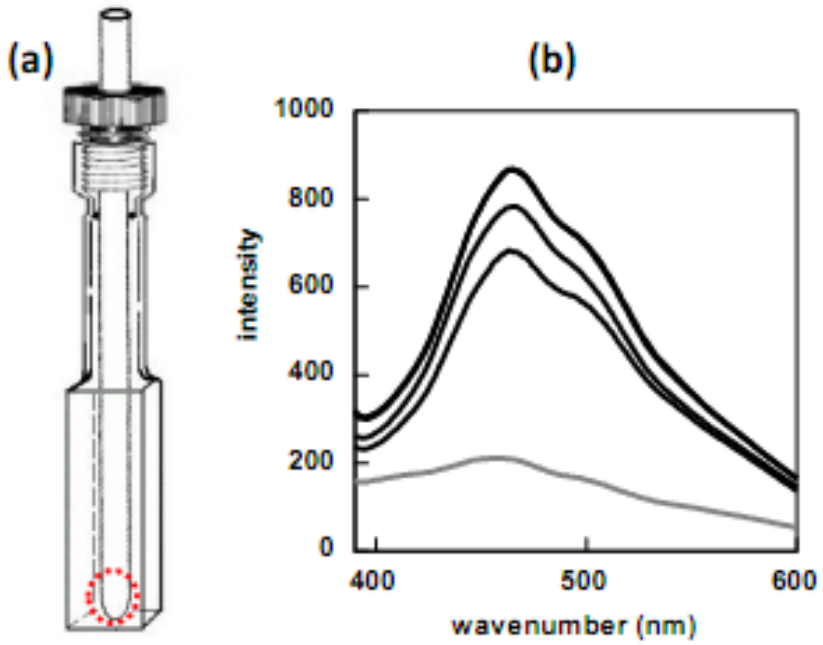

Figure 4.3-5. (a) Schematic of the modified quartz cuvette used to hold the tube in place. A magnet (not shown) is used to concentrate C_{18}-derivatized magnetic microparticles onto the tip of the tube (circled area), (b) fluorescence spectra of C_{18}-derivatized magnetic microparticles concentrated on the tip of the tube. Spectra in black are for C_{18}-derivatized magnetic microparticles vortexed with 5 mL of 265 ppb fluoranthene for 10 min. Bottom gray spectrum is for C_{18}-derivatized magnetic microparticles not exposed to fluoranthene.

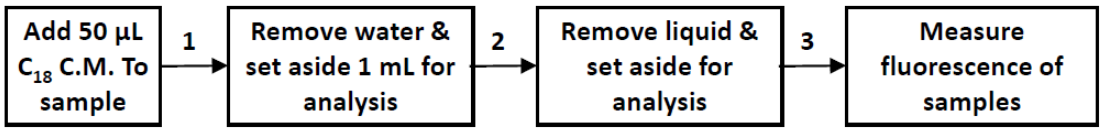

1. **Vortex for 10 min. Use magnet to separate C_{18} C.M. & liquid.**
2. **Add 1 mL acetonitrile & vortex for 10 min. Repeat twice more.**
3. **Measure flourescence of aqueous and acetonitrile samples. Spike first acetonitrile extraction with known amounts of fluoranthene in standard addition analysis.**

Figure 4.3-6. Schematic summarizing the steps required to detect and quantify PAHs using C_{18}-derivatized magnetic microparticles or capture matrices (C.M.).

Figure 4.3-7 shows the results of following those steps for a 5-mL sample containing 50-ppb fluoranthene in water. This sample contains 0.25 µg of fluoranthene. Figure 4.3-7a shows the fluorescence spectra obtained for a 5-mL aqueous solution before and after vortexing the sample with 50 µL of C18 capture matrices. Before vortexing, a peak due to fluoranthene is apparent. After vortexing, there is a decrease in peak intensity indicating that the capture matrices have taken up fluoranthene. Figure 4.3-7b shows the spectra obtained after subtracting the spectral contributions of water. Comparing the peak areas before and after vortexing, 75.1% of fluoranthene, or 0.188 ±0.019 µg, was extracted by the capture matrices.

We then used a magnet to separate the aqueous solution from the capture matrices. The water was removed and 1 mL of acetonitrile was added. After vortexing for 10 min, we used a magnet to

separate the capture matrices from the acetonitrile, placed the sample in a quartz cuvette, and measured the fluorescence. This procedure was repeated two more times. The resultant fluorescence spectra for the three acetonitrile extractions are shown in Figure 4.3-7c. For the first acetonitrile extraction, we observed a fluorescence peak caused by fluoranthene. Figure 4.3-7d are the spectra obtained after the second and third acetonitrile extractions showing weak fluoranthene peaks.

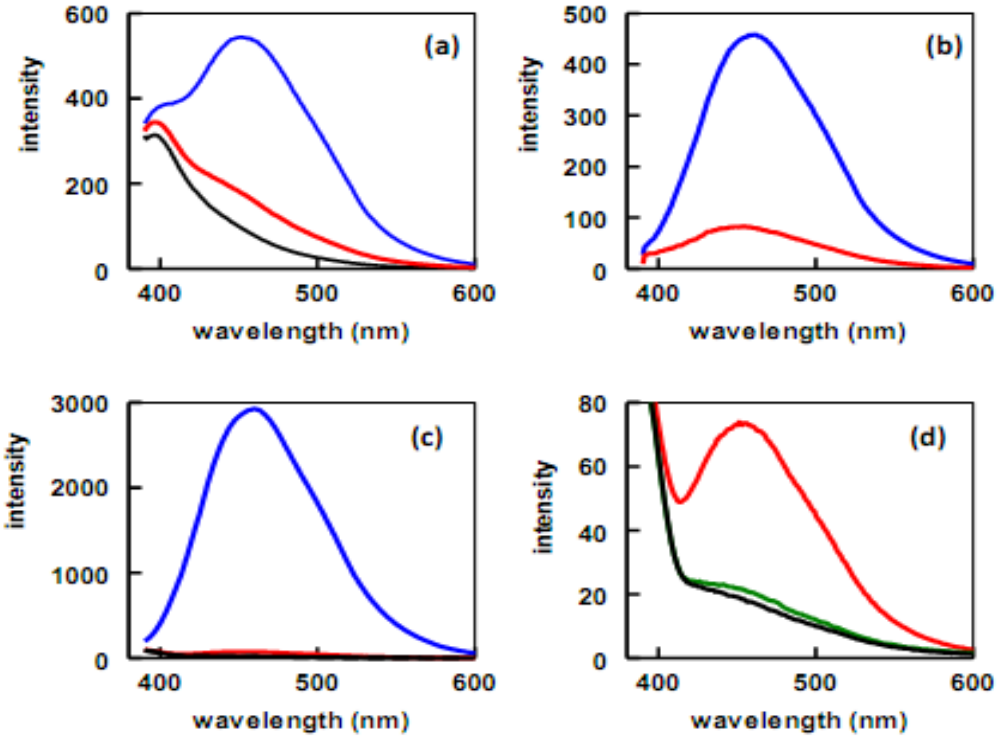

Figure 4.3-7. (a) Fluorescence spectra of deionized water and 50-ppb fluoranthene before (blue) and after (red) vortexing for 10 min with 50 µL of C_{18}- capture matrices (the spectrum for water is in black); (b) same spectra as (a) but with the spectral contributions of water subtracted out; (c) fluorescence spectra of acetonitrile and fluoranthene in acetonitrile after the first (blue), second (red), and third (green) extractions; (d) fluorescence spectra of acetonitrile and fluoranthene in acetonitrile after the second and third extractions. The spectrum caused by acetonitrile is in black.

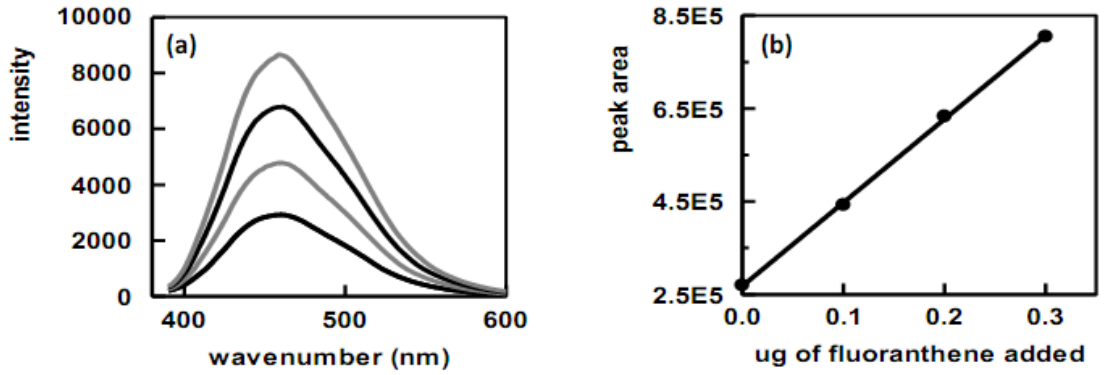

Figure 4.3-8. (a) Fluorescence spectra obtained by spiking the first acetonitrile extract (Figure4.3-7c) with known amounts of fluoranthene, (b) plot of fluoranthene peak area as a function of fluoranthene added to the sample.

The first acetonitrile extract was then spiked with known amounts of fluoranthene. The resultant fluorescence spectra are shown in Figure 4.3-8a. A plot of fluoranthene peak area as a function of micrograms of fluoranthene added to the sample is shown in Figure 4.3-8b. The plot is linear. Back extrapolation was used to determine the amount of fluoranthene in the first acetonitrile extract. We repeated this process for the second and third acetonitrile extracts. The amounts of fluoranthene in the three acetonitrile extracts are summarized in Table 4.3-1. The total amount of fluoranthene agrees reasonably well with the 0.188 ±0.019 µg taken up by the capture matrices from the aqueous solution.

Table 4.3-1. Summary of the fluoranthene extractions where C.M. is capture matrices. The uncertainty in the measurements is estimated to be 10%.

ppb Fluoranthene in Water	µg of Fluoranthene in 5-mL Aqueous Sample	% of Fluoranthene Extracted by C_{18} C.M.	µg of Fluoranthene Extracted by C_{18} C.M.	µg of Fluoranthene Eluted off C_{18} C.M. into ACN	
50	0.25	75.1	0.188 ± 0.019	**1st**	0.1496
				2nd	0.0030
				3rd	0.0001
				total	0.153 ± 0.015
5	0.025	88.7	0.0222 ± 0.0022	**1st**	0.0206
				2nd	0.0003
				3rd	0.0000
				total	0.0209 ± 0.0021
0.5	0.0025	cannot determine	cannot determine	**1st**	0.0028
				2nd	0.0000
				3rd	0.0000
				total	0.0028 ± 0.0003

The procedure summarized in Figure 4.3-6 was then applied to a 5-ppb solution of fluoranthene in water. Figure 4.3-9a shows the spectra before (blue) and after (red) vortexing. A fluorescence peak for fluoranthene is not apparent in the before spectrum. Figure 4.3-9b shows the spectra obtained after subtracting the spectral contributions of water. Comparing the peak areas before and after vortexing, the capture matrices extracted 88.7%, or 0.0222 ±0.0022 µg of fluoranthene.

Three acetonitrile extractions of the capture matrices were then completed, and the extracts were spiked with known amounts of fluoranthene. The results are summarized in Figure 4.3-10 and Table 4.3-1.

Figure 4.3-11 shows the results of following those steps for a 5-mL sample containing 500-pptr fluoranthene in water. This sample contains 0.0025 µg of fluoranthene. Figure 4.3-11a shows the fluorescence spectra obtained for a 5-mL aqueous solution before and after vortexing the sample with 50 µL of C_{18} capture matrices. There was no observable difference between the two spectra, indicating that we were below the instrument's detection limit.

We then used a magnet to separate the aqueous solution from the capture matrices. The water was removed and 1 mL of acetonitrile was added. After vortexing for 10 min, a magnet was used to separate the capture matrices from the acetonitrile. The sample was placed in a quartz cuvette and the fluorescence was measured. This procedure was repeated two more times. The resultant fluorescence spectra for the three acetonitrile extractions are shown in Figure 4.3-11b. For the first acetonitrile extraction, we observed a fluorescence peak caused by fluoranthene. No such peak was observed for the second and third extractions, indicating that all the fluoranthene taken up by the C_{18} capture

matrices had been released in the first extraction. The fluorescence spectra obtained for the second and third extractions were similar to that of neat acetonitrile.

The first acetonitrile extract was then spiked with known amounts of fluoranthene. The resultant fluorescence spectra are shown in Figure 4.3-11c. A plot of fluoranthene peak area as function of micrograms of fluoranthene added to the sample is shown in Figure 4.3-11d. The plot is linear. Back extrapolation determined that the amount of fluoranthene in the original 5 mL of aqueous sample was 0.0028 µg, which is in good agreement with the expected amount of 0.0025 µg.

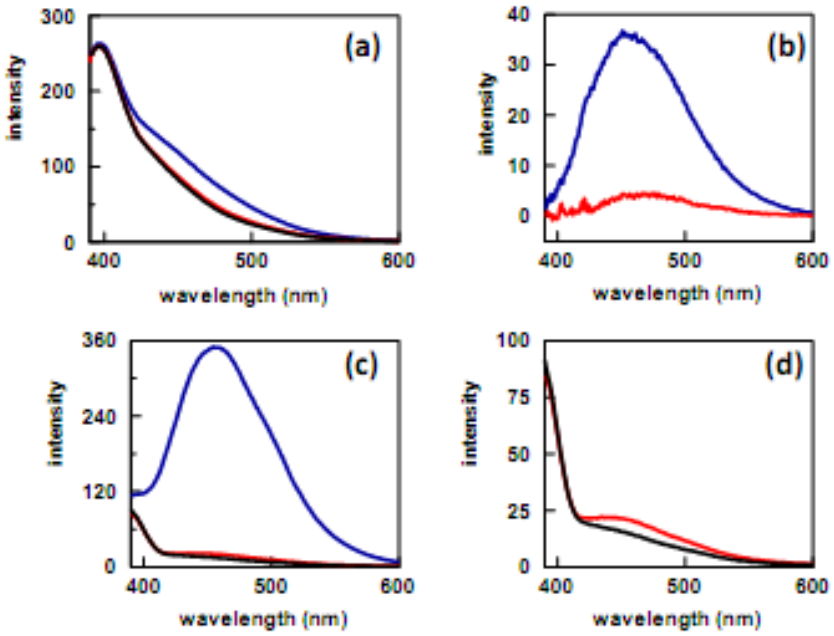

Figure 4.3-9. (a) Fluorescence spectra of deionized water and 5-ppb fluoranthene before (blue) and after (red) vortexing for 10 min with 50 µL of C_{18} capture matrices; (b) same spectra as (a) but with the spectral contributions of water subtracted out; (c) fluorescence spectra of acetonitrile and fluoranthene in acetonitrile after the first (blue), second (red), and third (black) extractions; (d) fluorescence spectra of acetonitrile and fluoranthene in acetonitrile after the second (red) and third (black) extractions.

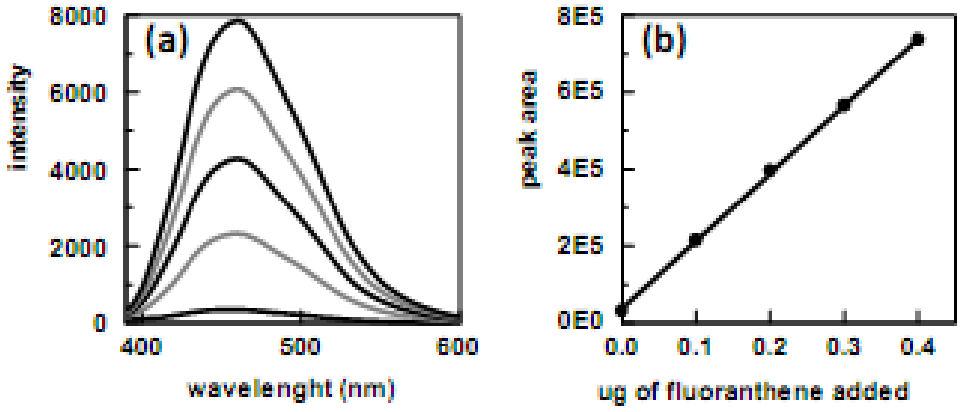

Figure 4.3-10. (a) Fluorescence spectra obtained by spiking the first acetonitrile extract (Figure 4.3-9c) with known amounts of fluoranthene, (b) plot of fluoranthene peak area as a function of fluoranthene added to the sample.

4.3.4 Other PAHs

We explored the use of C_{18} capture matrices to extract other PAHs. The results are summarized in Table 4.3-2. Each aqueous PAH sample was vortexed for 20 min. Fluorescence measurements were taken of the water after vortexing for 10 and 20 min. The table shows that the C_{18} capture matrices are more efficient in extracting the higher molecular weight PAHs. We expected this result, as these PAHs are also more lipophilic.

After 20 min of vortexing, we then used a magnet to separate the aqueous solution from the capture matrices. The water was removed and 1 mL of acetonitrile was added. This sample was vortexed for 10 min. A magnet was used to separate the capture matrices from the acetonitrile. We placed an acetonitrile in a cuvette and measured the fluorescence. This process was repeated two more times. The results are summarized in Table 4.3-2. The results show that more of the PAHs are eluted off the C_{18} capture matrices during the first acetonitrile extraction.

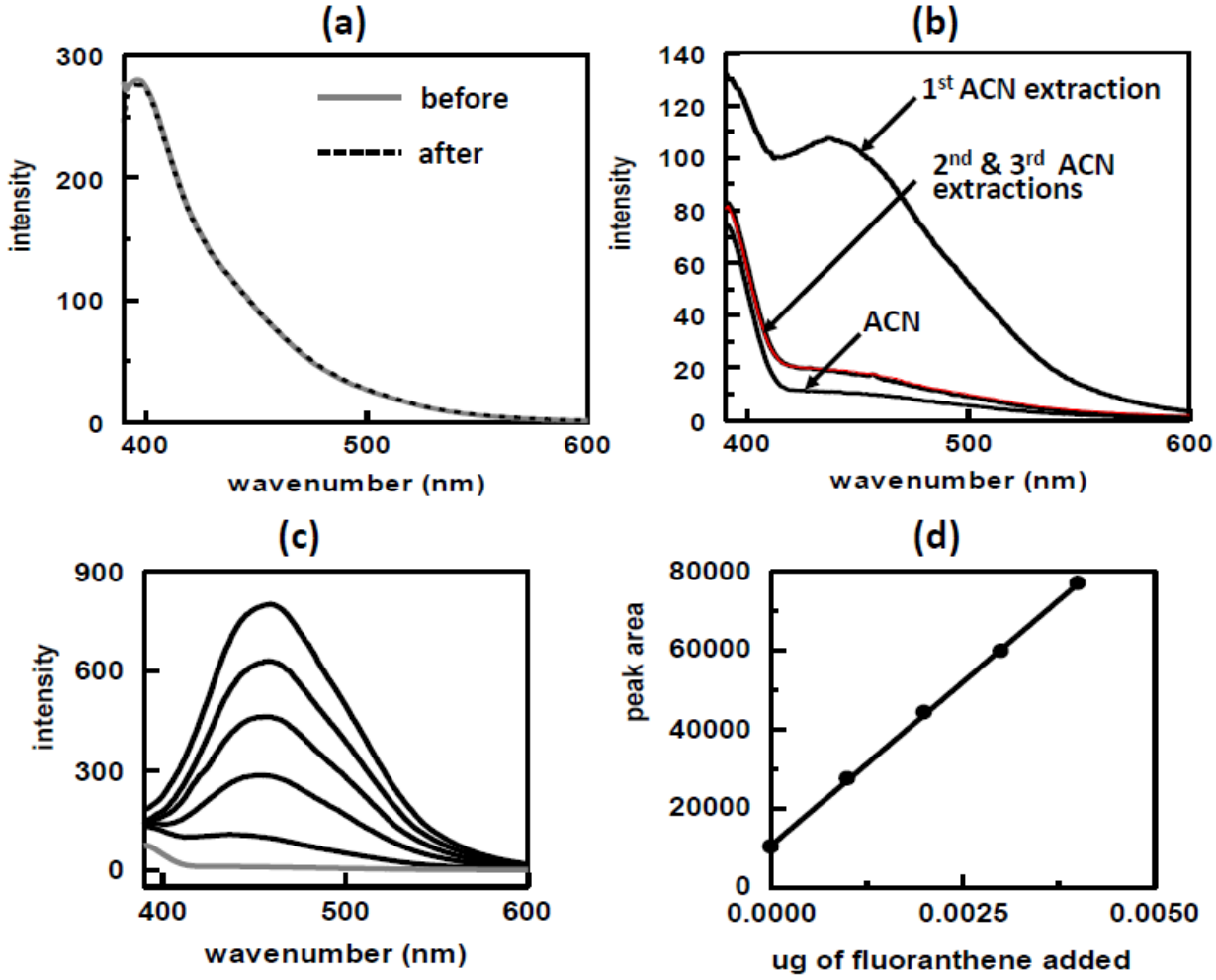

Figure 4.3-11. (a) Fluorescence spectra obtained for 500-pptr fluoranthene in water before and after vortexing with C_{18} capture matrices for 10 min, (b) fluorescence spectra obtained for the three acetonitrile extractions and neat acetonitrile, (c) fluorescence spectra obtained for neat acetonitrile (gray line) and the first acetonitrile extract before and after spiking the sample with known amounts of fluoranthene (black lines), (d) plot of fluoranthene peak area as a function of micrograms of fluoranthene added to the first acetonitrile extract.

Table 4.3-2. Summary of C_{18} capture matrices extractions of PAHs where C.M. is capture matrices, ACN is acetonitrile, and ND is not done.

PAH	Sample Concentration (ng/L)	λ_{EX} (nm)	λ_{EM} (nm)	% Extracted by C_{18} C.M. from Water		% Eluted off C_{18} C.M. into ACN	
Naphthalene	50	275	300-500	1st	15.0	1st	100
				2nd	26.4	2nd	0
						3rd	0
2-methyl Naphthalene	50	275	300-500	1st	10.8	1st	100
				2nd	19.8	2nd	0
						3rd	ND
Acenaphthalene	50	275	300-500	1st	18.6	1st	93.2
				2nd	24.1	2nd	3.8
						3rd	3
Anthracene	45	253	360-490	1st	25.7	1st	89.5
				2nd	25.2	2nd	6.2
						3rd	4.3
Pyrene	50	320	340-500	1st	63.7	1st	98.1
				2nd	66.2	2nd	1.9
						3rd	0
Fluoranthene (C_{18} C.M. prepared 5/30/13)	50	350	385-600	1st	75.1	1st	97.2
				2nd	ND	2nd	2.0
						3rd	0.8
Fluoranthene (C_{18} C.M. prepared 1/15/14)	50	350	385-600	1st	82.7	1st	96.3
				2nd	78	2nd	2.3
						3rd	1.4

4.4 DESIGN OF A PORTABLE SPECTROFLUOROMETER FOR FIELD USE

For use in the field, a spectrofluorometer must be inexpensive, compact, and robust, with very few moving parts. Figure 4.4-1 shows the basic components of a spectrofluorometer for use in the field. It is composed of a light source and a detector. We used a fiber-optic probe to deliver the light excitation to the sample and to collect and transmit the fluorescence emissions to the detector. The optical components and the sources of those components of the spectrofluorometer are summarized in Table 4.4-1.

The excitation source was a fiber-coupled, 275-nm ultraviolet (UV) LED light source. Figure 4.4-2 shows the LED, the LED driver, and the spectral response of the UV LEDs from Mightex Systems.[7] The fiber-optic probe used to deliver the excitation light to the sample is shown in Figure 4.4-3.[8] One end of the probe connects to the LED light source and the other end to the detector.

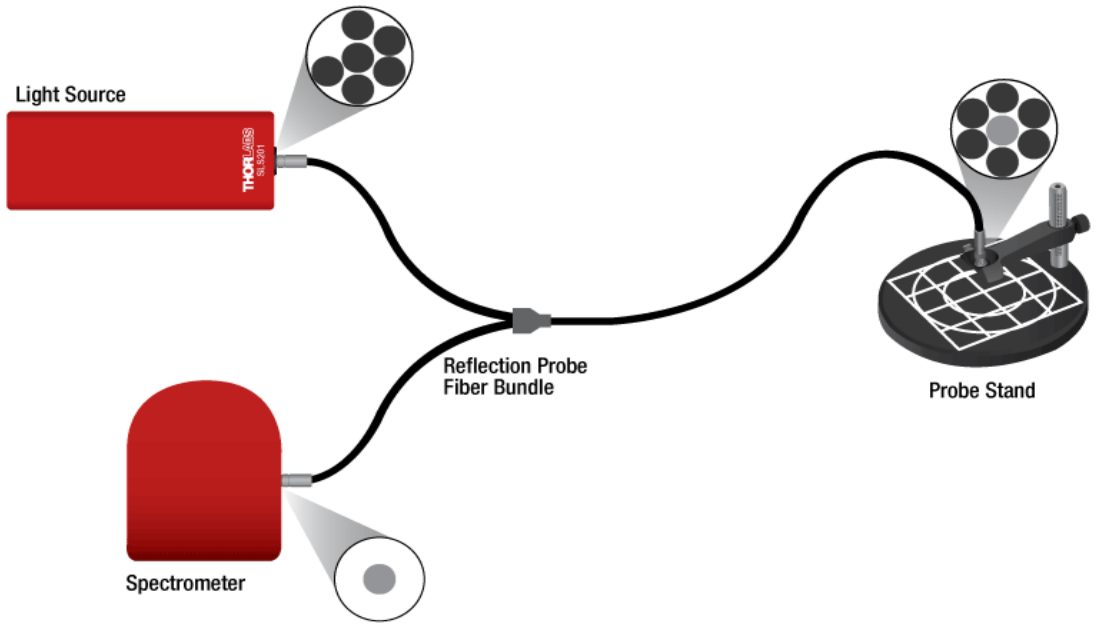

Figure 4.4-1. Schematic showing the basic components of a spectrofluorometer.

Table 4.4-1. Summary of components for a field-deployable spectrofluorometer.

Component Description	Source	Part Number
High-power, fiber-coupled LED light source, 275-nm UV	Mightex Systems	FCS-0275-000
Two-channel LED driver with manual and analog-input controls, maximum. Current: 100 mA	Mightex Systems	SLA-0100-2
Reflection probe, 200 µm, high-OH (250 to 1200 nm), SMA connectors, 2-m Long	Thorlabs Inc.	RP20
Broadband Multialkali amplified photomultiplier (PMT), 280 to 630 nm; includes retaining ring, interface connector cable, power supply, and thread adapter	Thorlabs Inc.	PMM01
SMA fiber adapter plate with external SM1 (1.035"-40) thread	Thorlabs Inc.	SM1SMA
200- to1000-nm CCD spectrometer	Thorlabs Inc.	CCS200
> 85% 308- to 420-nm longpass filter	Semrock	FF01-300/LP-25

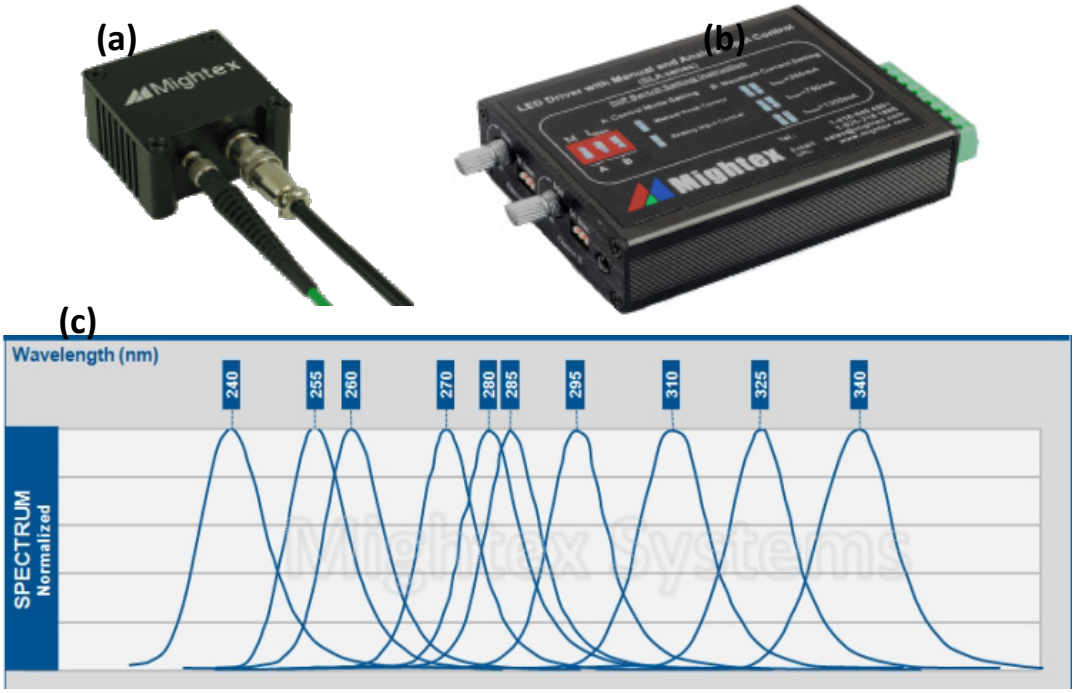

Figure 4.4-2. (a) Fiber-optic coupled LED excitation source, (b) two-channel LED driver, (c) spectral response of Mightex Systems UV LEDs.

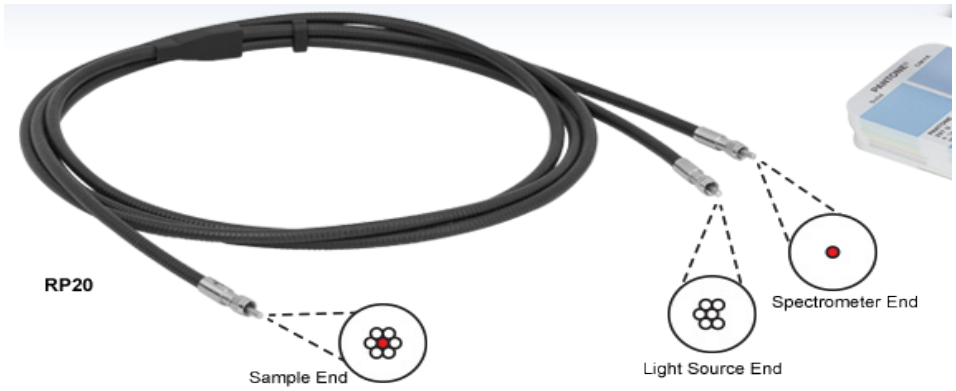

Figure 4.4-3. Fiber-optic probe used to deliver the excitation light to the sample and transmit the fluorescence emissions to the detector.

One of two kinds of detectors can be used. One is a PMT, as shown in Figure 4.4-4a.[8] The sensitivity of the PMM01and PMM02 PMTs are shown in Figure 4.4-4b. PMT PMM01 shows greater sensitivity between 290 to 600 nm than PMT PMM02. Table 4.3-2 shows that the PAHs fluoresce in the spectral window between 300 to 600 nm. Consequently, PMT PMM01 is the better detector to use. With a PMT, no spectral information is provided, just total counts. Consequently, there is no speciation and the output is proportional to the total PAHs. If speciation is desired, a portable CCD spectrometer can be used, Figure 4.4-4c. Regardless of which detector is used, a long-pass filter between the sample and the detector is needed to block the excitation source while

allowing the fluorescence emissions to enter the detector. Figure 4.4-5 shows the spectral response of an appropriate long-pass filter.[9]

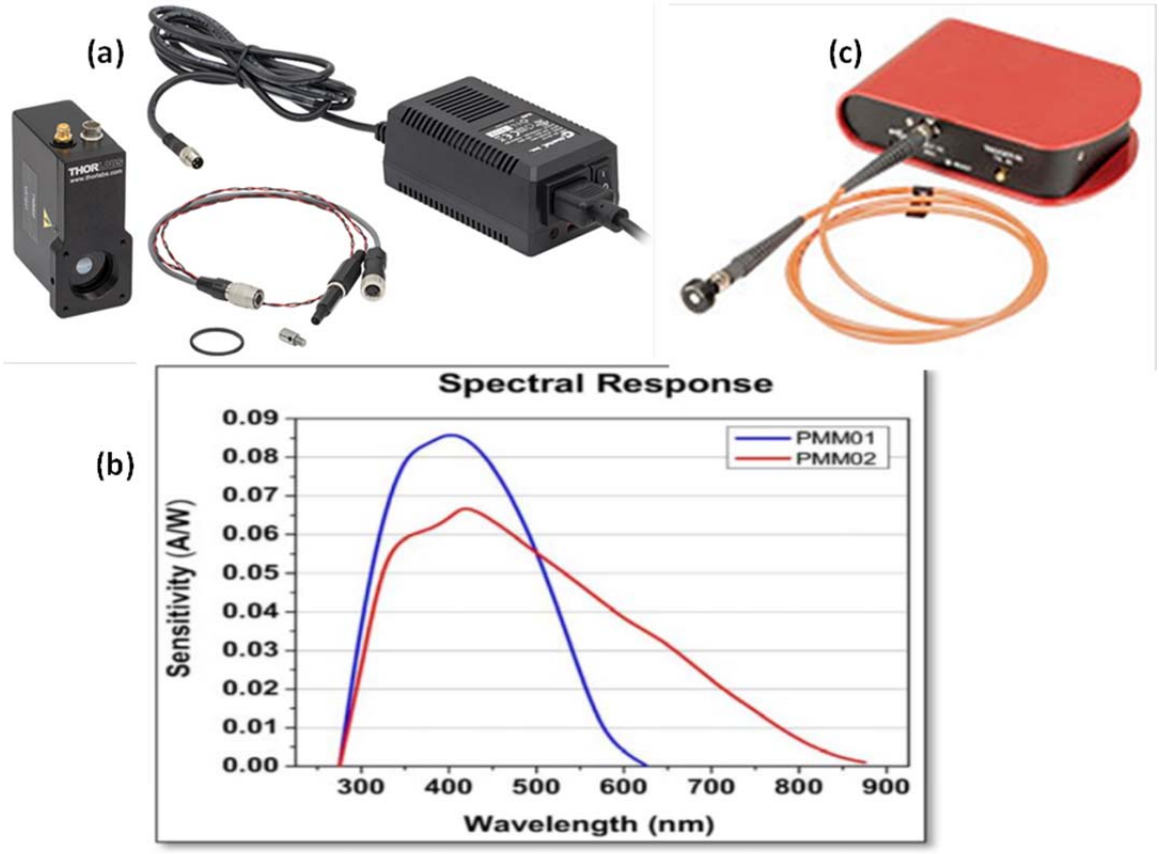

Figure 4.4-4. (a) PMT, (b) sensitivity of the PMM01 and PMM02 PMTs as a function of wavelength, (c) a portable CCD spectrometer.

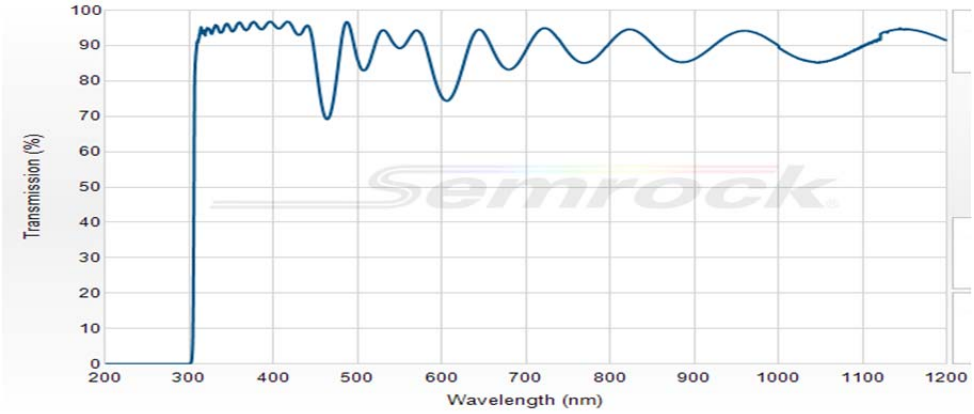

Figure 4.4-5. Transmission curve of a longpass filter for detecting PAHs.

4.5 REFERENCES

1. http://www.dionex.com/en-us/webdocs/4449-AN95_LPN0570.pdf

2. W. Kanchanamayoon and N. Tatrahun. 2008. "Determination of Polycyclic Aromatic Hydrocarbons in Water Samples by Solid Phase Extraction and Gas Chromatography," *World Journal of Chemistry* *3*:51–54.

3. M. R. Shishehbore, A. Afkhami, and H. Bagheri. 2011. "Salicylic Acid Functionalized Silica-coated Magnetite Nanoparticles for Solid Phase Extraction and Preconcentration pf Some Heavy Metal Ions from Various Real Samples," *Chemistry Central Journal* *5*:41–50.

4. I. Šafařik and M. Šafařikova. 2002. "Detection of Low Concentrations of Malachite Green and Crystal Violet in Water**,"** *Water Research* *36*:196–200.

5. F. P. Schwarz and S. P. Wasik. 1976. "Fluorescence Measurements of Benzene, Naphthalene, Anthracene, Pyrene, Fluoranthene, and Benzo[E]Pyrene In Water," *Analytical Chemistry* *48*:524–528.

6. http://www.chroma.com

7. http://www.mightexsystems.com

8. http://www.thorlabs.us/index.cfm

9. http://www.semrock.com/

5. BARE Au CAPTURE MATRICES FOR THE DETECTION OF TNT, DNT, AND RDX BY SERS

5.1 INTRODUCTION

Hatab, Eres, Hatzinger, and Gu[1] showed that RDX could be detected by SERS using bare Au colloidal particles. Figure 5.1-1a shows SERS spectra obtained for aqueous samples containing RDX. They used the standard addition method to determine the amount of RDX present in the sample, Figure 5.1-1b. Besides RDX, bare Ag and Au colloidal particles can be used to detect TNT[2] and 2,4-DNT.[3] SERS spectra for TNT and 2,4-DNT are shown in Figure 5.1-2. These materials adsorb onto the Ag/Au surfaces through their nitro groups.

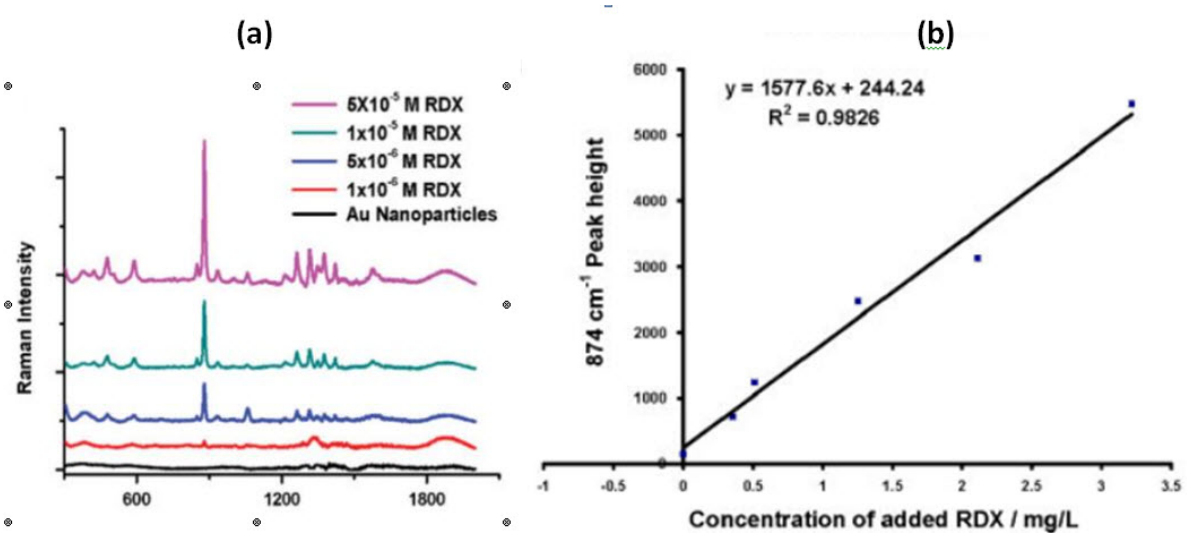

Figure 5.1-1. (a) SERS spectra of RDX at concentrations ranging from 1 x 10^{-6} to 1 x 10^{-5} M., (b) standard addition curve for determining the RDX concentration in groundwater.[1]

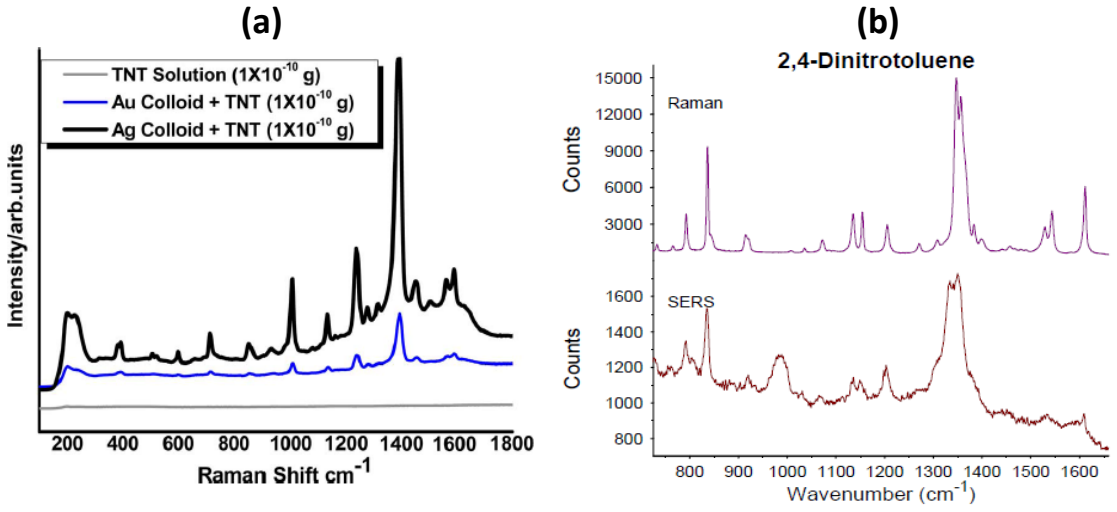

Figure 5.1-2. (a) SERS spectra of TNT on Ag and Au colloids,[2] (b) normal Raman and SERS spectra of 2,4-DNT.[3] SERS substrate is roughened gold.

5.1.1 Brief Description of Detection Scheme

In this detection method, a suspension of bare Au capture matrices and the sample to be analyzed are injected into a mixer that has folded flow mixing to increase capture efficiency (mixers are discussed in Section 9). Once mixed, the sample/capture matrices suspension goes into a flow-through cell where a magnet pulls the capture matrices down onto an optical surface. A Raman spectrometer, operating at 785-nm excitation, measures the SERS response of the TNT/DNT/RDX adsorbed on the capture matrices. The advantage of this detection method is that the TNT/DNT/RDX does not need to be eluted off the capture matrices prior to detection.

5.2 SYNTHESIS OF BARE Au CAPTURE MATRICES

5.2.1 Reagents

Hydrogen tetrachloroaurate (III) trihydrate (Aldrich), sodium citrate (Aldrich), and water (HPLC grade, Aldrich), were used as received.

A 0.5-mL aliquot of 5-μm-diameter, amine-terminated, silica-coated iron oxide microparticles (Bioclone, part number FA-104) was washed 10 times with 1-mL aliquots of HPLC water to remove surfactant. Between washes, we used a NdFeB magnet to separate the magnetic microparticles from the water. After the washes, the volume of the amine terminated and the magnetic microparticles adjusted to 1.0 mL with water.

5.2.2 Preparation of Gold Colloid

An aqueous solution of 100 mL of 0.01% (g/mL) of hydrogen tetrachloroaurate (III) trihydrate was brought to a vigorous boil in a 250-mL round-bottom flask equipped with a condenser. Once boiling, we added 0.85 mL of 1 % sodium citrate. After 40 min of refluxing, the solution had changed from a light yellow color to red-violet. We removed the flask from the heat and allowed it to cool to room temperature. The colloidal suspension was then concentrated by centrifugation to a final volume of ~ 2 mL.

5.2.3 Preparation of Bare Au Capture Matrices

A 100-μL aliquot of the washed, amine-terminated, magnetic microparticles was pippetted into a glass vial containing 1 ml of water (HPLC grade, Aldrich). A 200-μL aliquot of the concentrated gold colloidal suspension was added to the glass vial and the vial was placed on a roller. The amine groups of the magnetic microparticles bind to the gold colloidal particles. After rolling for 2 h, we used a NdFeB magnet to separate the microparticles from the liquid. If the liquid was clear, half the volume was removed and another 200-μL aliquot of the concentrated gold colloidal suspension was added to the glass vial and placed on the roller. The process was repeated until the surface of the magnetic microparticles was completely covered with colloidal gold particles, as indicated when the liquid remained red-violet in color. The gold-covered magnetic microparticles were then washed three times with water (HPLC grade, Aldrich). The volume of the Au capture matrices was adjusted to 1 mL using water. We refrigerated the capture matrices between uses.

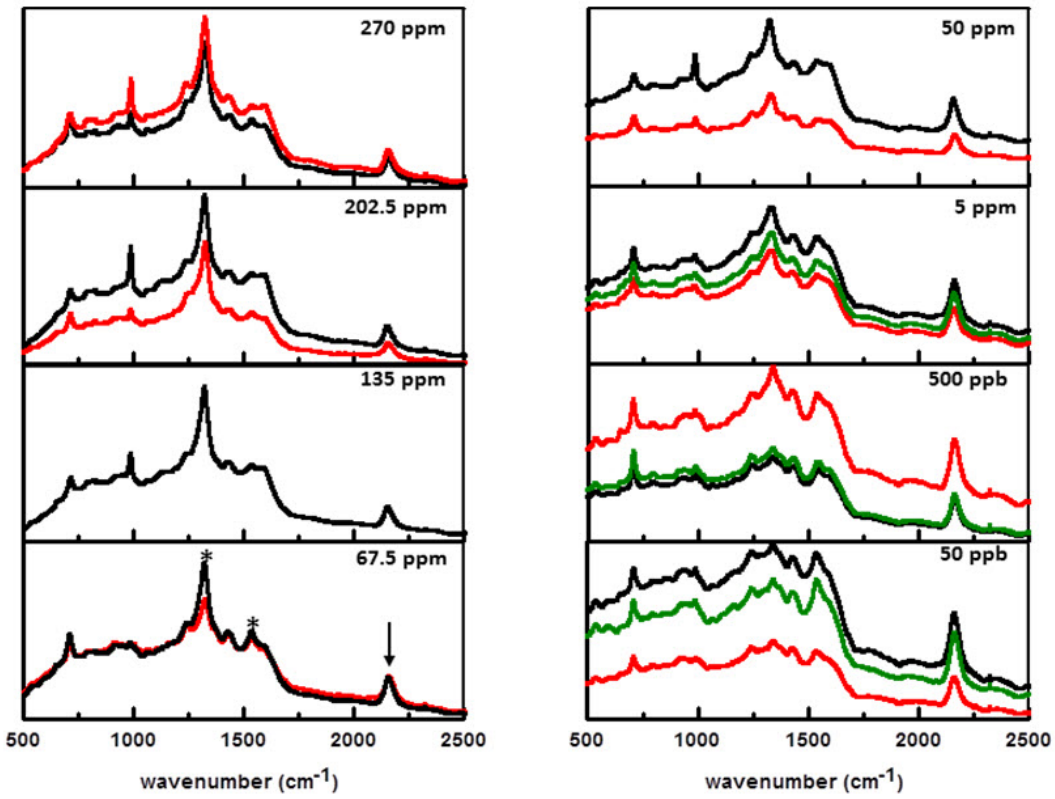

Figure 5.3-1 SERS spectra obtained for bare Au capture matrices exposed to varying concentrations of 2,4-DNT. Spectra were obtained using 785-nm laser excitation.

5.3 BARE Au CAPTURE MATRICES AND 2,4-DNT

Aqueous samples of 2,4-DNT were prepared with 2,4-DNT concentrations between 50 ppb and 270 ppm. We added 50-µL aliquots of the bare Au capture matrices to 1-mL volumes of these samples. We allowed the samples to equilibrate overnight. Afterwards, a pipette was used to transfer the capture matrices and solution to a cell with an Au foil optical surface. We used a NdFeB magnet on the other side of the Au foil to concentrate the capture matrices in a single spot. The spectra are shown in Figure 5.3-1. Multiple spectra were obtained for most of the concentrations of 2,4-DNT. The spectra obtained for each concentration was reproducible. We noticed that as the concentration of 2,4-DNT decreased, the intensity of the peak at 2163 cm^{-1} (indicated by an arrow in the 67.5-ppm 2,4-DNT spectra in Figure 5.3-1) increased relative to the peaks at 1328 and 1553 cm^{-1} (indicated by asterisks in the same spectra in Figure 5.3-1). We ratioed the intensities of the peaks at 1328 and 1553 cm^{-1} to the 2163 cm^{-1} peak. The results are summarized in Figure 5.3-2. The figure shows that reasonable calibration curves can be obtained by this method.

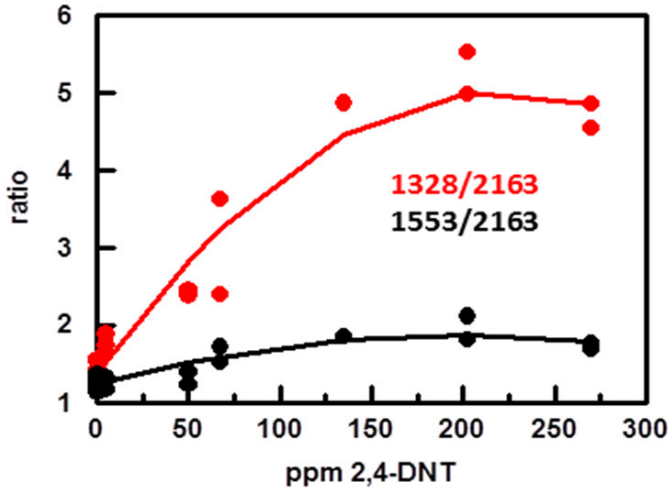

Figure 5.3-2. Calibration curves obtained for 2,4-DNT obtained by ratioing the peaks at 1328 and 1553 cm^{-1} to the 2163 cm^{-1} peak.

5.4 BARE Au CAPTURE MATRICES AND RDX AND TNT

We were unable to obtain samples of either RDX or TNT for testing purposes.

5.5 REFERENCES

1. N. A. Hatab, G. Eres, P .B. Hatzinger, and B. Gu. 2010. "Detection and Analysis of Cyclotrimethylenetriamine (RDX) in Environmental Samples by Surface-enhanced Raman Spectroscopy," *Journal of Raman Spectroscopy 41*:1131–1136.

2. J. I. Jerez-Rozo, O. M. Primera-Pedrozo, M. A. Barreto-Cabán, and S. P. Hernández-Rivera. 2008. "Enhanced Raman Scattering of 2,4,6-TNT Using Metallic Colloids," *IEEE Sensors Journal 8*:974–982.

3. J. M. Sylvia, K. M. Spencer, and J. A. Janni. 2001. "Sniffing Landmines with Surface-Enhanced Raman. Spectroscopy," *Journal of Process Analytical Chemistry 6*:146–147.

6. PREPARATION OF PYRIDINE-DERIVATIZED CAPTURE MATRICES FOR THE DETECTION OF RDX BY FLUORESCENCE

6.1 INTRODUCTION

Andrew and Swager have shown that TMEDA-Zn(H_2Ac)$_2$ photochemically reacts, selectively, with RDX and pentaerythritol tetranitrate (PETN) to form TMEDA-Zn(Ac)$_2$ that fluoresces when excited at 356 nm.[1] Several attempts were made to fabricate the Zn(H_2Ac)$_2$ complex on dimethylaminoethyl-derivatized magnetic microparticles. These microparticles were prepared by reacting dimethylaminoethane-trimethoxysilane with silica magnetic particles. Using the Hitachi spectrofluorometer, we saw no evidence that the dimethylamino groups on the magnetic microparticles had reacted with the zinc and acridine to form the Zn(Ac)$_2$ and Zn(H_2Ac)$_2$ complexes.

Because the TMEDA-Zn(Ac)$_2$ and TMEDA-Zn(H_2Ac)$_2$ complexes exhibit low solubility, we then tried mixing suspensions of the complexes and C_{18} capture matrices in acetonitrile. Again, there was no evidence that the complexes partitioned inside the C_{18} chains of the capture matrices.

Solid phase extraction (SPE) of RDX from aqueous samples was explored by Anspach, Jones, and Kitchens.[2] Resins tested included several styrene-divinylbenzene co-polymers, several acrylic esters, several carbonaceous materials, a polyvinylpyrrolidone, a polyvinylpyrridine, an acrylonitrile divinylbenzene copolymer, a C_{18} reversed-phase silica, an activated carbon, and a reversed-phase cyanopropyl bonded material. Overall, the researchers concluded that resins containing polyvinylpyrrolidone and polyvinylpyrridine generally outperformed the other materials for preconcentration of the nitroaromatics (TNT, DNT) and nitramines (RDX, HMX).

6.1.1 Brief Description of Detection Scheme

Pyridine-derivatized capture matrices are used to extract RDX from the sample. Once extracted, the RDX is eluted off the capture matrices using a smaller volume of acetonitrile. To this solution, the TMEDA-Zn(H_2Ac)$_2$ powdered complex is added. The suspension is irradiated at 313 nm to induce the photochemical reaction between RDX and TMEDA-Zn(H_2Ac)$_2$ to form TMEDA-Zn(HAc^+)$_2$. The fluorescence of the suspension can then be measured. This is essentially the way in which Timothy Swager used this complex to detect RDX and PETN.[1] Figure 6.1-1 shows vials containing suspensions of TMEDA-Zn(H_2Ac)$_2$ powder in a solvent and in a solvent containing TNT, RDX, and PETN. The figure shows that only fluorescence is observed for RDX and PETN.

6.2 PYRIDINE-DERIVATIZED CAPTURE MATRICES

6.2.1 Reagents

We used 2(4-pyridyethyl)triethoxysilane (Gelest™), toluene (Aldrich), and ethanol (HPLC grade, Aldrich) as received. A 0.5-mL aliquot of 5-µm-diameter, silica-modified magnetic microparticles (Bioclone, part no. FF-104) was washed 10 times with 1-mL aliquots of HPLC water to remove surfactant. Between washes, we used a NdFeB magnet to separate the magnetic microparticles from the water.

6.2.2 Synthesis

After the water washes, the microparticles were soaked overnight in 0.1-M HCl solution to remove impurities on the surfaces of the microparticles. A NdFeB magnet was used to separate the microparticles from the HCl solution and the microparticles were washed three times with water. A NdFeB magnet was used to separate the microparticles from the water and a 1:1 solution composed of 50% $H2SO_4$ and 30% $H2O_2$ was added. This step activates the microparticles by increasing the hydroxyl

group concentration on their surfaces. After reacting for 30 min, separate and wash the microparticles three times with water, three times with ethanol, then three times with toluene. If the microparticles are activated, they will not disperse homogeneously in toluene. Add 500 µL of 2(4-pyridyethyl) triethoxysilane and 100 µL of n-butylamine (a transesterification catalyst) to the microparticles. This action will cause the microparticles to disperse homogeneously in toluene. The suspension is then transferred, using toluene, to a 25-mL round-bottom flask and refluxed for ~ 2 h. Afterwards, the microparticles are transferred to a glass microvial and washed three times with ethanol. The volume of the pyridine-derivatized capture matrices was adjusted to 1 mL using ethanol. Capture matrices were refrigerated between uses.

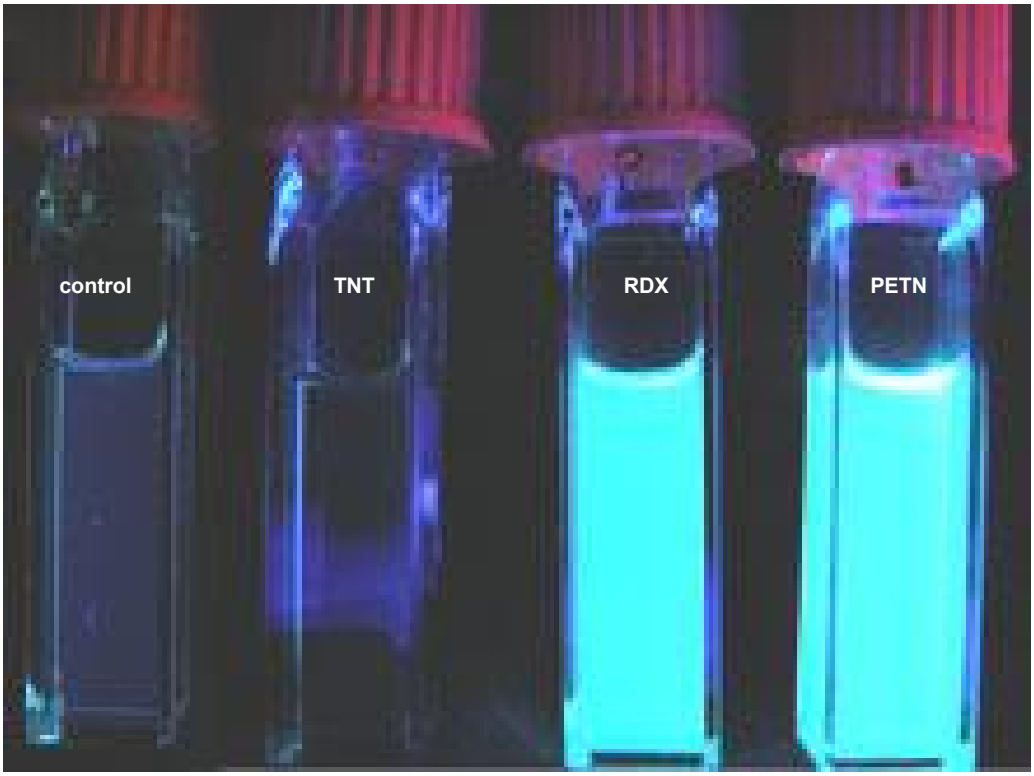

Figure 6.1-1. Vials containing TMEDA-Zn($H_2Ac)_2$ glow only in the presence of two explosives, RDX and PETN, and not in the presence of TNT (second vial from the right). The vial on the far left is a control. All four vials are illuminated with invisible ultraviolet light.[3]

6.3 TMEDA-ZN($H_2AC)_2$

6.3.1 Reagents

We used acridine (Fluka), zinc nitrate hydrate (Aldrich), tetramethylethylenediamine (TMEDA, Aldrich), sodium tetraphenylborate (Aldrich), sodium borohydride (Aldrich), water (HPLC grade, Aldrich), acetonitrile (Aldrich), diethyl ether (Aldrich), and tetrahydrofuran (Aldrich) as received.

6.3.2 Synthesis

Figure 6.3-1 summaries the reaction steps in the synthesis of the TMEDA-Zn($H_2Ac)_2$ complex.[1] First, the TMEDA-Zn$(Ac)_2$ complex needs to be synthesized, Figure 6.3-1a. The apparatus used to do this synthesis is shown in Figure 6.3-2a. All glassware was dried in an oven at ~110 ^{O}C overnight. A four-neck, 50-mL round-bottom flask equipped with two stoppers, a funnel with a stopper, and a condenser were assembled. While argon gas flowed through the apparatus, a heat gun was used to

drive off any water and oxygen adsorbed on the glass. When it had cooled, 0.289 g of zinc nitrate hydrate, 0.835 g of acridine, and 20 mL of ethanol was added to the round-bottom flask through one of the necks of the flask under a positive pressure of argon. Ethanol was added to the funnel to replace any ethanol carried away by the argon during the reaction. The resulting solution in the round-bottom flask was refluxed for 10 min under a positive pressure of argon. When the solution cooled to room temperature, 0.189 g of TMEDA was then added to the round-bottom flask under a positive pressure of argon. The resulting solution was refluxed for 12 h under argon. Ethanol was added periodically to replace that which had been carried away by the flowing argon. After refluxing for 12 h, the assembly was allowed to cool to room temperature. Once cooled, we placed a magnetic stir bar inside the round-bottom flask and placed the assembly on top of a magnetic hot plate. With argon flowing though the assembly, a solution of 1.044-g sodium tetraphenylborate in 6 mL of HPLC water was added dropwise with vigorous stirring. The reaction mixture was stirred for 15 min under argon. Afterwards, the resulting orange solid was filtered onto a 0.1-µm Anodisc™ filter. The solid was washed with cold ethanol, cold water, and then with cold diethyl ether. A photograph of the resultant product is shown in Figure 6.3-3a. The Andrew–Swager[1] synthesis stipulates purification using Soxhlet extraction. A Soxhlet thimble was filled with the product. Soxhlet extraction was done overnight using diethyl ether, Figure 6.3-2b. Acridine is soluble in diethyl ether, but TMEDA-Zn(Ac)2 is not. Afterwards, the material in the thimble was transferred to a beaker. Hot acetonitrile was added to the yellow-orange material. A white residue precipitated out. This material was vacuum-filtered out using a 0.1-µm Whatman™ Anodisc™ filter. The filtrate was placed in a beaker. When cold water was added to the beaker, yellow-orange crystals precipitated out. These crystals were collected by filtering through a fluted filter paper. The crystals were allowed to air-dry. A photograph of the crystals is shown in Figure 6.3-3b. The researchers found that Soxhlet extraction was unnecessary. The same results were obtained by adding ~ 20-mL acetonitrile to the yellow-orange product, Figure 6.3-3a. The white residue that formed was filtered off and 80 mL of cold water was added to the filtrate. The resultant yellow-orange, flakey crystals, Figure 6.3-3b, were isolated by filtering through a fluted filter paper.

Figure 6.3-1b summaries the reaction steps to synthesize TMEDA-Zn$(H_2Ac)_2$. In this process, 0.1 g of TMEDA-Zn$(Ac)_2$ was weighed into a 50-mL, four-neck flask, Figure 6.3-2c. Under positive pressure of argon, 15 mL of THF and 15 mL of water was added to the flask. The flask and its contents were then placed in an ice bath. Once cooled, 0.185 g of sodium borohydride was added to the solution in small portions over a 30-min period. The reaction flask was taken out of the ice bath. A magnetic stir bar was added to the flask and the apparatus was placed on a magnetic hot plate. With argon flowing through the apparatus, the reaction was stirred for 1 h at room temperature. The resulting white solid was vacuum-filtered onto a 0.02-µm Whatman™ Anodisc™ filter, Figure 6.3-3c, and washed with copious amounts of water.

Some of the yellow-orange crystals shown in Figure 6.3-3b were dissolved in acetonitrile. Figure 6.3-4a shows the fluorescence spectrum obtained for this solution using excitation at 356 nm. This spectrum matches the one for TMEDA-Zn$(Ac)_2$ reported by Andrew and Swager.[1] The white solid exhibits limited solubility in acetonitrile, pyridine, DMF, and DMSO. A suspension of the white solid in acetonitrile was prepared. Figure 6.3-4a shows the fluorescence spectrum obtained for this suspension using excitation at 316 nm. This spectrum matches the one for TMEDA-Zn$(H2Ac)_2$ reported by Andrew and Swager.[1]

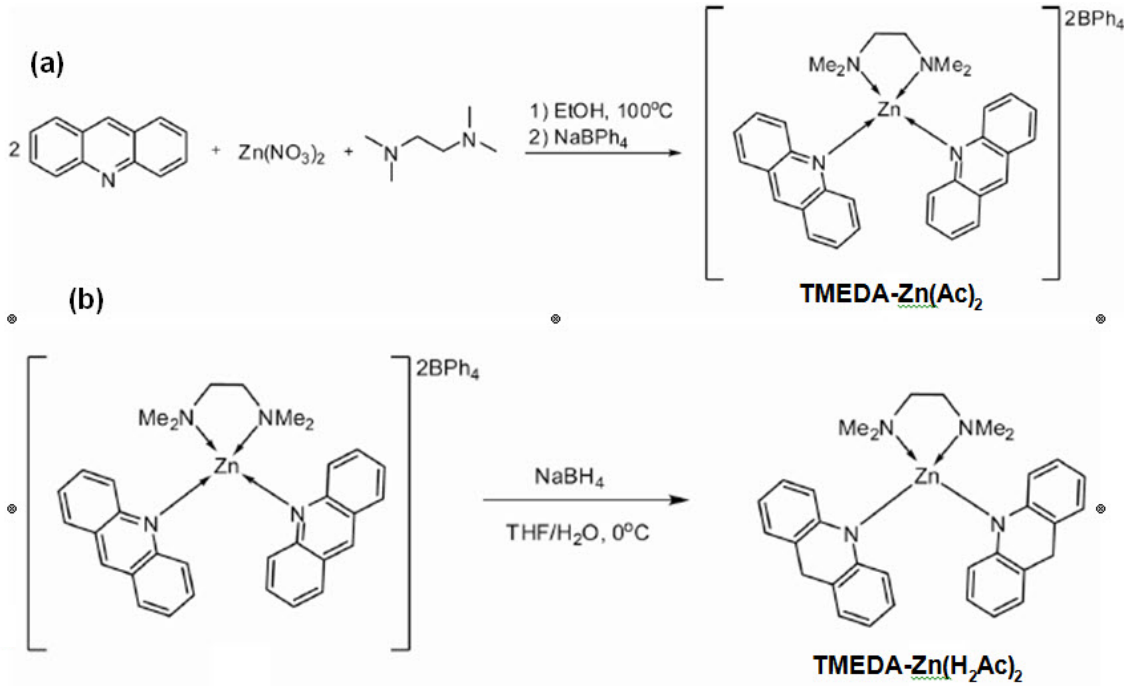

Figure 6.3-1. Summary of synthesis steps to create (a) TMEDA-Zn$(Ac)_2$, and (b) TMEDA-Zn$(H_2Ac)_2$.

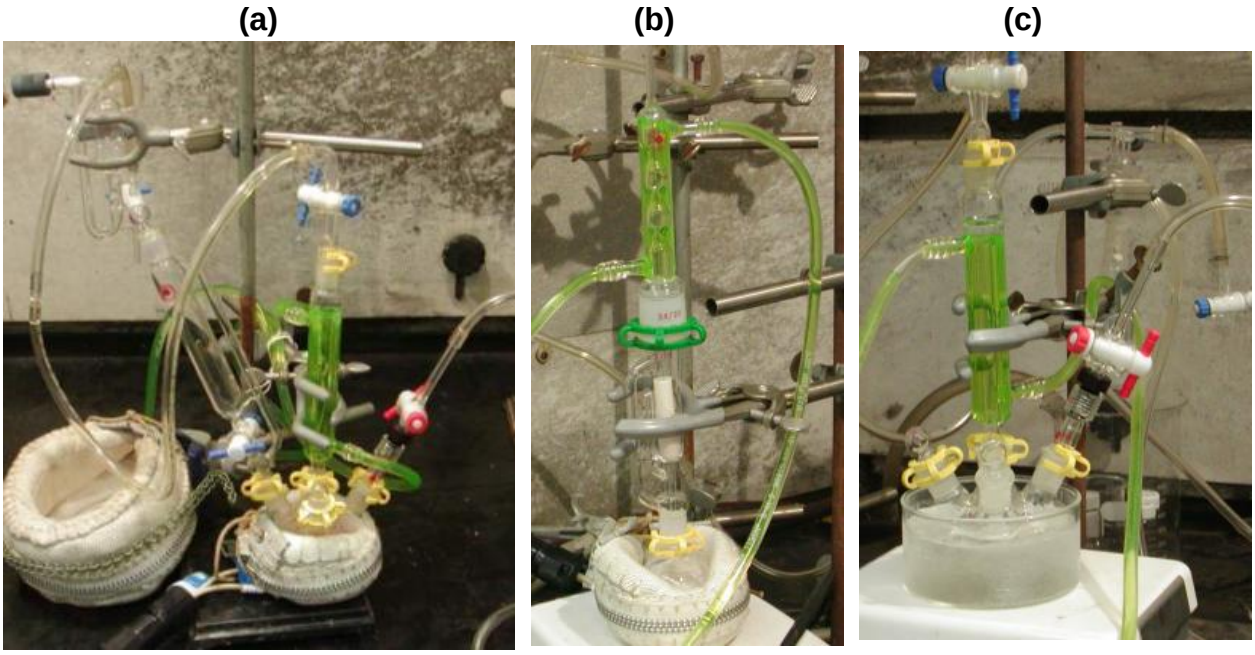

Figure 6.3-2. (a) Reaction apparatus used to synthesize the TMEDA-Zn$(Ac)_2$, (b) Soxhlet extraction apparatus used to purify TMEDA-Zn$(Ac)_2$, (c) reaction apparatus used to synthesize TMEDA-Zn$(H_2Ac)_2$.

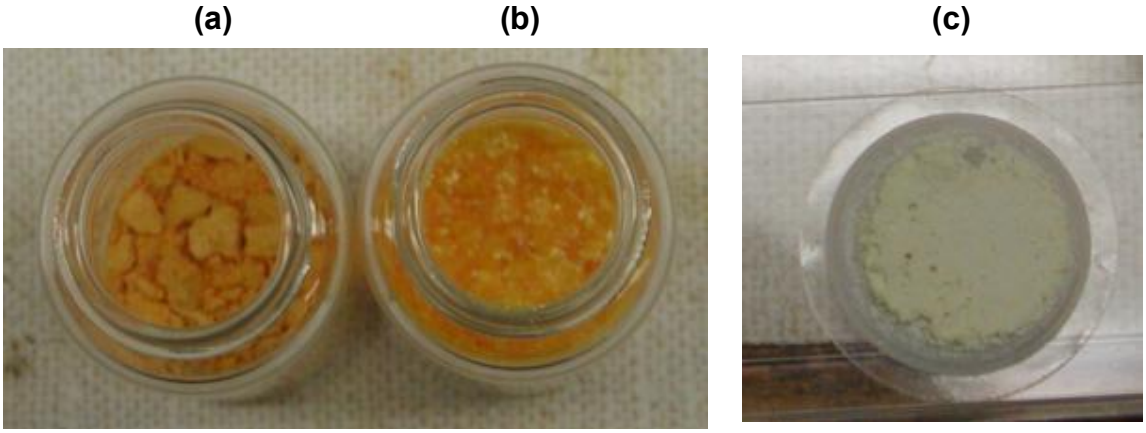

Figure 6.3-3. (a) TMEDA-$Zn(Ac)_2$ isolated after the washings, (b) TMEDA-$Zn(Ac)_2$ isolated after Soxhlet extraction and recrystallization, (c) TMEDA-$Zn(H_2Ac)_2$ isolated after reduction of TMEDA-$Zn(Ac)_2$.

Raman spectra for acridine and the yellow crystals are shown in Figure 6.3-4b. The Raman spectrum for acridine agrees with that reported in the literature.[4] Molecular modeling of TMEDA, acridine, TMEDA-$Zn(Ac)_2$, and TMEDA-$Zn(H_2Ac)_2$ was done using the Hartree–Fock model with the 3-21G basis set. This modeling aided in determining the vibrational modes causing the peaks observed in the Raman spectra. These vibrational modes are summarized in Table 6.3-1. The table shows that the spectral contributions of TMEDA in both complex species is minimal. This is because TMEDA is a weaker Raman scatterer than the acridine and dihydrogen acridine moieties of the complexes. In the Raman spectrum of acridine, we observed a large peak at ~ 1400 cm^{-1}. This large peak is caused by the symmetric A_1 ring vibrational mode. This peak is observed for the yellow crystals, indicating that acridine moieties are present in the sample. The Raman spectrum of the white powder, Figure 6.3-3c, is also shown in Figure 6.3-4b. In this spectrum, the peak caused by the symmetric A_1 ring vibrational mode has disappeared. The Raman spectra also show that, at 785-nm excitation, acridine exhibits a broad fluorescence background. This fluorescence background is suppressed upon formation of the TMEDA-$Zn(Ac)_2$ complex because of the withdrawal of electron density from the acridine moieties by the Zn. This fluorescence background is further suppressed when the acridine moieties of the TMEDA-$Zn(Ac)_2$ complex are reduced to form the TMEDA-$Zn(H_2Ac)_2$ complex. Both the fluorescence and Raman spectra verify that both TMEDA-$Zn(Ac)_2$ and TMEDA-$Zn(H_2Ac)_2$ were successfully synthesized.

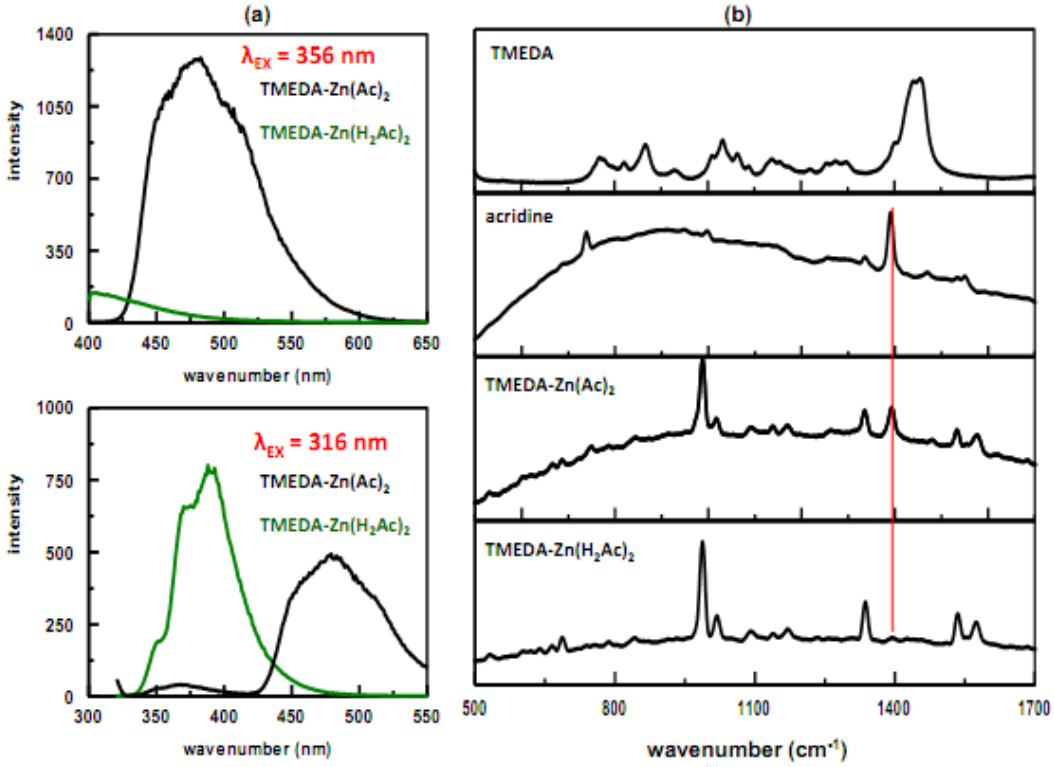

Figure 6.3-4. (a) Fluorescence spectra obtained for TMEDA-$Zn(Ac)_2$ and TMEDA-$Zn(H_2Ac)_2$. (excitation wavelengths are indicated), (b) Raman spectra obtained for TMEDA, acridine, TMEDA-$Zn(Ac)_2$, and TMEDA-$Zn(H_2Ac)_2$. Spectra were obtained using 785-nm laser excitation. Red line indicates the acridine A_1 ring vibrational mode at ~ 1400 cm^{-1}.

Table 6.3-1. Vibrational assignments for TMEDA, acridine, TMEDA-$Zn(Ac)_2$, and TMEDA-$Zn(H_2Ac)_2$, where oop = out of plane, vw = very weak, w = weak, m = moderate, s = strong.

TMEDA	Acridine	TMEDA-$Zn(Ac)_2$	TMEDA-$Zn(H_2Ac)_2$	Assignment
	421 vw	414 vw	423 vw	Symmetric ring stretch
447 vw				CNC bending
499 w				CH_2 rocking
	532 vw	534 w	534 w	CH bending
		582 w		oop C-H bending
		608 w	608 w	Symmetric ring stretch
	643 vw	625 w	625 w	Asymmetric ring stretch
	661 vw	645 w	645 w	Asymmetric ring stretch
	693 w	670 w	670 vw	oop C-H bending
		688 w	688 w	Asymmetric ring stretch
	740 m	723 w	723 vw	Asymmetric ring stretch
		752 vw	744 vw	Asymmetric ring stretch
770 m		772 vw		CH_2 rocking-twisting
		791 vw	791 vw	oop C-H bending
820 m				CH_2 rocking-twisting, CH_2-CN stretch
	850 vw	846 w	844 w	Asymmetric ring stretch
869 m		876 vw	876 vw	C-C stretching
		913 vw	918 vw	oop C-H bending

Table 6.3-1. Continued. Vibrational assignments for TMEDA, acridine, TMEDA-Zn$(Ac)_2$, and TMEDA-Zn$(H_2Ac)_2$ where oop = out of plane, vw = very weak, w = weak, m = moderate, s = strong.

TMEDA	Acridine	TMEDA-Zn$(Ac)_2$	TMEDA-Zn$(H_2Ac)_2$	Assignment
934 w				CNC symmetric stretch
		934 vw	936 vw	oop C-H bending
	952 vw	956 vw		oop C-H bending
	1000 w	988 s	988 s	oop C-H bending
	1005 m			Asymmetric ring stretch
1034 m		1020 m	1020 m	CH_2 rocking-twisting
	1032 w			Asymmetric ring stretch
1065 m				CH_2 rocking-twisting
	1069 vw			Asymmetric ring stretch
1091 w				CH_2 rocking-twisting
	1104 vw	1096 w	1096 w	oop C-H bending
1140 m	1124 vw	1124 vw		CNC asymmetric stretch
	1154 vw	1140 w	1140 w	Asymmetric ring stretch
1157 m				CNC asymmetric Stretch, C-C stretch
1178 m				CH_3 terminal rocking, CH_2 rocking
	1207 vw	1173 w	1173 w	Asymmetric ring stretch
1223 w				CH_3 terminal rocking
1259 w				CH_3 terminal rocking, CH_2 rocking
1262 w				Asymmetric ring stretch
1280 w		1267 w		CH_3 terminal rocking, CH_2 rocking
1304 w		1281 w		CH_3 terminal rocking, CH_2 rocking
	1319 w			Asymmetric ring stretch
	1337 w	1338 m	1338 m	Asymmetric ring stretch
	1392 s	1395 m	1398 vw	Symmetric ring stretch
1445 s		1445 vw		CH_3 terminal rocking, CN stretching
1458 s				CH_2 rocking, CN stretching
	1474 w	1463 w	1463 vw	Asymmetric ring stretch
	1519 vw			Asymmetric ring stretch
	1538 w	1536 m	1536 m	Asymmetric ring stretch
	1553 m	1577 m	1577 m	Asymmetric ring stretch
2834 m				methyl CH stretch
2879 s				Methyl and methylene CH stretch
2937 m				Methyl CH stretch
	3009 w	3010 m	3010 m	C-H stretch
3086 m				Methyl and methylene CH stretch

6.4 TESTING TMEDA-ZN($H_2AC)_2$ WITH A SIMULANT

A sample containing 0.0022 g of 2,4-DNT in 1 mL of acetonitrile was prepared and placed in a quartz cuvette. A suspension containing 0.0038 g of TMEDA-Zn($H_2Ac)_2$ in 1-mL acetronitrile was also prepared. A 50-µL aliquot of this TMEDA-Zn($H_2Ac)_2$ suspension was pipetted into the cuvette containing the 2,4-DNT. We placed the cuvette in the holder, shown schematically in Figures 6.4-1a and b. We then used a Hg lamp (Oriel Corp. Model No. 6047) to irradiate the sample. As shown in Figure 6.4-1c, Hg emits a line at 313 nm. Fluorescence spectra measured as a function of irradiation time are shown in Figure 6.4-2a. The total time the sample was irradiated was 26 min. We observed no change in sample color. As the sample is irradiated, the intensity of the fluorescence peak decreases. We attribute this to the TMEDA-Zn($H_2Ac)_2$ particles in the sample settling out. The normalized spectra are shown in Figure 6.4-2b. The figures show that the normalized spectra completely overlap. These results indicate that 2,4-DNT does not photochemically react with the TMEDA-Zn($H_2Ac)_2$ complex.

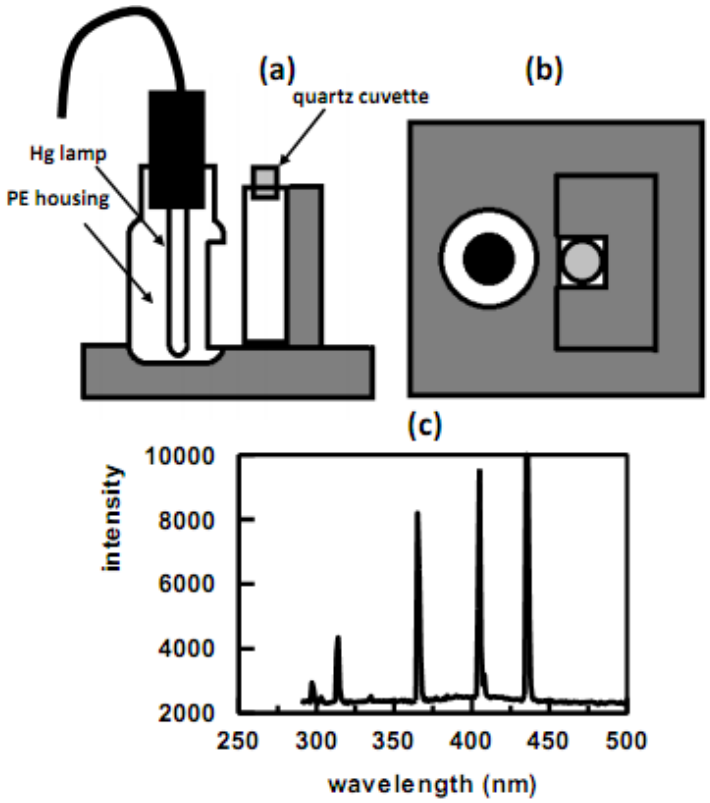

Figure 6.4-1. Schematic of a holder for the Hg lamp and sample cuvette: (a) side view, (b) top view, (c) emission spectrum of a Hg lamp.

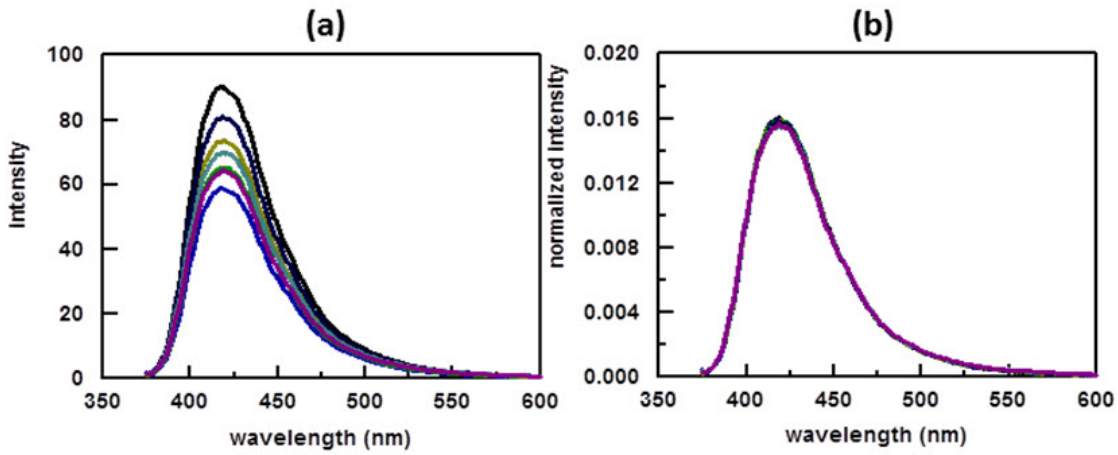

Figure 6.4-2 (a) Fluorescence spectra measured for the 2,4-DNT sample as a function of time where λ_{EX} = 356 nm, scan rate = 60 nm/min, EX slit = 10 nm, and EM slit = 20 nm, and (b) normalized fluorescence spectra in (a).

6.5 TESTING TMEDA-ZN($H_2AC)_2$ WITH RDX

We were unable to obtain samples of either RDX or TNT for testing purposes.

6.6 REFERENCES

1. T. L. Andrew and T. M. Swager. 2007. "A Fluorescence Turn-On Mechanism to Detect High Explosives RDX and PETN," *Journal of the American Chemical Society 129*:7254–7255.

2. G. L. Anspach, W. E. Jones, and J. F. Kitchens. 1992. "Evaluation of Solid Sorbents for Sampling and Analysis of Explosives from Water." USATHAMA Report DRXTH-TE-CR-82142. Aberdeen Proving Ground, MD.

3. http://www.technologyreview.com/news/408010/easier-detection-of-explosives/.

4. S. T. Oh, K. Kim, and M. S. Kim. 1991. "Adsorption and Surface Reaction of Acridine in Silver Sol: Surface-enhanced Raman Spectroscopic Study," *Journal of Physical Chemistry 95* :8844–8849.

7. EDTA CAPTURE MATRICES FOR THE DETECTION OF HEAVY METALS BY SWV

7.1 INTRODUCTION

Rahman, Won, and Shim[1] immobilized EDTA onto a glassy carbon electrode (GCE) by reacting EDTA, in the presence of a catalyst, on a conducting polymer modified electrode. The conducting polymer was formed by electropolymerization of 3',4'-diamino-2,2;5',2"-terthiophene monomer on a GCE. A schematic of this EDTA bonded conducting polymer modified electrode (EDTA-CPME) is shown in Figure 7.1-1a. To detect metal ions, the researchers immersed the EDTA-CPME in a buffered aqueous sample for 10 min with stirring. The EDTA portion of the electrode forms complexes with the metal ions. After accumulation of the metal ions in the preconcentration step, they took the electrode out of the solution and washed it with distilled water. The electrode was then taken to a cell containing a blank solution of sodium acetate/acetic acid buffer. The metal ions complexed on the electrode surface were reduced at -0.9 V for 10 s. The researchers used square wave voltammetry to detect Pb, Cu, and Hg simultaneously. Figure 7.1-1b shows these voltammograms as a function of concentration. The resultant calibration plots are shown in Figure 7.1-1c. The researchers found that the film properties of the electrode changed with time. As a result, these electrodes could only be used for a few days.

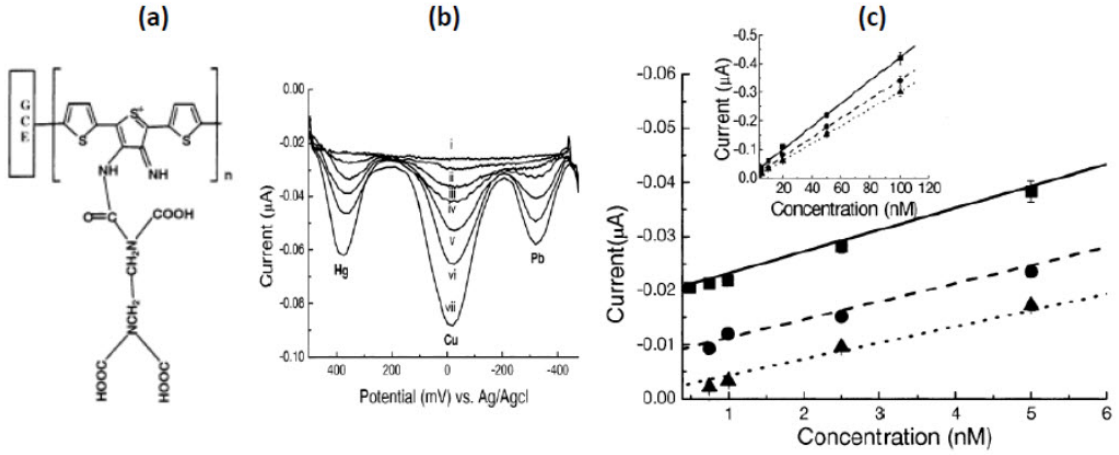

Figure 7.1-1. (a) Schematic of the EDTA-CPME; (b) square wave voltammograms[1] recorded using EDTA-CPME for (i) blank and (ii) 5.0 x 10^{-10}, (iii) 7.5 x 10^{-10}, (iv) 1.0 x 10^{-9}, (v) 2.5 x 10^{-9}, (vi) 5.0 x 10^{-9}, and (vii) 1.0 x 10^{-8} M Pb^{2+}, Cu^{2+}, and Hg^{2+} ions in sodium acetate buffer solution of pH 4.3 (deposition time 10 min at 30 ^{o}C); (b) calibration plots[1] constructed for Cu (solid line), Hg (dashed line), and Pb (dotted line) from square wave voltammetric measurements.

7.1.1 Brief Description of Detection Scheme

In this detection method, a suspension of EDTA-capture matrices and buffered aqueous sample are injected into a mixer that has folded flow mixing to increase capture efficiency (mixers are discussed in Section 9). Once mixed, the sample/capture matrices suspension goes into a chamber housing an Au working electrode. A magnet inside the working electrode concentrates the capture matrices on the gold surface of the electrode. Once concentrated, the electrode and capture matrices are rinsed with distilled water and placed in a blank buffer solution. The metal ions complexed to the EDTA are then reduced. Square wave voltammograms are then measured using a commercial off-the-shelf,

portable potentiostat. The advantage of this method of detection is that the heavy metals do not need to be eluted off the capture matrices prior to detection.

7.2 EDTA-CAPTURE MATRICES

Both 5- and 1-µm-diameter EDTA-modified magnetic microparticles are commercially available (Bioclone, part number FQ-104). They come as dry particles. Before use, some material needs to be suspended in water.

7.3 HARDWARE FOR THE DETECTION

Due to time constraints in the project, we never got to the point of doing any measurements. For instance, it took 6 mos. to acquire a portable potentiostat. However, we did set up the hardware for the measurements, which is discussed below.

7.3.1 Electrochemical Cell

Figure 7.3-1 shows the electrochemical cell that we would have used to perform the voltammetric measurements. This electrochemical cell would be used after the EDTA-derivatized capture matrices had been mixed with sample using the in-line mixer discussed in Section 9. The electrochemical cell houses a Pt counter electrode/bubbler combination, a Ag/AgCl reference electrode, and the Au working electrode. Figure 7.3-2a shows a schematic of the working electrode. An Au foil is wrapped around a glass tube. A Pt wire provides ohmic contact with the Au foil. Heat-shrink tubing holds the Au foil and Pt wire in place. To concentrate the EDTA-derivatized capture matrices onto the surface of the working electrode, a magnet mounted on a support is placed inside the tube. Figure 7.3-2b shows the working electrode that has concentrated capture matrices on its surface. The magnet is mounted on a substrate and can be lowered to the required depth inside the tube of the working electrode.

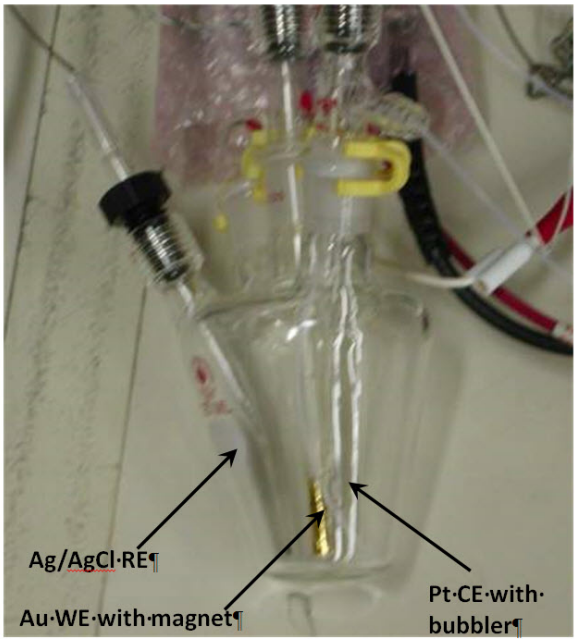

Figure 7.3-1. Electrochemical cell showing the placement of Au working electrode (WE), Ag/AgCl reference electrode (RE), and the Pt counter electrode (CE) with bubbler.

7.4 PORTABLE POTENTIOSTAT

A portable potentiostat is needed to conduct measurements in the field. A survey of portable potentiostats was done and the one chosen was the WaveNow AFTP1 by Pine Research Instrumentation, Figure 7.4-1. The instrument has a voltage range (potentiostat mode) of ±4 volts and current ranges (galvanostat mode) of ±100 mA, ±5 mA, ±200 µA, and ±10 µA. This instrument can perform potential sweep methods such as linear sweep voltammetry, cyclic voltammetry, and staircase voltammetry. It can also perform potential pulse methods such as differential pulse voltammetry and square-wave voltammetry.

7.5 REFERENCES

1. A. Rahman, M.-S. Won, and Y.-B. Shim. 2003. "Characterization of an EDTA Bonded Conducting Polymer Modified Electrode: Its Application for the Simultaneous Determination of Heavy Metal Ions," *Analytical Chemistry* *75*:1123–1129.

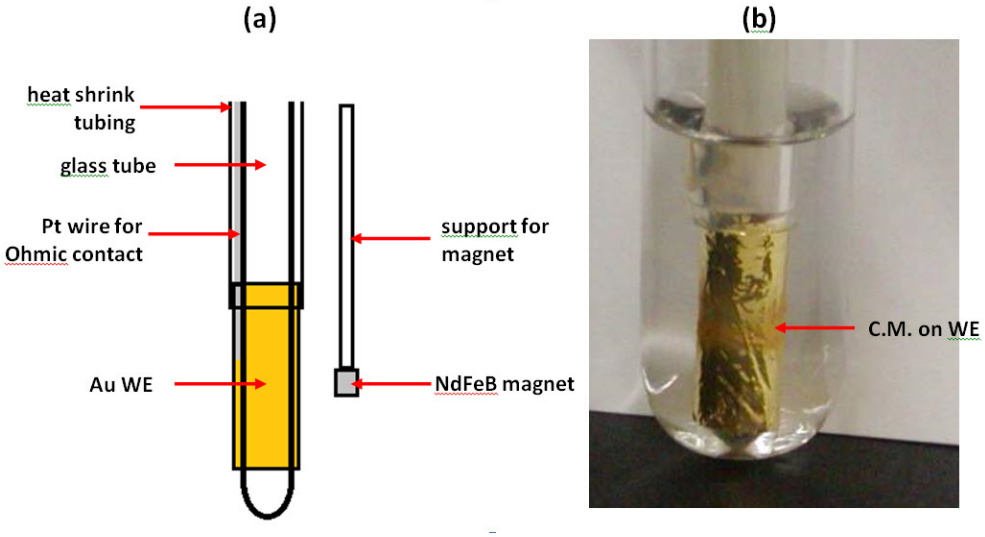

Figure 7.3-2. (a) Schematic of the Au working electrode, (b) Au working electrode. A magnet inside the electrode has concentrated the capture matrices onto its surface.

Figure 7.4-1. Pine Research Instrumentation WaveNow AFTP1 portable potentiostat.

8. SERS-ACTIVE CAPTURE MATRICES FOR THE DETECTION/IDENTIFICATION OF PHARMACEUTICALS

Depending on the chemical nature of the affinity ligands, capture matrices can be used to enhance the detection of toxic industrial chemicals (TICs), explosive materials, chemical warfare agents, as well as pharmaceuticals. In 2005, SPAWAR Systems Center (SSC) San Diego had a Cooperative Research and Development Agreement (CRADA) with Parallax Biosystems, a small San Diego-based company, to explore using SERS-active capture matrices in accessing the efficacy of drugs. Working collaboratively with Parallax Biosystems, SSC San Diego showed that the SERS technique could be used to detect and differentiate nifedipine and midazolam and their derivatives.

Figure 8-1 shows structures of nifedipine and its metabolite. Nifedipine is a calcium channel blocker. This drug is used to treat high blood pressure. It relaxes the blood vessels so that the heart does not have to pump as hard. Nifedipine is also used to treat migraine headaches, Raynaud's syndrome, congestive heart failure, and cardiomyopathgy. It is metabolized by the CYP3A subfamily of enzymes, specifically the cytochrome P450 3A4 system, which is located in both the intestinal mucosa and in the liver. CYP designates a host of enzymes that use iron to oxidize chemical compounds, often as part of the body's strategy to dispose of potentially harmful substances by making them more water-soluble. About 50 CYP enzymes have been identified. As shown in Figure 8-1, the only difference between nifedipine and its metabolite is that the heterocyclic ring of nifedipine is protonated. Currently, speciation of these compounds is done by separation using liquid chromatography (LC) followed by identification using electrospray ionization mass spectrometry (ESI-MS). To demonstrate that SERS could be an inexpensive, less time-consuming alternative to detecting these compounds, Ag/t-BuS derivatized capture matrices were used to concentrate the compounds onto the SERS active surfaces. SERS spectra were obtained and are shown in Figure 8-2. Despite the similarities in structure, the SERS spectra of nifedipine and its metabolite are significantly different. These results clearly indicate that the SERS technique can differentiate between these two species.

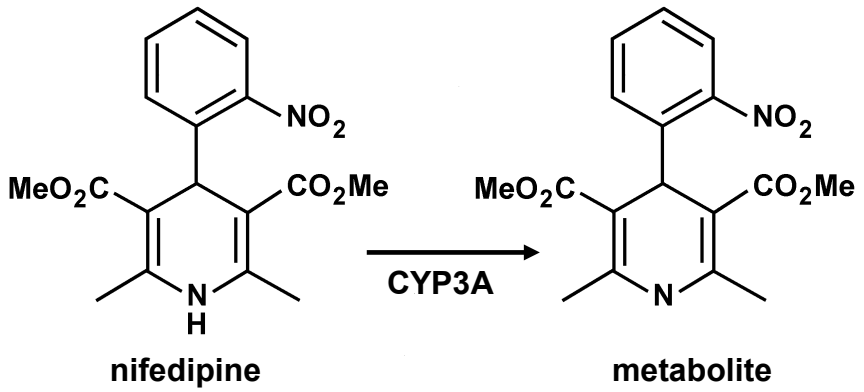

Figure 8-1. Structures of nefedipine and its metabolite.

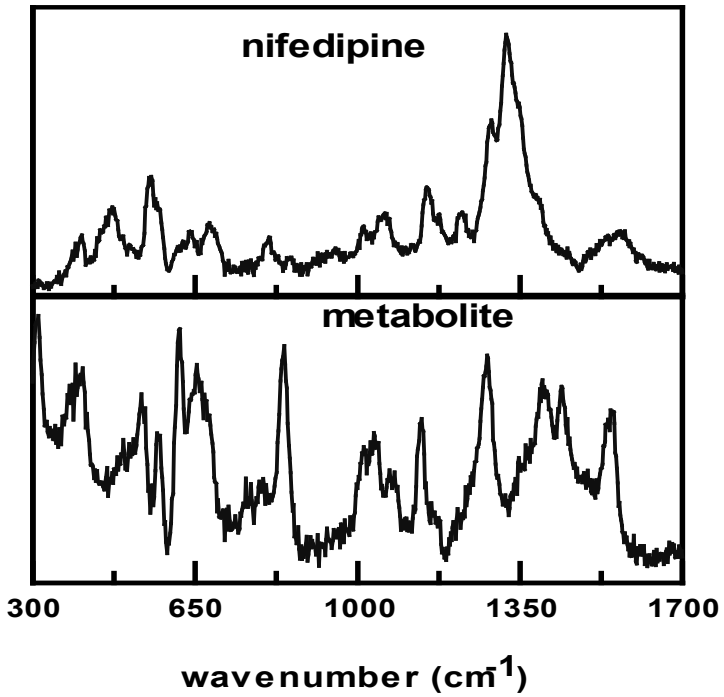

Figure 8-2. SERS spectra of Ag/t-BuS on magnetic microspheres immersed in 200-μM aqueous samples of nifedipine and its metabolite. The spectral contributions of the t-BuS coating were subtracted out.

Additional feasibility studies were done to determine whether or not the SERS technology using capture matrices could be used to differentiate midazolam and its metabolites. The structures of midazolam and its two metabolites are shown in Figure 8-3. The primary metabolite is 1-hydroxymidazolam. Midazolam is a short-lived benzodiazepine central nervous system depressant that is used to induce unconsciousness in a patient before or during surgery to relieve patent anxiety. CYP3A4 is a cytochrome P450 isoform that metabolizes midazolam. As discussed *vide supra*, speciation of these compounds is currently done by separation using liquid LC followed by identification using ESI-MS. Au/t-BuS derivatized magnetic microparticles were used to concentrate the compounds onto the SERS active surfaces. SERS spectra were obtained and are shown in Figure 8-4. Although the differences in the spectra are not as dramatic as was observed for nifedipine and its metabolite, SERS can still be used to differentiate midazolam and its metabolites.

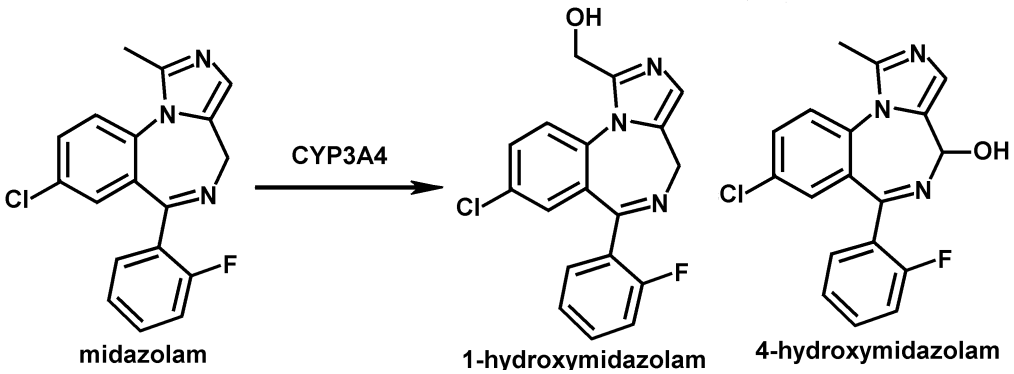

Figure 8-3. Structures of midazolam and its metabolites.

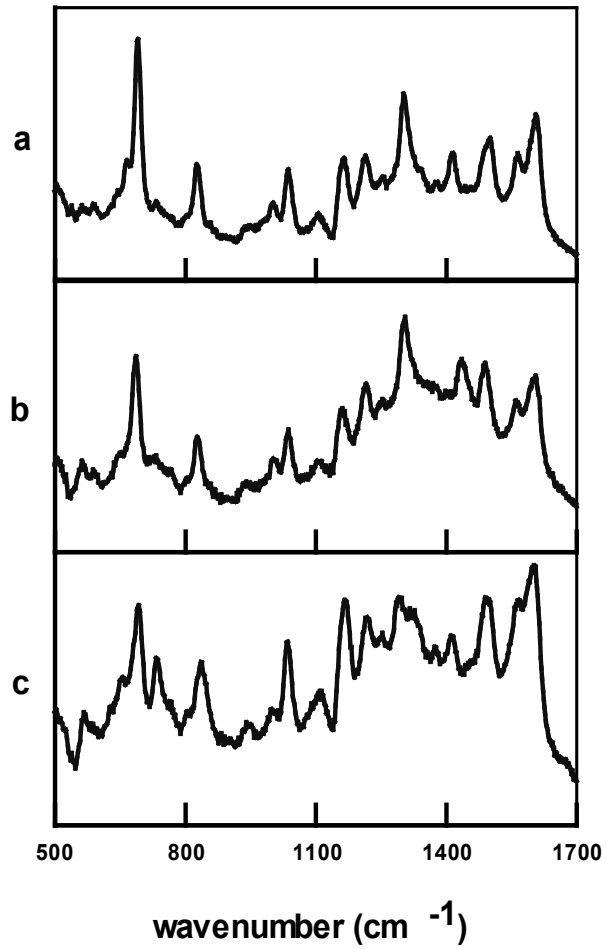

Figure 8-4. SERS spectra of Au/t-BuS on magnetic microspheres immersed in aqueous solutions of (a) 300 μM midazolam, (b) 50-μM 1-hydroxymidazolam, (c) 123 μM 4-hydroxymidazolam. The spectral contributions of the t-BuS- coating were subtracted out.

9. IN-LINE MIXER FOR HYDROPHILIC CAPTURE MATRICES

9.1 INTRODUCTION

For capture matrices, the efficiency of the analyte extraction depends on the contact time of the sample with the capture matrices. The greater the capture efficiency, the lower the detection limit of the analyte. To improve the probability of contact between the analyte and the capture matrices, Shishehbore, Afkhami, and Bagheri[1] used ultrasonication for 10 min to disperse the capture matrices in aqueous samples. Šafařik and Šafařiková[2] stirred their aqueous samples for 4 h after adding their capture matrices. For hydrophobic samples, we showed that vortexing could be used to improve the capture efficiency. Vortexing would probably work as well for hydrophilic capture matrices. However, vortexing does not lend itself well to automation. The use of folded flow mixing to increase capture efficiency was then explored. Increasing the contact area between the species to be mixed is one of the most efficient means of enhancing the diffusive mixing effect.[3] One approach to do this is to increase the contact area between the mixing species by designing the microchannel configurations so that the species are folded multiple times as they flow along the mixing channel.

9.2 DESIGN OF IN-LINE MIXER

Figure 9.2-1 shows an in-line mixing assembly. The flow-through mixer assembly consists of two syringe pumps (Razel® Scientific Instruments) and a low-flow, Hyper Shear static, in-line mixer from Analytical Scientific Instruments. One syringe pump houses a 10-mL plastic syringe that delivers the sample at a given rate. The other syringe pump houses a 3-mL plastic syringe that delivers the capture matrices at another given rate. To keep the capture matrices suspended during delivery, a 3-VDC microvibration motor (RadioShack® Corporation, part number 273-107) was attached to the barrel of the syringe. The motor was also wired to a battery pack and an on/off switch. The microvibration motor is slightly magnetic. Consequently, magnetic beads were concentrating on the side of the syringe adjacent to the motor. To alleviate that problem, 3-mm-thick Tygon® tubing was placed around the barrel of the 3-mL syringe. The micro-vibration motor was epoxied to a plastic clip, Figure 9.2-2. The combination of the Tygon® tubing and clip provided enough distance between the microvibration motor and magnetic beads that the beads remained suspended as they were injected into the mixer.

Both syringe pumps inject sample and capture matrices into the low-flow, Hyper Shear-static, in-line mixer, Figure 9.2-3a. The mixer is an example of a folding flow mixer that consists of a chain of elements. In each element, the flow is folded upon itself, Figure 9.2-3b. This decreases the length scale for mixing and reduces the mixing time.

The combined suspension of sample and capture matrices is transported from the mixer to a flow-through cell that has a NdFeB magnet below the optical surface. Initially, the first-generation flow-through cell, Figure 3.5-1, was used. As the capture matrices flowed through this cell, the magnets did pull the capture matrices out of the suspension and concentrated them onto the optical surface, Figure 9.2-4a. However, air bubbles would accumulate that hampered the efficiency of concentrating the capture matrices onto the optical surface, Figure 9.2-4b. To eliminate these air bubbles, we fabricated a second-generation cell that incorporated another microvibration motor in the cell body, Figure 9.2-5. The magnets on this second-generation cell were also mounted on a plunger with solenoid used to move the magnets to and away from the optical surface. When the magnets are moved away from the optical surface, the capture matrices can be flushed off the optical surface.

When the project ended, we were working on automation of the mixer assembly. This was not completed.

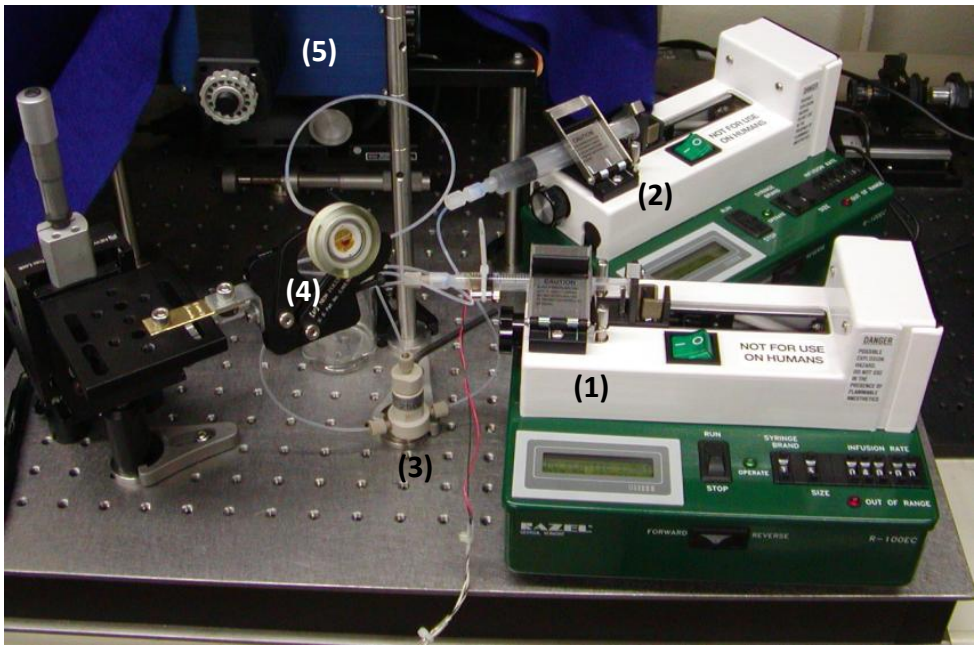

Figure 9.2-1. In-line mixer assembly composed of (1) syringe pump with 3-mL syringe for capture matrices, (2) syringe pump with 10-mL syringe for the sample, (3) low-flow, Hyper Shear static, in-line mixer, and (4) flow-through cell. The portable Raman spectrometer (5) is also shown.

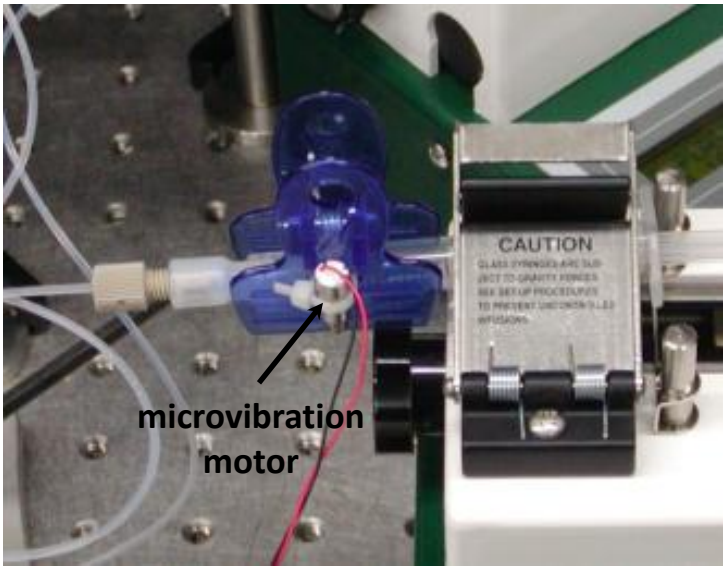

Figure 9.2-2. Syringe used to deliver the capture matrices. The microvibration motor was used to keep the capture matrices suspended is indicated.

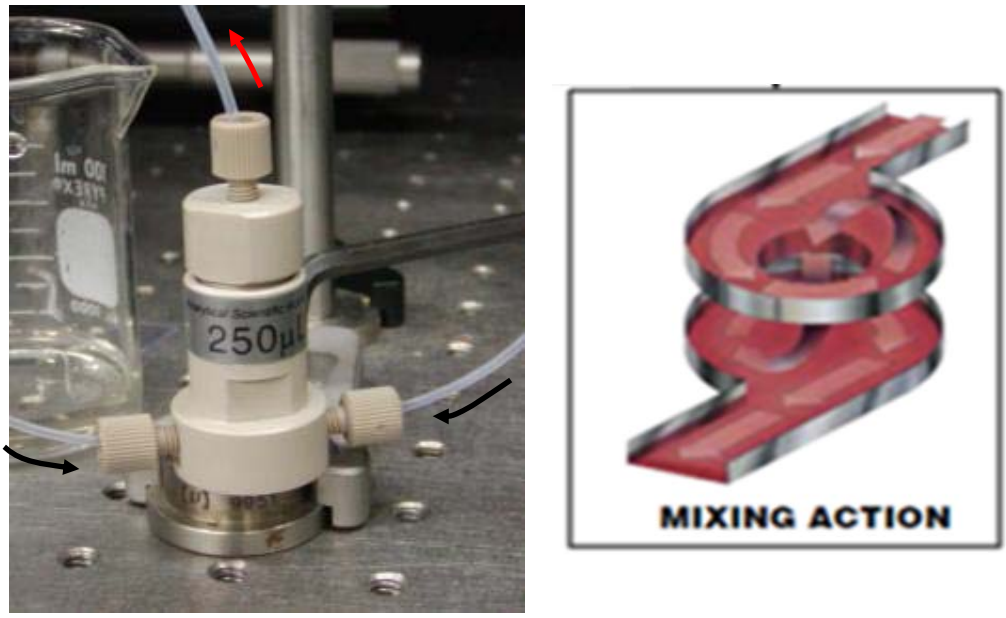

Figure 9.2-3. (a). Folding flow mixer (flows are indicated), (b) schematic showing folded flow mixing between two elements of the mixer.

9.3 REFERENCES

1. M. R. Shishehbore, A. Afkhami, and H. Bagheri. 2011. "Salicylic Acid Functionalized Silica-Coated Magnetite Nanoparticles for Solid Phase Extraction and Preconcentration of Some Heavy Metal Ions from Various Real Samples," *Chemistry Central Journal* *5*:41–50.

2. I. Šafařik and M. Šafařikova. 2002. "Detection of Low Concentration of Malachite Green and Crystal Violet in Water," *Water Research* *36*:196–200.

3. Y. Lee, C.-L. Chang, and L.-M. Fu. 2011. "Microfluidic Mixing: A Review," *International Journal of Molecular Sciences* *12*:3263–3287.

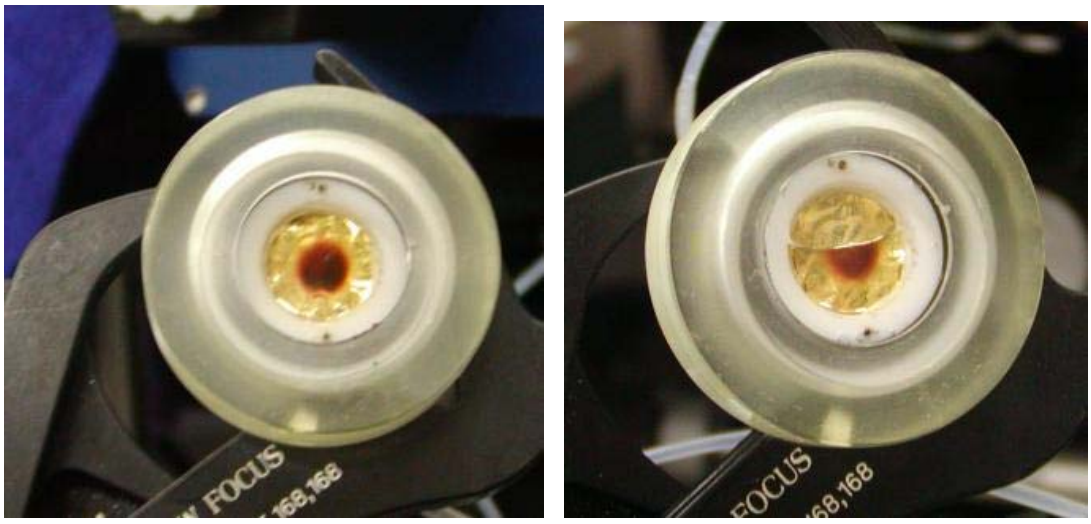

Figure 9.2-4. First-generation flow cell concentrating capture matrices onto the optical surface where (a) has no air bubbles, and (b) has air bubbles.

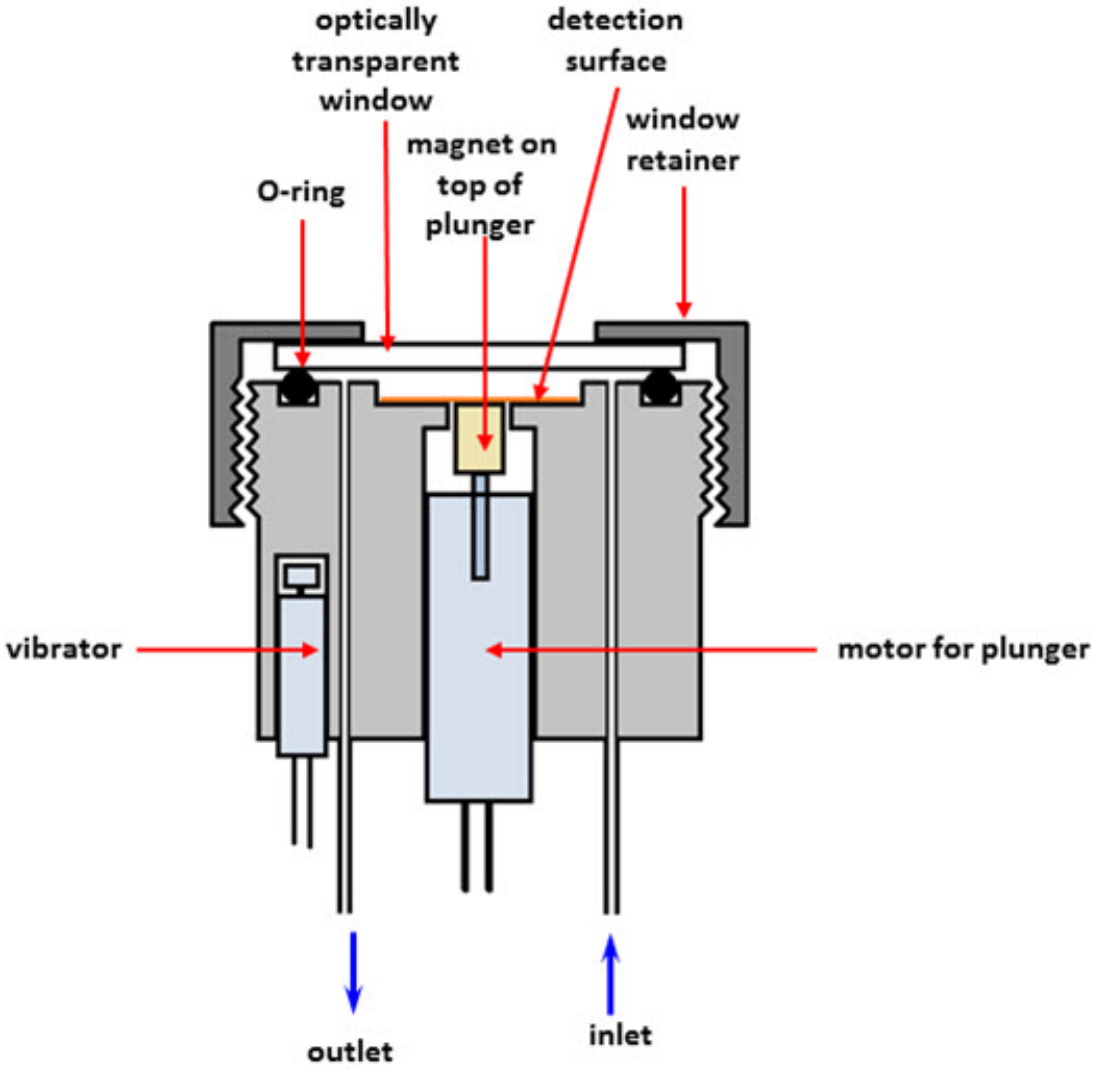

Figure 9.2-5. Schematic of second-generation flow-through cell.

APPENDIX

CAPTURE MATRICES PUBLICATIONS

The publications included in this appendix describe the fabrication and use of surface-enhanced Raman spectroscopy (SERS)-active capture matrices to detect naphthalene, hexavalent chromium, and perchlorate:

1. P. A. Mosier-Boss and S. H. Lieberman. 2005, "Surface-Enhanced Raman Spectroscopy Sunstrate Composed of Chemically Modified Gold Colloid Particles Immobilized on Magnetic Particles," *Analytical Chemistry 77*:1031–1037.

2. P.A. Mosier-Boss and M.D. Putnam. 2013. "Detection of Hexavalent Chromium using Gold/4-(2-Mercaptoethyl)Pyridinium Surface Enhanced Raman Scattering-Active Capture Matrices," *Analytica Chimica Acta 801*:70–77.

3. P.A. Mosier-Boss and M.D. Putnam. 2014. "Detection of Perchlorate using Ag/DMAH+ SERS-active Capture Matrices," *Spectrochimica Acta Part A: Molecular and Biomolecular Spectroscopy 133*:156–164.

Anal. Chem. **2005,** *77,* 1031−1037

Surface-Enhanced Raman Spectroscopy Substrate Composed of Chemically Modified Gold Colloid Particles Immobilized on Magnetic Microparticles

P. A. Mosier-Boss* and S. H. Lieberman

SPAWAR Systems Center San Diego, Code 236, San Diego, California 92152

In this paper, immobilization of gold colloidal particles onto amine-modified magnetic microparticles is demonstrated. Once immobilized, the gold was then reacted with pentachlorothiophenol (PCTP) to form a self-assembled monolayer. The PCTP−gold colloid on magnetic microparticles was then used to extract naphthalene from aqueous samples. A magnet was used to concentrate the microparticles onto the side of the sample vial, allowing detection of naphthalene by surface-enhanced Raman spectroscopy. Using the PCTP−gold colloid on magnetic microparticles the limit of detection for naphthalene achieved was 0.3 μg mL^{-1}. Multiple extractions can be done with the PCTP−gold colloid on magnetic microparticles to further lower the detection limit.

Silver and gold colloids are perhaps the most versatile of substrates used for surface-enhanced Raman spectroscopy (SERS). Aqueous solutions of the colloids are easy to prepare and are stable for long periods of time.[1] The colloids can be prepared with a wide range of diameters (2.5−120 nm). Colloids have been used as a tool to probe the SERS phenomenon. They have been used to examine the roles of surface-active sites and chemical enhancement in SERS[2] and to evaluate the effects of size and morphology on the magnitude of the SERS effect.[3,4] Colloids have also been used to detect bacteria,[5−7] nitrogen-containing drugs,[8] and other chemical species.[9,10] Using running buffers containing silver colloid suspensions, on-column SERS detection in capillary electrophoresis has been demonstrated.[11] Individual colloidal particles have been labeled with reporter molecules and then encapsulated in glass.[12,13] The focus of these efforts was to create alternatives to fluorescent tags currently used in genome sequencing, PCR, and immunoassays. In other efforts, silver/gold colloids have been immobilized on TLC plates,[14] plastic,[15] silica microspheres,[16] and on glass slides.[1,17] They have also been incorporated in sol−gel films to create stable SERS substrates with long shelf lives.[18−20] Immobilized gold colloidal particles on glass have been coated with a C-18 alkylsilane layer and used to detect trace amounts of polycyclic aromatic hydrocarbons.[21,22]

While silver/gold colloidal particles have been bound to plastic, glass, and silica microspheres, to our knowledge they have not been immobilized on magnetic microparticles. Magnetic microparticles have been used primarily in the areas of biosciences and biotechnologies for the capture of biomolecules, cells, and cell organelles.[23] Advantages of the use of magnetic microparticles for these applications are extraction/concentration of the target analyte from a complex sample matrix, ease of separation, and suitability for automation. These same features make magnetic microparticles attractive for use to extract/concentrate/separate chemical species. In this work, pentachlorothiophenol (PCTP)-modified colloidal gold is immobilized on magnetic microparticles that have amine groups on their surface. Use of the Au−PCTP colloid on magnetic microparticles to detect naphthalene by SERS is demonstrated.

EXPERIMENTAL SECTION

Reagents. Naphthalene (Fluka), hydrogen tetrachloroaurate-(III) trihydrate (Aldrich), sodium citrate (Aldrich), pentachlorothiophenol,[24] water (HPLC grade, Aldrich), and ethanol (HPLC

* To whom correspondence should be addressed. E-mail: pam.boss@navy.mil.

(1) Grabar, K. C.; Allison, K. J.; Baker, B. E.; Bright, R. M.; Brown, K. R.; Freeman, R. G.; Fox, A. P.; Keating, C. D.; Musick, M. D.; Natan, M. J. *Langmuir* **1996**, *12*, 2353−2361.
(2) Doering, W. E.; Nie, S. *J. Phys. Chem. B* **2002**, *106*, 311−317.
(3) Suzuki, M.; Niidome, Y.; Kuwahara, N.; Inone, K.; Yamada, S. *J. Phys. Chem. B* **2004**, *108*, 11660−11665.
(4) Freeman, R. G.; Bright, R. M.; Hommer, M. B.; Natan, M. J. *J. Raman Spectrosc.* **1999**, *30*, 733−738.
(5) Efrima, S.; Bronk, B. V. *J. Phys. Chem. B* **1998**, *102*, 5947−5950.
(6) Jarvis, R. M.; Goodacre, R. *Anal. Chem.* **2004**, *76*, 40−47.
(7) Jarvis, R. M.; Brooker, A.; Goodacre, R. *Anal. Chem.* **2004**, *76*, 5198−5202.
(8) Torres, E. L.; Winefordner, J. D. *Anal. Chem.* **1987**, *59*, 1626−1632.
(9) Garrell, R. L. *Anal. Chem.* **1989**, *61*, 401A−411A.
(10) Angel, S. M.; Myrick, M. L.; Milanovich, F. P. *Appl. Spectrosc.* **1990**, *44*, 335−336.
(11) Nirode, W. F.; Devault, G. L.; Sepaniak, M. J.; Cole, R. O. *Anal. Chem.* **2000**, *72*, 1866−1871.
(12) Mulvaney, S. P.; Musick, M. D.; Keating, C. D.; Natan, M. J. *Langmuir* **2003**, *19*, 4784−4790.
(13) Doering, W. E.; Nie, S. *Anal. Chem.* **2003**, *75*, 6171−6176.
(14) Roth, E.; Kiefer, W. *Appl. Spectrosc.* **1994**, *48*, 1193−1195.
(15) Supriya, L.; Claus, R. O. *Langmuir* **2004**, *20*, 8870−8876.
(16) Fleming, M. S.; Walt, D. R. *Langmuir* **2001**, *17*, 4836−4843.
(17) Grabar, K. C.; Freeman, R. G.; Hommer, M. B.; Natan, M. J. *Anal. Chem.* **1995**, *67*, 735−743.
(18) Lucht, S.; Murphy, T.; Schmidt, H.; Kronfeldt, H.-D. *J. Raman Spectrosc.* **2000**, *31*, 1017−1022.
(19) Bao, L.; Mahurin, S. M.; Dai, S. *Anal. Chem.* **2004**, *76*, 4531−4536.
(20) Bao, L.; Mahurin, S. M.; Haire, R. G.; Dai, S. *Anal. Chem.* **2003**, *75*, 6614−6620.
(21) Olson, L. G.; Lo, Y.-S.; Beebe, T. P., Jr.; Harris, J. M. *Anal. Chem.* **2001**, *73*, 4268−4276.
(22) Olson, L. G.; Uibel, R. H.; Harris, J. M. *Appl. Spectrosc.* **2004**, *58*, in press.
(23) Šafařík, I.; Šafaříkková, M. *Monatsh. Chem.* **2002**, *133*, 737−759.
(24) PCTP was generously provided by Prof. Keith Carron of the University of Wyoming.

10.1021/ac048647f Not subject to U.S. Copyright. Publ. 2005 Am. Chem. Soc.
Published on Web 01/19/2005

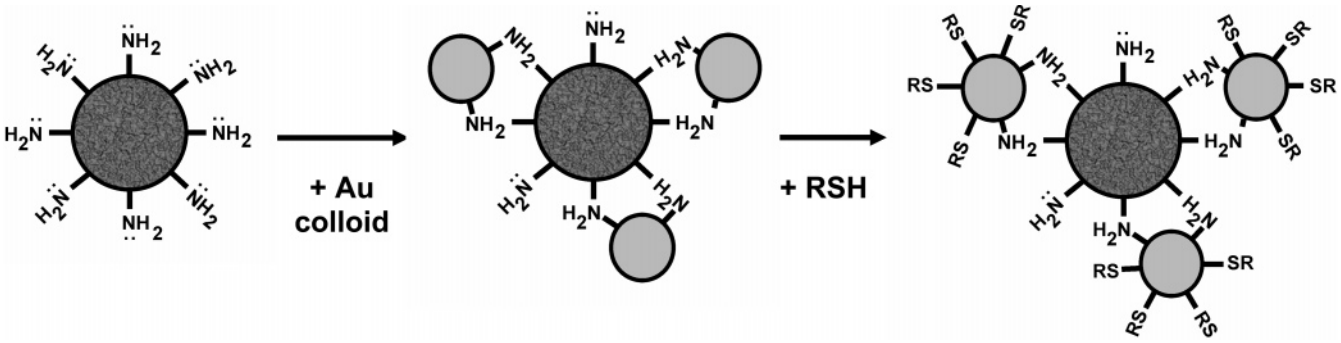

Figure 1. Procedure used to fabricate thiol-modified Au colloidal particles on magnetic microparticles.

grade, Aldrich) were used as received. A 0.5-mL aliquot of 5 wt % BioMag, amine-terminated superparamagnetic microparticles (Bangs Laboratories, part no. BM546), was washed 12 times with 1-mL aliquots of HPLC water to remove surfactant. Afterward, the volume of the BioMag amine-terminated superparamagnetic microparticles was adjusted to 2.5 mL.

Preparation of Conventional SERS Substrates. An insulated copper wire was soldered to a 0.75-cm length of 2-mm-diameter gold wire (Aldrich, 99.9%). The gold wire was potted inside a 5-mm-outer diameter glass tube with a chemically resistant epoxy (Epoxy Patch 1C, Hysol). Prior to use, the gold disk of the electrode was electrochemically roughened in a 0.1 M KCl solution using a PAR 173 potentiostat under computer control. The gold surface was roughened by cycling the electrode from −280 (holding 10 s) to 1220 mV (holding 5 s) at 500 mV s^{-1} for 25 times. After electrochemical roughening, the gold electrode was rinsed with water (HPLC grade, Aldrich) and then ethanol (HPLC grade, Aldrich). The electrode was immersed in a dilute thiol solution in ethanol and allowed to react for ~24 h to form a self-assembled monolayer (SAM). Before use, the substrates were rinsed thoroughly with ethanol and stored in water between uses.

Preparation of Gold Colloid. A solution of 100 mL of 0.01% (g/mL) hydrogen tetrachloroaurate(III) trihydrate, in a 250-mL round-bottom flask equipped with a condenser, is brought to a vigorous boil while being stirred rapidly. Once the solution reaches a boil, 0.85 mL of of 1% sodium citrate is added. Within 1 min, the color of the solution changes from light yellow to blue. After refluxing for 40 min, the solution is red-violet. The flask is removed from the heat and allowed to cool to room temperature. The colloidal suspension is then concentrated, by centrifugation, to a final volume of ~3 mL.

Preparation of Chemically Modified Gold Colloid Immobilized on Magnetic Microparticles. Figure 1 summarizes the procedure used to prepare chemically modified gold colloid that has been immobilized on magnetic microspheres. To 1 mL of the concentrated gold colloid, 0.250 mL of the washed BioMag amine-terminated superparamagnetic microparticles was added and rolled for 2 h. The gold colloidal particles bind to the amine groups of the superparamagnetic microparticles. The gold colloid immobilized on magnetic microparticles is washed three times with ethanol. Between washes, a NdFeB magnet is used to separate the magnetic microparticles from the liquid. The magnetic microparticles used in these experiments are ~1.5 μm in size and have a greater than 90% iron oxide content. Both of these attributes allow for faster magnetic separations. Afterward a dilute ethanolic solution of pentachlorothiophenol (PCTP) is added and PCTP is allowed to react with the immobilized colloidal particles for ~24 h to form a SAM. The chemically modified gold colloid immobilized on magnetic microparticles is washed three times with ethanol, as described above. The particles are stored in ethanol. Prior to use, an aliquot of PCTP-derivatized gold colloid on magnetic microsheres is pipetted into a 1.75-mL amber glass vial and washed three times with 0.5 mL of water. A NdFeB magnet is used to separate the magnetic microparticles from the liquid between washes. Afterward a 0.25−0.5-mL aliquot of aqueous sample containing naphthalene is added and allowed to equilibrate prior to analysis by SERS.

Evaluation of the SERS Substrates. The flow-through cell to evaluate the concentration response of the conventional Au/PCTP SERS substrate to naphthalene has been described elsewhere.[25] The spacing between the SERS surface and the sapphire window of the cell is ~0.5 mm. The flow-through cell is held in place with an Opti-Claw optical mount (New Focus, P/N 9832). The Opti-Claw is mounted on an *x*,*y*,*z* translation stage (Newport Corp., P/N 460A). SERS measurements were made using the Raman Solution 785 system (Detection Limit), which has an *f* number of 2, a fixed-position 1200 grooves/mm grating, and a TE-cooled Kodak 0400 CCD. A fiber-optic sampling probe operating at 785 nm (InPhotonics, model RPS785-12-10) is used to deliver the laser excitation to the sample and transfer the Raman emissions to the spectrometer. The excitation source is a tunable, continuous-wave laser diode (Spectra Diode Laser, SDL-8630) operating at 785 nm. A tunable optical isolator (Optics for Research, model IO-7-NIR) is used to prevent backscatter of the laser beam into the laser cavity. The 785-nm laser line is focused into the silica/silica clad, 100-μm, excitation fiber using a 5× microscope objective lens. To obtain spectra of the conventional SERS substrate, a laser power of 100 mW (measured out of the fiber-optic probe) was used.

After equilibration, a 3.175-mm-diameter disk NdFeB magnet is used to concentrate the PCTP-derivatized gold colloid on magnetic microparticles onto the side of the amber glass vial. Rigorous shaking is required to dislodge the magnetic microparticles from the glass surface. SERS measurements were made using the Raman Solution 785 system described above. The vial is placed in front of the output of the fiber-optic sampling probe and the laser beam is focused into the area where the magnetic microparticles are concentrated. A laser power of 50 mW was used to obtain spectra of the Au/PCTP immobilized on magnetic microparticles. Unlike the conventional SERS substrate, there is

(25) Mosier-Boss, P. A.; Lieberman, S. H. *Appl. Spectrosc.* **2000**, *54*, 1126−1135.

no water layer between the inside of the vial and the magnetic microparticles. In the case of the conventional SERS substrate, the layer of water between the optical window and the SERS substrate absorbs near-IR excitation from the laser requiring the use of higher laser power than that used to obtain spectra of the magnetic microparticles.

All manipulations of the spectral data were done using GRAMS/AI7 (ThermoGalactic), a software package that can be used to subtract spectra interactively as well as integrate peak areas.

Imaging of Gold Colloids and Magnetic Microparticles. The 10-μL aliquots of the concentrated gold colloid, washed amine magnetic microparticles, and gold colloid bound magnetic microparticles were added to 5 mL of water and vacuum filtered onto 0.02-μm-pore size anodizc membranes (Whatman). The membranes were then mounted on microscope slides; coverslips were placed over the membranes and subjected to microscopic examination. Images were obtained using an Eclipse E600 epifluorescent microscope (Nikon) and CoolSnap HQ CCD camera (Photometrics). The light source was a mercury lamp. Images were taken using either a DAPI (filters from Chroma technology: exciter D360/40X, dichroic 400DCLP, emitter D460/50M) or CY5 (filters from Chroma technology: exciter HQ620/60X, dichroic Q660LP, emitter HQ700/50M) filter cube. A magnification of 1000× was used.

RESULTS AND DISCUSSION

Detection of Naphthalene Using Conventional Au/PCTP SERS Substrates. It has been shown that thiols react on Ag/Au surfaces to form SAMs.[26] It has also been shown that the thiol coating can be chosen to attract and concentrate an analyte to the Ag/Au surface allowing its detection and identification by SERS. Thiol-coated SERS substrates have been used to detect aromatic compounds,[27−29] chlorinate solvents,[29,30] MTBE,[29] and anions.[25,31] Depending on the analyte and coating, analyte detection limits in the ppb−ppm concentration range have been reported. SERS spectra for molecules directly adsorbed onto the metal surface are often significantly different from their normal Raman spectra.[9,32] However, in the investigations using thiol-coated SERS substrates, the spectral features (peak positions as well as peak shape and intensity) of the analytes in the SERS spectra directly correspond to the spectral features in the normal Raman spectra of the neat compounds. This is attributed to the fact that the thiol coating prevents the analyte molecule from directly adsorbing onto the metal surface.

To detect an analyte, thiols are chosen that have an affinity for the analyte. Another consideration is the availability of a spectral window to detect the analyte. The coating itself exhibits a SERS spectrum, which can be used for calibration purposes as will be discussed vide infra. However, a coating must be chosen whose SERS spectrum minimally interferes with the Raman spectrum of the analyte. Naphthalene is an aromatic compound that should be attracted to an aromatic thiol such as PCTP. Comparing the SERS spectrum of PCTP with the normal Raman spectrum of naphthalene, Figure 2A, it can be seen that the peaks due to PCTP should not interfere in the detection of naphthalene. The concentration response of a conventional gold SERS surface that has been derivatized with a PCTP SAM is summarized in Figure 2B−D. Figure 2B shows SERS spectra obtained with increasing concentration of naphthalene (1.5−30 μg mL^{-1}). As can be seen, there is little variation in the background response and intensity of the PCTP peaks in the spectra. This is attributed to the fact that the gold SERS substrate is held in a fixed position throughout the course of the experiment. Consequently, it is not necessary to reference the naphthalene peak area to that of an internal standard. With the addition of naphthalene, new peaks emerge, which are indicated by asterisks (*) in Figure 2B, and these peaks are attributed to naphthalene that has partitioned into the PCTP coating on the gold substrate. The naphthalene peaks are smaller than the peaks due to PCTP. This results because PCTP is directly bound to the metal surface and naphthalene is not. It has been well documented that the SERS enhancement factor decays exponentially as a function of distance.[33−35] Figure 2D shows a plot of the 1381-cm^{-1} naphthalene peak area as a function of concentration of naphthalene. The response is linear up to a concentration of 16 μg mL^{-1} naphthalene. At higher amounts of naphthalene, the response begins to level off. Figure 2C is an expansion of the 1300−1425-cm^{-1} spectral region. The detection limit for naphthalene is defined as the concentration that produces a net line intensity equivalent to three times the standard deviation of the background.[36] For the conventional Au/PCTP SERS surface, the limit of detection for naphthalene is 1.5 μg mL^{-1}. Similar results for naphthalene were obtained using octadecyl-modified silver SERS substrates.[27] The substrates used in this earlier study were prepared by chemically etching the silver surface with 30% nitric acid. In this study, the limit of detection for naphthalene was 2.3 μg mL^{-1}.

Immobilization of Gold Colloid on Magnetic Microparticles. Gold colloidal particles are not luminescent when viewed using the DAPI filter cube. However, when viewed through the CY5 filter cube, the gold colloidal particles are weakly luminescent. Such luminescence has been characterized for silver nanoparticles.[37−39] While the gold colloidal particles were luminescent, the magnetic microparticles were not. Therefore, in this investigation, the luminescence of the gold colloidal particles is used to (1) show that the colloidal gold particles are associated with the magnetic microspheres and (2) to determine the homogeneity of the distribution of the gold colloid on the surface of the magnetic microparticles. As shown in Figure 3A for images obtained using the DAPI filter cube, the magnetic microparticles used in this investigation exhibit an irregular shape. This is because they are composed of magnetic iron oxide particles with a coating that provides primary amine groups for covalent coupling. It can also be seen in Figure 3A that the microspheres are aggregated.

(26) Bryant, M. A.; Pemberton, J. E. *J. Am. Chem. Soc.* **1991**, *113*, 3629−3637.
(27) Carron, K.; Peitersen, L.; Lewis, M. *Environ. Sci. Technol.* **1992**, *26*, 1950−1954.
(28) Carron, K. T.; Kennedy, B. J. *Anal. Chem.* **1995**, *67*, 3353−3356.
(29) Mosier-Boss, P. A.; Lieberman, S. H. *Anal. Chim. Acta* **2003**, *488*, 15−23.
(30) Mullen, K.; Carron, K. *Anal. Chem.* **1994**, *66*, 478−483.
(31) Mosier-Boss, P. A.; Lieberman, S. H. *Appl. Spectrosc.* **2003**, *57*, 1129−1137.
(32) Mosier-Boss, P. A.; Lieberman, S. H. *Recent Res. Dev. Appl. Spectrosc.* **1999**, *2*, 83−98.
(33) Murray, C. A.; Allara, D. L. *J. Chem. Phys.* **1982**, *76*, 1290−1303.
(34) Ye, Q.; Fang, J.; Sun, L. *J. Phys. Chem. B* **1997**, *101*, 8221−8224.
(35) Tsen, M.; Sun, L. *Anal. Chim. Acta* **1995**, *307*, 333−340.
(36) Sabsabi, M.; Cielo, P. *Appl. Spectrosc.* **1995**, *49*, 499−507.
(37) Doering, W. E.; Nie, S. *J. Phys. Chem. B* **2002**, *106*, 311−317.
(38) Geddes, C. D.; Parfenov, A.; Gryczyski, I.; Lakowicz, J. R. *J. Phys. Chem. B* **2003**, *107*, 9989−9993.
(39) Anderson, P. C.; Jacobson, M. L.; Rowlen, K. L. *J. Phys. Chem. B* **2004**, *108*, 2148−2153.

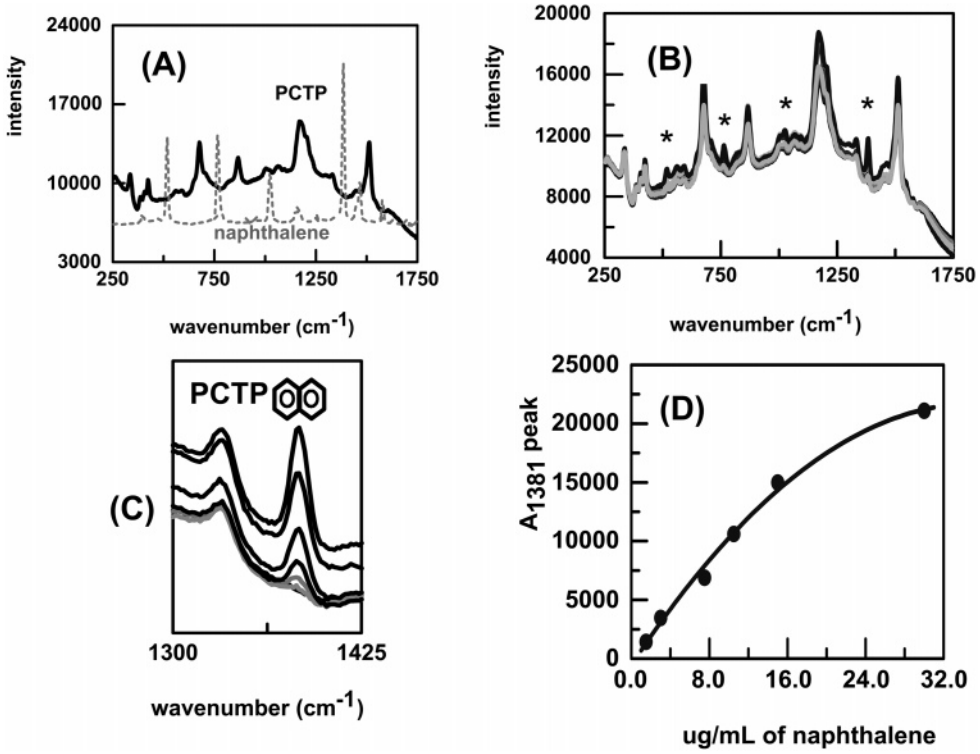

Figure 2. (A) SERS and Raman spectra of Au/PCTP (solid black line) and naphthalene (gray dotted line), respectively, illustrating the spectral windows in the SERS spectrum of PCTP available to detect naphthalene. (B) SERS spectra obtained for PCTP-derivatized, electrochemically roughened, conventional gold SERS substrate as a function of naphthalene concentration. Spectra obtained using 785-nm excitation at 100 mW and averaging 10 10-s acquisitions. (C) Spectra of the 1300−1425-cm^{-1} region. Naphthalene concentration varies from 1.5 to 30 μg mL^{-1}. (D) Concentration response obtained for naphthalene. The curve is described by the following relationship: $A_{1381} = (-17.746)x^2 + 1257.1x - 538.22$, where x is the concentration of naphthalene (in μg mL^{-1}) and $R^2 = 0.994$.

Aggregation of the microparticles occurs in the absence of a surfactant. It should be noted that prior to using the gold-immobilized magnetic microparticles, vortexing is used to resuspend the particles. When the gold-immobilized magnetic microparticles are viewed using the CY5 filter cube, it can be seen that the luminescence is evenly distributed over the surface of the magnetic microparticles, suggesting that binding of the gold colloidal particles onto the surface of the magnetic microparticles is homogeneous, Figure 3B.

SERS Response of Au/PCTP on Magnetic Microparticles. Aliquots (50 μL) of the magnetic microparticles and gold colloid-immobilized on magnetic microparticles were pipetted into 0.5 mL of water in amber glass vials. A 3.175-mm-diameter disk NdFeB magnet was then placed on the side of the glass vial to concentrate the microparticles onto the side of the vial prior to obtaining the Raman spectra. After ~2 min, it was observed that the magnetic microparticles had concentrated on the surface of the glass vial adjacent to the position of the magnet. Raman spectra were then obtained for the microparticles that had been concentrated on the side of the glass. For both the magnetic microparticles and gold-immobilized magnetic microparticles, the spectra were characterized by featureless, broad continua. These experiments were then repeated using the PCTP-derivatized gold colloid on magnetic microparticles. Specifically, 50-μL aliquots of the ethanolic suspensions were pipetted into two 1.75-mL amber glass vials. After washing the microparticles three times with water to remove the ethanol, 0.5-mL aliquots of water and naphthalene-saturated water (concentration 30 μg of naphthalene/mL) were pipetted into each of the glass vials. The samples were allowed to equilibrate for ~30 min. Spectra of the suspended microparticles were obtained, and they are shown in Figure 4c and d. Peaks due to the PCTP SAM can be discerned; however, they are very weak. The fact that peaks can be seen indicates that the colloidal gold particles immobilized on the magnetic microparticles are SERS active and the weakness of the signal is attributed to the fact that the microparticles are dispersed throughout the sample. The NdFeB disk magnet was used to concentrate the magnetic microparticles onto the side of the glass vial. SERS spectra, traces a and b of Figure 4 for water and naphthalene-saturated water, respectively, were obtained by focusing the laser beam from the fiber-optic probe onto the magnetic microparticles concentrated on the side of the glass. The SERS spectra exhibit highly resolved, intense peaks. The naphthalene peaks are indicated by asterisks (*). When the spectral contributions of PCTP are subtracted from the spectrum shown in Figure 4b, the spectral features of the resultant difference spectrum, Figure 4f, match those of neat naphthalene, Figure 4e, in peak position, intensity, and line width.

Figure 5 shows five replicate measurements made for the same sample. The time between each measurement was 1 h. Between each measurement, the magnetic microparticles were resuspended. Prior to measurement, the magnetic microparticles were concentrated on the side of the glass vial using a magnet. The vial was placed in front of the laser beam as described vide supra. As can be seen in Figure 5, great variability in the intensity of the peaks due to PCTP and naphthalene (indicated by asterisks) is observed. This fluctuation in peak intensity and background level

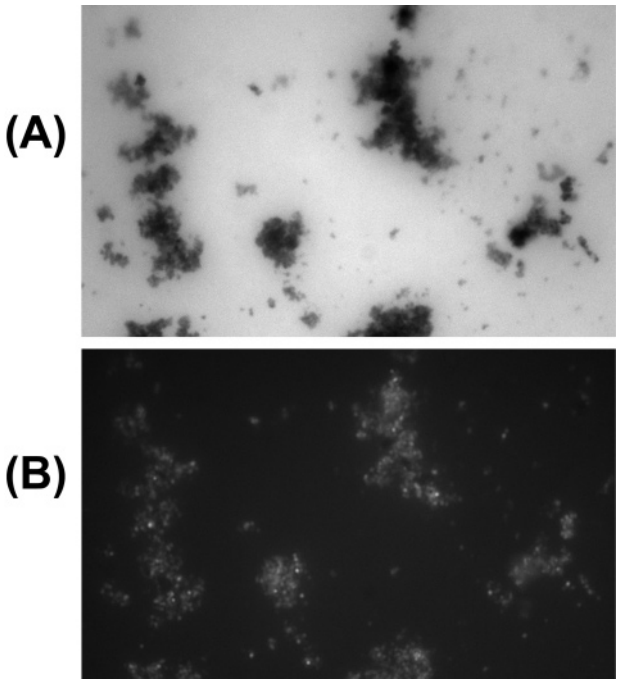

Figure 3. Images of colloidal gold immobilized on magnetic microparticles obtained using an epifluorescent microscope and CCD camera. (A) Image obtained using the DAPI filter cube and 500-ms acquisition time. No luminescence is observed. (B) Image obtained in the same optical region as (A) but using the CY5 filter cube and 100-s acquisition time. Luminescence from the colloidal gold particles bound to the magnetic microparticles is observed.

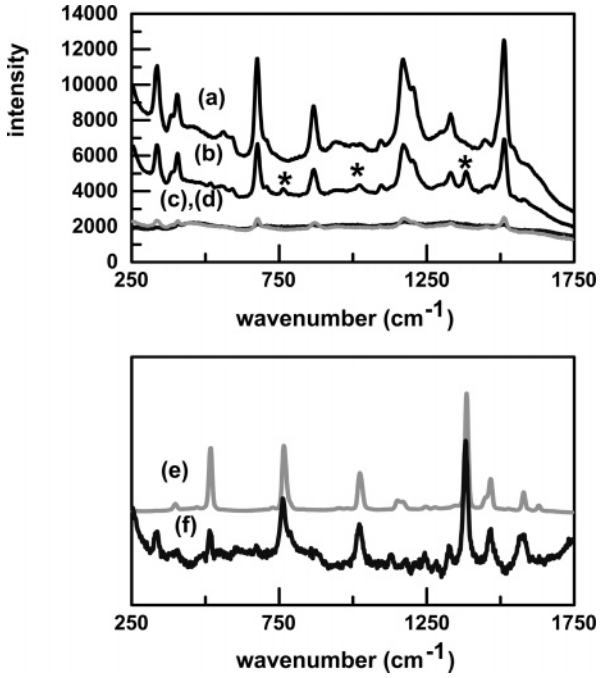

Figure 4. Spectra obtained for naphthalene and Au/PCTP colloid on magnetic microparticles using 785-nm excitation at 50 mW and averaging five 10-s acquisitions. (a) SERS spectrum of Au−PCTP magnetic microparticles in 0.5 mL of water. A magnet has been used to concentrate the magnetic particles onto the side of the glass vial. (b) SERS spectrum of Au/PCTP magnetic microparticles in 0.5 mL of 30 μg mL^{-1} naphthalene in water. A magnet has been used to concentrate the magnetic particles onto the side of the glass vial. Asterisks (*) note the appearance of new peaks. (c) and (d). SERS spectra obtained for Au/PCTP magnetic microparticles suspended in 0.5 mL of water and 30 μg mL^{-1} naphthalene, respectively. (e) Normal Raman spectrum of naphthalene. (f) SERS spectrum of (b) in which the spectral contributions of PCTP have been subtracted.

is attributed to variability in the density of the concentrated magnetic microparticles between samples as well as variability in positioning the vial in front of the laser from sample to sample. To compare different samples of the derivatized gold colloid on magnetic microparticles, the area of the analyte peak needs to be referenced to an internal standard.[40] It would be ideal to use one of the peaks due to the SAM as the internal standard. To be used as an internal standard, the SAM peak needs to be relatively intense and not change as increasing amounts of analyte partitions into the SAM. It was found that the PCTP peak at 1331 cm^{-1} meets both of these criteria. In Figure 5, the naphthalene peaks are indicated by asterisks. The peak at 1381 cm^{-1} is the most intense and will be used for quantification purposes. Table 1 summarizes the peak area of the PCTP peak at 1331 cm^{-1} and the naphthalene peak at 1381 cm^{-1} as well as the ratio of the peak areas, A_{1381}/A_{1331}. The relative standard deviation in the peak areas are 22.9 and 24.5% for the PCTP and naphthalene peaks, respectively. In contrast, the relative standard deviation in the ratio of the peak areas, A_{1381}/A_{1331}, is 1.5%. This normalization procedure increases the precision of the analyte signal by more than 1 order of magnitude.

Spectral data as a function of time for the Au/PCTP on magnetic microparticles and naphthalene were obtained to determine the time needed for equilibration. The data, which can be found in Figure S-1 of the Supporting Information, indicate that the interaction between naphthalene and PCTP is initially rapid and then levels off. To ensure that the samples have reached

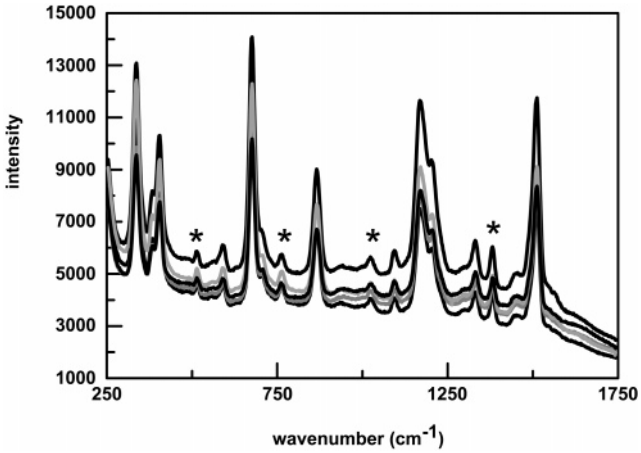

Figure 5. Replicate SERS measurements of a sample of 25 μL of Au/PCTP colloid on magnetic microparticles in 0.5 mL of 30 μg mL^{-1} naphthalene in water. Prior to each measurement, a magnet is used to concentrate the magnetic microparticles onto the side of the glass vial. Peak areas for the 1381- and 1331-cm^{-1} peaks are summarized in Table 1.

equilibrium, measurements are made 30 min or more after the naphthalene sample has been added to the Au/PCTP on magnetic microparticles.

Concentration Response of Au/PCTP on Magnetic Microparticles to Naphthalene. Aliquots (50 μL) of Au/PCTP on

(40) Lorén, A.; Engelbrektsson, J.; Eliasson, C.; Josefson, M.; Abrahamsson, J.; Abrahamsson, K. *Nano Lett.* **2004**, *4*, 309−312.

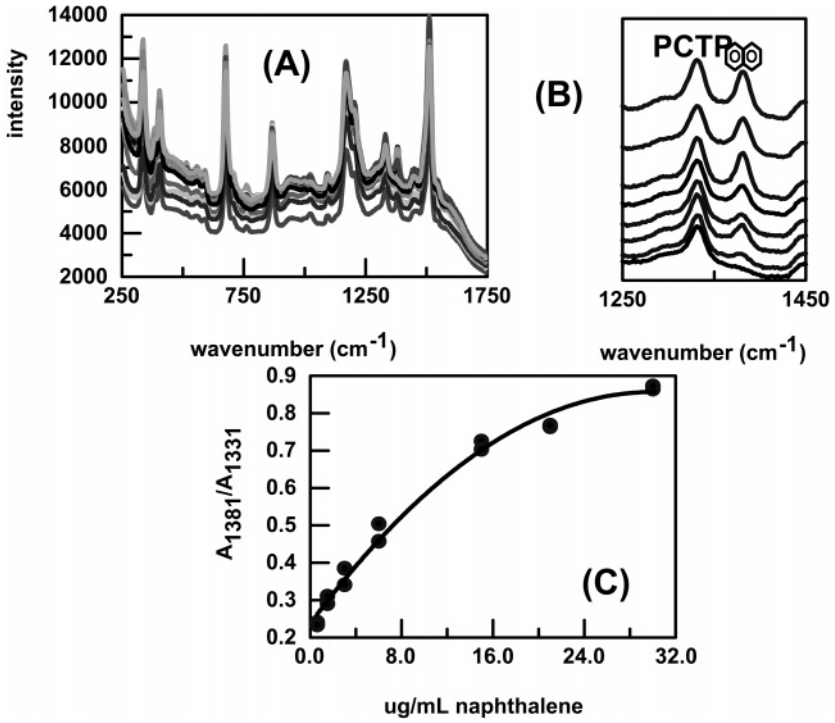

Figure 6. (A) SERS spectra obtained for PCTP-derivatized, gold colloid immobilized on magnetic microparticles as a function of naphthalene concentration. Spectra obtained using 785-nm excitation at 50 mW and averaging five 10-s acquisitions. (B) Spectra of the 1250−1450-cm^{-1} region. Naphthalene concentration varies from 0.6 to 30 μg mL^{-1}. (C) Concentration response obtained for naphthalene. The curve is described by the following relationship: $A_{1381}/A_{1331} = (-0.00069)x^2 + 0.0412x + 0.2376$, where x is the concentration of naphthalene (in μg mL^{-1}) and $R^2 = 0.990$.

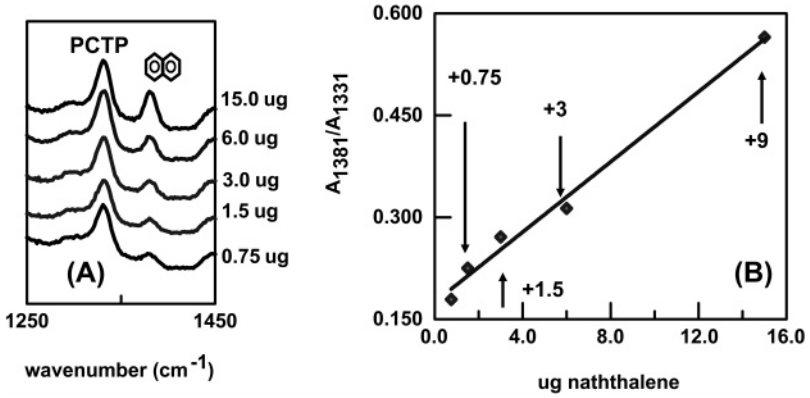

Figure 7. SERS spectra obtained after multiple extractions of naphthalene. (A) Spectra of the 1250−1450-cm^{-1} region are shown. Amount of naphthalene in the vial after additions is indicated. (B) Plot of the ratio of the peak areas, A_{1381}/A_{1331}, versus amount of naphthalene. Amount (μg) of naphthalene added prior to each measurement is indicated.

magnetic microparticles were pipetted into 1.75-mL glass amber vials. The magnetic microparticles were washed three times to remove ethanol as described vide supra. To one vial, 500 μL of water was added for a blank. Into the remaining vials, 500-μL samples varying between 0.6 and 30 μg mL^{-1} naphthalene were added and allowed to equilibrate. After equilibration, the magnetic microparticles were concentrated on the side of the glass vials and SERS spectra obtained as described earlier. The measurements were done in duplicate. The microparticles were resuspended between each measurement. Figure 6 summarizes the spectral data. Figure 6A shows the SERS spectra. As was noted earlier, the intensity and background response of the PCTP and naphthalene peaks vary considerably, requiring the use of the 1331-cm^{-1} PCTP peak as an internal standard. Figure 6C shows a plot of the ratio of the peak areas, A_{1381}/A_{1331}, as a function of micrograms of naphthalene per milliliter. The shape of the plot is similar to that obtained for the PCTP-derivatized gold electrode, Figure 2D. The plot shown in Figure 6C is linear to 16 μg mL^{-1} naphthalene. At higher concentrations of naphthalene, the response begins to level off. Figure 6B is an expansion of the 1250−1450-cm^{-1} spectral region. Using the same definition as before,[36] the limit of detection for naphthalene using the Au/PCTP on magnetic microparticles is estimated to be 0.3 μg mL^{-1}.

Methods To Further Lower the Limit of Detection. One way to further lower the detection limit is to increase the volume of the sample size while keeping the aliquot size of the Au/PCTP on magnetic microparticles constant. In one such experiment, 0.25 mL of 3 μg mL^{-1} naphthalene in water was pipetted into a glass

Table 1. Reproducibility of the SERS Measurements of a Sample Containing 0.5 mL of 33 ppm Naphthalene in Water and 25 μL of Au/PCTP Immobilized on Magnetic Microparticles

measurement number	area of 1331-cm^{-1} PCTP peak	area of 1381-cm^{-1} naphthalene peak	A_{1381}/A_{1331}
1	13625.01	13497.62	0.99065
2	7548.107	7180.257	0.951266
3	10100.1	9804.469	0.97073
4	8266.482	7891.04	0.954583
5	8318.408	8054.123	0.968229
verage	9571.621	9285.502	0.967082
SD	2194.438	2276.143	0.013975
% RSD	22.93	24.51	1.45

vial containing 25 μL of Au/PCTP on magnetic microparticles. To a second vial containing 25 μL of Au/PCTP on magnetic microparticles, 1.75 mL of 3 μg mL^{-1} naphthalene in water was added. After equilibration, SERS spectra were measured. The ratio of the 1381-cm^{-1} naphthalene peak to the 1331-cm^{-1} PCTP peak was 0.11 for the 0.25-mL sample and 0.34 for the 1.75-mL sample. While larger sample volumes will result in lower detection limits, as the sample size gets larger it becomes more difficult to concentrate the magnetic microparticles onto the side of the glass vial. A similar approach would be to keep the sample volume constant and to vary the aliquot size of the derivatized gold magnetic microparticles. The results of this approach are summarized in Figure S-2 of the Supporting Information. In general, it was shown that as the aliquot size of the Au/PCTP on magnetic microparticles decreases, the ratio of the 1381-cm^{-1} naphthalene peak to the 1331-cm^{-1} PCTP peak increases.

Another way to lower the detection limit is to do multiple extractions, as summarized in Figure 7. In this approach, 25 μL of the PCTP-derivatized gold magnetic microparticles were added to a 0.5-mL sample containing 0.75 μg of naphthalene. After equilibration, a SERS spectrum was obtained as described vide supra. Afterward, a magnet was used to separate the magnetic microparticles from the sample. The liquid was removed and a second 0.5 mL of sample containing 0.75 μg of naphthalene was added and allowed to equilibrate. The SERS spectrum was obtained, and an increase in the ratio of the 1381-cm^{-1} naphthalene peak to the 1331-cm^{-1} PCTP peak was observed, which indicates that the PCTP-derivatized gold magnetic microparticles had taken up more naphthalene. The process was repeated again. After magnetic separation of the microparticles, the liquid was removed and 0.5 mL of sample containing 1.5 μg of naphthalene was added. Again an increase in the ratio of the 1381-cm^{-1} naphthalene peak to the 1331-cm^{-1} PCTP peak was observed in the SERS spectrum. The process was repeated two more times—first with a 0.5-mL sample containing 3 μg of naphthalene and then with a 0.5-mL sample containing 9 μg of naphthalene. In both cases, an increase in the ratio of the 1381-cm^{-1} naphthalene peak to the 1331-cm^{-1} PCTP peak was observed in the SERS spectra.

CONCLUSIONS

It has been shown that colloidal gold particles can be immobilized on magnetic microparticles while retaining their SERS activity. The gold colloid can then be reacted with a thiol to form a SAM. The SAM is used to attract the analytes of interest that are then identified/quantified by their characteristic SERS response. In this investigation, a pentachlorothiophenol SAM was used to enable detection of naphthalene. However, other thiols can be used instead of PCTP. The choice of thiol is contingent upon the physiochemical properties of the analyte. It was shown that the limit of detection for naphthalene is 0.3 μg mL^{-1} Au/PCTP on magnetic microparticles. Lower detection limits are achievable by either increasing sample size, decreasing the amount of modified magnetic microparticles added to the sample, or doing multiple extractions.

ACKNOWLEDGMENT

This work was supported by the Strategic Environmental Research and Development Program (SERDP) and the SSC-SD Independent Research (ILIR) Program.

SUPPORTING INFORMATION AVAILABLE

Additional information as noted in text. This material is available free of charge via the Internet at http://pubs.acs.org.

Received for review September 13, 2004. Accepted November 15, 2004.

AC048647F

Analytica Chimica Acta 801 (2013) 70–77

Contents lists available at ScienceDirect

Analytica Chimica Acta

journal homepage: www.elsevier.com/locate/aca

Detection of hexavalent chromium using gold/4-(2-mercaptoethyl) pyridinium surface enhanced Raman scattering-active capture matrices

P.A. Mosier-Boss*, M.D. Putnam

SPAWAR Systems Center Pacific, Code 71730, San Diego, CA 92152, United States

HIGHLIGHTS

- We prepared capture matrices specific for hexavalent chromium.
- Capture matrices were prepared by immobilizing gold colloidal particles on amine-derivatized magnetic microparticles.
- The gold colloid was reacted with a thiol to form a SAM selective for hexavalent chromium.
- The thiol was 4-(2-mercaptoethyl) pyridinium (MEP) hydrochloride.
- The SERS response of the capture matrices was compared to that of conventional SERS substrates.

GRAPHICAL ABSTRACT

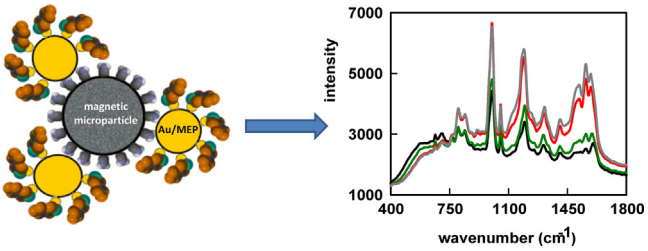

ARTICLE INFO

Article history:
Received 22 April 2013
Received in revised form 2 September 2013
Accepted 5 September 2013
Available online 12 September 2013

Keywords:
Surface enhanced Raman scattering spectroscopy
Hexavalent chromium
Capture matrices

ABSTRACT

In this communication, the fabrication of SERS-active capture matrices for the detection of hexavalent chromium is described. The amine groups of amine-modified magnetic microparticles were used to immobilize gold colloidal particles. Once immobilized, the gold was reacted with 4-(2-mercaptoethyl) pyridinium (MEP) hydrochloride to form a self-assembled monolayer (SAM). The MEP SAM exhibits great selectivity for hexavalent chromium. It was shown that calibration curves could be generated by ratioing MEP peaks that increased in intensity upon complexation with chromate with a peak that did not change. Flow experiments, using Au/MEP capture matrices held in place by a magnet, showed instantaneous response to changes in chromate concentration.

Published by Elsevier B.V.

1. Introduction

Hexavalent chromium, Cr(VI), has been used in hard-chromium plating of structural components of ships and planes; as conversion coatings and primers to protect aluminum aircraft alloys; and in electrochemical processes to thicken and toughen the naturally occurring protective elements in aluminum parts [1]. Hexavalent chromium is a strong oxidizer and is both highly toxic and carcinogenic [2,3]. It is very water soluble and has little interaction with the soil. Consequently, this pollutant is mobile and has resulted in widespread groundwater contamination. Chromium contamination is present in over half of the superfund sites. Recently, the Environmental Working Group (EWG) issued a report showing widespread occurrence of hexavalent chromium in tap water across the US [4]. It is believed that this report will result in increased requirements on monitoring surface and subsurface waters for the presence of hexavalent chromium.

Currently monitoring of hexavalent chromium is done by conventional soil and water sampling followed by laboratory analysis using ion chromatography (IC) followed by a post column reaction

* Corresponding author. Tel.: +1 619 553 1603.
E-mail address: pam.boss@navy.mil (P.A. Mosier-Boss).

0003-2670/$ – see front matter. Published by Elsevier B.V.
http://dx.doi.org/10.1016/j.aca.2013.09.006

with diphenylcarbohydrazide (DPC) [5]. This method of monitoring is time consuming and is not field deployable. Direct push sensors using either X-ray fluorescence (XRF) or laser induced breakdown spectroscopy (LIBS) have been developed to detect heavy metals such as lead and chromium [6]. However, these sensors cannot differentiate between Cr(VI), Cr(III), or metallic Cr. Although these direct push probes can be used to detect the total amount of chromium in the subsurface as a function of depth without the need of reagents, the limit of detection (depending upon the soil type) is on the order of 100 ppm or higher. This limit of detection is significantly higher than the federal government's current total chromium standard of 100 ppb [7]. While these direct push sensors are good for real-time, in situ, site characterization, they are not ideal for long-term monitoring.

For long term monitoring purposes, it would be desirable to detect hexavalent chromium in samples on-site in near real time so as to minimize sample handling, processing and costs. It would also be desirable to detect hexavalent chromium in the low ppb concentration range with little or no sample preparation and with no interferences. One technology that meets many of these criteria is SERS using chemically modified silver/gold substrates. The coatings used on the SERS substrate are chosen to attract the analyte of interest. The advantages of SERS using chemically derivatized substrates are: (i) all polyatomic species exhibit a characteristic SERS spectrum, (ii) the SERS lines are narrow allowing simultaneous detection of multiple polyatomic species, (iii) SERS can result in a 10^5–10^{10} enhancement of the Raman signal, (iv) water is a very poor Raman scatterer and does not interfere, and (v) the selective coating also exhibits SERS lines that can be used as an internal standard. The main limitation of the SERS technology has to do with the coating itself. The sensitivity of SERS to detect the desired analyte is dependent upon the selectivity of the coating for that analyte. However, there is a trade off between selectivity and reversibility. The stronger the interaction between an analyte and the coating, the greater the selectivity of the coating for that analyte and the greater the sensitivity. However, reversibility is sacrificed. The only practical way to address this trade off is to provide a fresh SERS-active surface between sampling.

Earlier we demonstrated that SERS-active substrates could be fabricated by immobilizing silver/gold colloidal particles on amine-derivatized magnetic microspheres to form SERS-active capture matrices [8]. We showed that the colloidal particles could be reacted with a thiol to form a self-assembled monolayer (SAM). In this earlier investigation, we demonstrated the detection of naphthalene using pentachlorothiophenol-derivatized, SERS-active capture matrices. Besides providing a fresh SERS surface between sampling, additional advantages of capture matrices in chemical detection are extraction/concentration of the target analyte from a complex sample matrix, ease of separation, and suitability for automation.

In order to detect hexavalent chromium using SERS-active capture matrices, a coating selective for hexavalent chromium needs to be identified. Earlier Turyan and Mandler [9] used 4-(2-mercaptoethyl) pyridinium (MEP) hydrochloride to detect hexavalent chromium by square wave voltammetry (SWV). MEP binds to the Au surface through its sulfhydryl group to form a SAM. This Au/MEP electrode was used to preconcentrate chromate on the electrode surface prior to detection/quantification by cathodic SWV. Turyyan and Mandler showed that the analysis of 0.1 ppb Cr(VI) was not affected by the presence of a 1000-fold excess of Cr(III). They also showed that the anions chloride, nitrate, phosphate, acetate and perchlorate did not interfere in the detection of chromate.

The use of conventional Au/MEP substrates to detect chromate by SERS has also been demonstrated [10]. It was shown that, when the chromate concentration is in M, the concentration response is described by a Frumkin isotherm. The shape of the Frumkin isotherm is determined by two parameters – K, the ion-pair constant between the anion and the coating, and g, the Frumkin parameter that takes into account interactions between adsorbed species. Measurements were also done for other anions [11]. The selectivity for MEP for anions, as measured by SERS was (ion pair constants are indicated): CrO_4 = (K = 142 700) ⋙ CN^- (K = 1090) ≫ Cl^- (K = 92) > ClO_4^- (K = 38) »» $SO_4^=$, NO_3^-, $H_2PO_4^-$ (K = 0). Molecular modeling of the SAM showed the presence of microcavities between adjacent MEP moieties on the SERS surface with a three-dimensional structure complementary in both shape and chemical functionality to that of the chromate anion [11]. This complementary three-dimensional structure is responsible for the high selectivity of the MEP SAM for chromate.

Both the earlier SWV [9] and SERS [10] work indicate that MEP is a highly selective coating for the detection of hexavalent chromium. In this communication, we describe the fabrication of SERS-active Au/MEP capture matrices and discuss their use to detect hexavalent chromium.

2. Experimental

2.1. Reagents

Hydrogen tetrachloroaurate (III) trihydrate (Aldrich), sodium citrate (Aldrich), sodium chromate (Aldrich), potassium chloride (Aldrich), 4-(2-mercaptoethyl) pyridinium (MEP) hydrochloride (Toronto Research Chemicals), water (HPLC grade, Aldrich), and ethanol (HPLC grade, Aldrich) were used as received. Aqueous solutions of chromate were prepared using deionized water.

A 0.5 mL aliquot of 5 wt% BioMag, amine-terminated, superparamagnetic, microparticles (Bangs Laboratory, part no. BM546) was washed ten times with 1 mL aliquots of HPLC water to remove surfactant. Between washes, a NdFeB magnet is used to separate the magnetic microparticles from the water. After the washes, the volume of the amine-terminated, magnetic microparticles was adjusted to 1.0 mL.

2.2. Preparation of conventional Au/MEP SERS substrates

An insulated copper wire was soldered to a 0.75-cm length of 2 mm diameter gold wire (Aldrich, 99.9%). The gold wire was potted inside a 5-mm outer diameter, borosilicate glass tube using a chemically resistant epoxy (Epoxy Patch 1C, Hysol). Prior to use, the gold disk of the electrode was electrochemically roughened in a 0.1 M KCl solution using a PAR 273A potentiostat/galvanostat under computer control. The gold surface was roughened by cycling the electrode potential 25 times between −280 mV (holding 10 s) and 1220 mV (holding 5 s) at a sweep rate of 500 mV s^{-1}. After electrochemical roughening, the gold electrode was rinsed with water (HPLC grade, Aldrich) and then ethanol (HPLC grade, Aldrich). The electrode was immersed in a dilute solution of MEP in ethanol and allowed to react for ∼24 h to form a SAM. Before use, the electrode was rinsed thoroughly with ethanol and water.

2.3. Preparation of gold colloid

An aqueous solution of 100 mL of 0.01% (g mL^{-1}) of hydrogen tetrachloroaurate (III) trihydrate, in a 250 mL round bottom flask equipped with a condenser, was brought to a vigorous boil. Once boiling, 0.85 mL of 1% sodium citrate was added. After 40 min of refluxing, the solution had changed from a light yellow color to red-violet. The flask was removed from the heat and allowed to cool to room temperature. The colloidal suspension was then concentrated, by centrifugation, to a final volume of ∼2 mL.

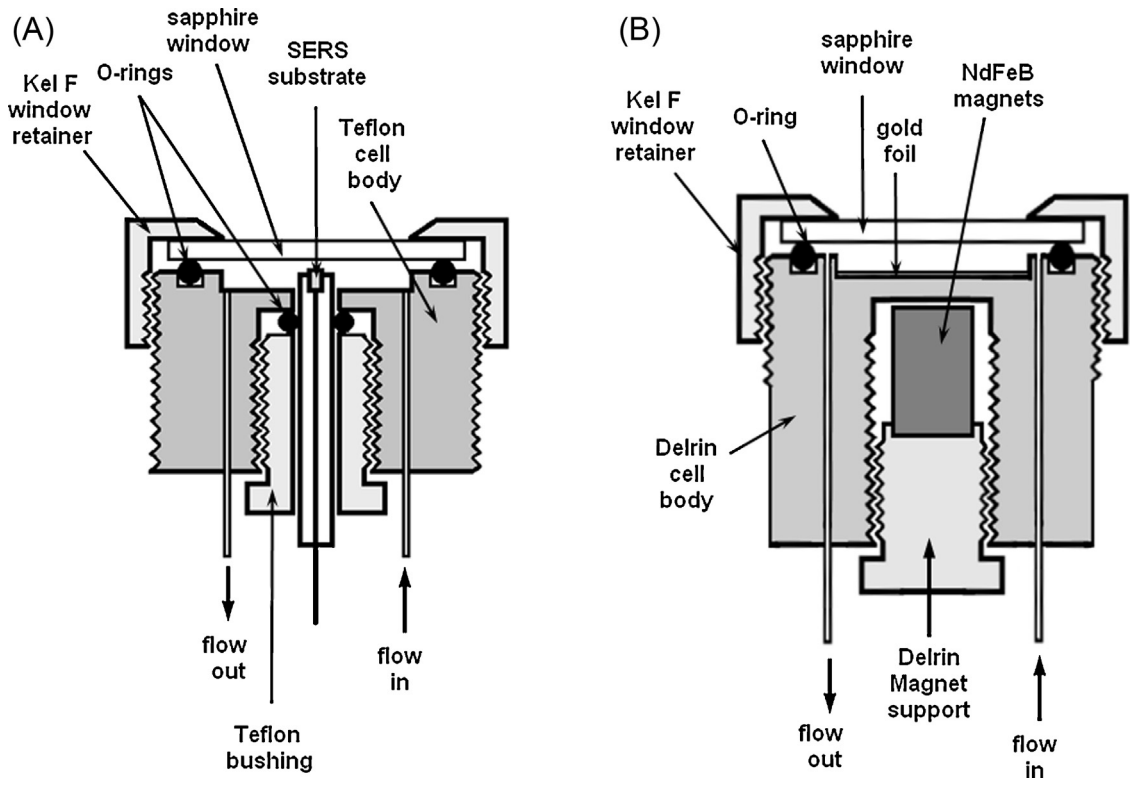

Fig. 1. Schematics of (a) the cell used to measure the concentration response of conventional Au/MEP SERS substrates to chromate and (b) the cell used to evaluate the response of Au/MEP capture matrices to chromate.

2.4. Preparation of Au/MEP capture matrices

A 100 μL aliquot of the washed, amine-terminated, magnetic microparticles was pipetted into a glass vial containing 1 mL of water (HPLC grade, Aldrich). A 200 μL aliquot of the concentrated gold colloidal suspension was added to the glass vial and the vial was placed on a roller. The amine groups of the magnetic microparticles bind to the gold colloidal particles. After rolling for 2 h, a NdFeB magnet was used to separate the microparticles from the liquid. If the liquid was clear, half the volume was removed and another 200 μL aliquot of the concentrated gold colloidal suspension was added to the glass vial and placed on the roller. The process was repeated until the surface of the magnetic microparticles was completely covered with colloidal gold particles as indicated when the liquid remained red-violet in color. The Au-covered, magnetic microparticles were then washed three times with water (HPLC grade, Aldrich) and then three times with ethanol (HPLC grade, Aldrich). Between washings, a NdFeB magnet is used to separate the Au-covered magnetic microparticles. Afterwards a dilute ethanolic solution (~0.09 M) of MEP was added to the glass vial. The MEP was allowed to react with the immobilized gold colloidal particles for ~24 h to form a SAM. The Au/MEP capture matrices were then washed three times in ethanol, as described above. The volume of the Au/MEP capture matrices was adjusted to 1 mL using ethanol.

2.5. Evaluation of the SERS substrates

SERS measurements of the conventional Au/MEP substrate and the Au/MEP capture matrices were made using the Snowy Range Instruments Sierra portable Raman system. The system has a 785 nm laser that can operate at 100 mW and a 3000 element, linear, cooled, NIR enhanced CCD array, dispersive spectrometer (operational range is 200–3200 cm^{-1} and resolution is 10 cm^{-1}). This particular system has three-way sampling for side, bottom, and point and shoot. To evaluate the conventional SERS substrates and the capture matrices, the instrument was operated in the point and shoot mode.

A schematic of the flow-through cell to evaluate the concentration response of the conventional Au/MEP SERS substrate to chromate is shown in Fig. 1a. The body of the flow-through cell is constructed of Teflon®. A 25 mm diameter, 2 mm thick sapphire disk was used as the optically transparent window. A Kel-F window retainer holds the window in place. An O-ring provides a leak-tight seal between the window and the cell body. A Teflon® bushing holds the SERS substrate in place. A second O-ring provides a leak-tight seal around the glass tube of the SERS substrate. The inlet and outlet consist of 20 gauge stainless steel tubes that have been epoxied in place using a chemically resistant epoxy (Epoxy Patch 1C, Hysol). The volume of the cell is ~0.5 mL. For SERS measurements, the flow-through cell was held in place below the point and shoot optics of the spectrometer with the "Opti-Claw" optical mount (New Focus, part no. 9832) mounted on an *x*,*y*,*z*-translation stage (Newport Corporation, part no. 460A).

To evaluate the chromate concentration response of Au/MEP capture matrices, a 75 μL aliquot of the capture matrices were pipetted into a glass vial. A NdFeB magnet was used to separate the capture matrices from the ethanol. The capture matrices were washed three times with 0.5 mL of water. A NdFeB magnet was used to separate the capture matrices from the liquid between washes. Afterwards a 1 mL aliquot of an aqueous chromate solution of a known concentration was added to the vial. The sample was allowed to equilibrate overnight. Afterwards, a syringe was used to transfer the capture matrices to a glass, 1.1–1.2 mm ID melting point tube (Corning part no. 9530-2) and flame sealed. Prior to SERS measurement, a NdFeB magnet was used to concentrate the capture matrices in one spot inside the glass tube. The sample was placed on a flat surface, that was mounted on an *x*,*y*,*z* translation stage (Newport Corporation, part no. 460A). The sample was then placed below the point and shoot optics of the spectrometer.

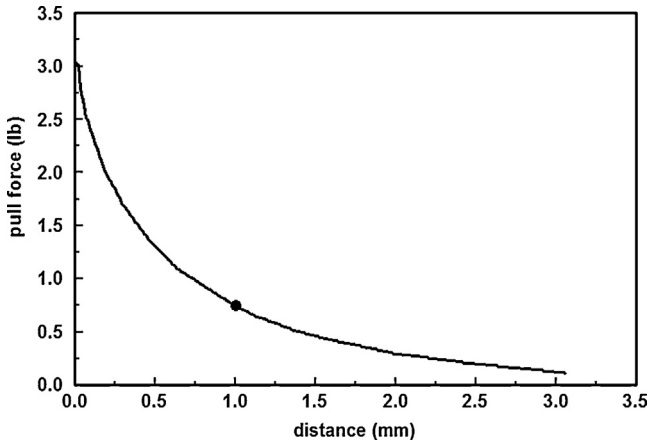

Fig. 2. Magnetic pull force as a function of distance calculated for the NdFeB magnets used in the cell shown in Fig. 1b where ● shows the separation between the magnets and the Au foil surface of the cell.

A schematic of the flow-through cell to evaluate the concentration response of Au/MEP SERS active capture matrices to chromate is shown in Fig. 1b. The body of the flow-through cell is constructed of Delrin®, which is harder than Teflon®. A harder plastic is required to minimize the distance between the NdFeB magnets and the detection surface of the cell body. A chemically resistant epoxy (Epoxy Patch 1C, Hysol) was used to epoxy a gold foil on the inside surface of the cell, as shown in Fig. 1b. A 25 mm diameter, 2 mm thick sapphire disk was used as the optically transparent window. A Kel-F window retainer holds the window in place. An O-ring provides a leak-tight seal between the window and the cell body. The inlet and outlet consist of 20 gauge stainless steel tubes that have been epoxied in place using a chemically resistant epoxy (Epoxy Patch 1C, Hysol). A Delrin® support holds two NdFeB magnets (part number ZD6, K&J Magnetics) below the gold-covered sample surface as shown in Fig. 1b. The distance between the surface of the magnets and the gold covered sample surface is ~1 mm. Fig. 2 shows a plot of the pull force of the magnets calculated as a function of distance [12]. As shown in Fig. 2, the pull force of the magnet decreases as the distance between the capture matrices and the magnet increases. For a distance of 1 mm, the pull force of the magnets is 0.78 lb. This pull force was found to be sufficient to hold the capture matrices in place when chromate solution was flowed through the cell. For SERS measurements, the flow-through cell was held in place below the point and shoot optics of the spectrometer with the "Opti-Claw" optical mount (New Focus, part no. 9832) mounted on an *x*,*y*,*z*-translation stage (Newport Corporation, part no. 460A).

All manipulations of the spectral data were done using GRAMS/AI7 (Thermogalactic), a software package that can be used to subtract spectra interactively as well as integrate peak areas and measure peak heights.

3. Results and discussion

3.1. Conventional Au/MEP SERS substrate

SERS spectra were obtained using a conventional Au/MEP substrate. These spectral results were used to evaluate the performance of the Au/MEP capture matrices. To obtain the SERS spectra, the conventional Au/MEP substrate was mounted in the cell shown in Fig. 1a. The cell was filled with water and the substrate was scanned in the *x*, *y*, and *z* directions to optimize the signal. Once optimized, the cell was locked in place and all spectra were obtained at this fixed location on the substrate. A reference spectrum was obtained with the cell filled with water. The water was then sequentially replaced with solutions of varying concentrations of chromate, going from the lowest chromate concentration to the highest. The response of the MEP coating to chromate was instantaneous.

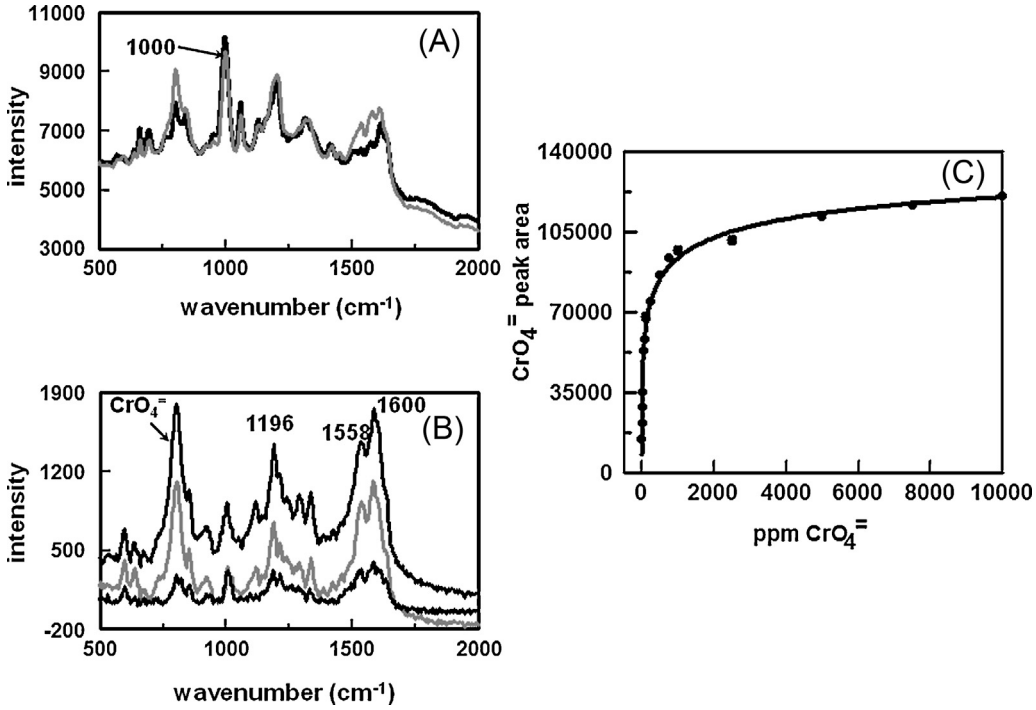

Fig. 3. (a) SERS spectra of a conventional Au/MEP SERS substrate obtained at chromate concentrations of 0 (black) and 2500 (gray) ppm. Spectra were obtained using 785 nm excitation at 30 mW and averaging ten 2 s spectra. (b) Difference spectra obtained by subtracting the 0 ppm spectrum from the 1 (bottom), 100 (middle), and 500 (top) ppm chromate Au/MEP spectra. The chromate peak is indicated. (c) Plot of chromate peak area as a function of chromate concentration. Equation describing the curve is summarized in Table 1.

Table 1
Summary of the equations that describe the observed calibration curves.

Curve	Equation describing curve[a]	R^2	Values of parameters
Fig. 3c	$y = c + a(1 - \exp(-bx^{0.2}))$	0.9879	$a = 188\,000 \pm 6000$ $b = 0.346 \pm 0.047$ $c = -47\,100 \pm 9400$
Fig. 5a and b	$y = c + a(1 - \exp(-bx^{0.3}))$	0.9894	$a = 0.546 \pm 0.029$ $b = 0.143 \pm 0.021$ $c = 0.360 \pm 0.017$
Fig. 6a and b	$y = c + a(1 - \exp(-bx^{0.5}))$	0.9923	$a = 0.567 \pm 0.036$ $b = 0.176 \pm 0.024$ $c = 0.269 \pm 0.024$
Fig. 7c	$y = ax^2 + bx + c$	0.9975	$a = -1200 \pm 290$ $b = 7630 \pm 790$ $c = -126 \pm 470$
Fig. 7d, 1196 cm^{-1} MEP peak	$y = ax^2 + bx + c$	0.9978	$a = -30 \pm 9$ $b = 220 \pm 23$ $c = -3 \pm 13$
Fig. 7d, 1558 cm^{-1} MEP peak	$y = ax^2 + bx + c$	0.9992	$a = -2 \pm 9$ $b = 297 \pm 16$ $c = -53.6 \pm 6.0$
Fig. 7d, 1600 cm^{-1} MEP peak	$y = ax^2 + bx + c$	0.9996	$a = -2 \pm 9$ $b = 391 \pm 15$ $c = -75.4 \pm 5.5$
Fig. 8b, 1196 cm^{-1} MEP peak	$y = ax + b$	0.9778	$a = 0.0176 \pm 0.0022$ $b = 0.6180 \pm 0.0037$
Fig. 8b, 1558 cm^{-1} MEP peak	$y = ax^2 + bx + c$	0.9964	$a = -0.0295 \pm 0.0057$ $b = 0.147 \pm 0.015$ $c = 0.4049 \pm 0.0091$
Fig. 8b, 1600 cm^{-1} MEP peak	$y = ax^2 + bx + c$	0.9991	$a = -0.0154 \pm 0.0022$ $b = 0.0993 \pm 0.0060$ $c = 0.4747 \pm 0.0036$

[a] In the equations, y is either the chromate peak area or the ratio of peak intensities and x is ppm chromate.

Fig. 3a shows SERS spectra of a conventional Au substrate coated with MEP at chromate concentrations of 0 and 2500 ppm. Additional spectra are shown in Fig. S1 of the supplementary material. When exposed to chromate, a peak due to the symmetric and asymmetric Cr—O stretching modes of chromate grows in at ~835 cm^{-1}. The chromate peak overlaps with peaks due to the MEP coating. To determine the chromate peak area, the spectral contributions of the coating need to be subtracted out. As shown in Figs. 3a and S1, the spectra exhibit similar baselines and the spectral peaks lineup. Under these circumstances, the spectral contributions of the reference spectrum can be subtracted out resulting in the difference spectra shown in Fig. 3b. Experience has shown that when these conditions are not met, such as in those instances when the cell has moved and another area of the SERS substrate is being interrogated, spectral subtraction of the reference spectrum does not result in well defined peaks whose areas can be measured. An example of a difference spectrum obtained for a Au/MEP substrate that had moved after the reference spectrum was obtained is shown in Fig. S2 of the supplementary material. The difference spectrum does not show a clean chromate peak.

Supplementary material related to this article can be found, in the online version, at http://dx.doi.org/10.1016/j.aca.2013.09.006.

Supplementary material related to this article can be found, in the online version, at http://dx.doi.org/10.1016/j.aca.2013.09.006.

Difference spectra were obtained by subtracting the reference spectrum from the spectra obtained in the presence of chromate. These difference spectra are shown in Fig. 3b. In the difference spectra, the broad band due to chromate is indicated. The difference spectra also show increased intensity of the MEP peaks at 1196, 1558 and 1600 cm^{-1}. These peaks are primarily assigned to the pyridine ring vibrational modes [12]. The intensity changes indicate that the chromate anion is interacting with the pyridine ring of MEP. Molecular modeling showed that hydrogen bonding was occurring between the chromate oxygens and pyridine ring protons and that this hydrogen bonding was responsible for the observed changes in the bands due to pyridine [12]. The raw and difference spectra show that the one MEP peak that is not dramatically affected by the presence of chromate is the peak at ~1000 cm^{-1}. This peak is due to a ring breathing mode of the pyridinium ion.

A plot of chromate peak area as a function of chromate concentration is shown in Fig. 3c. This is the calibration curve. At low chromate concentration, the chromate peak area increases with concentration. At higher chromate solution concentrations, the response levels off as the adsorption sites on the MEP SAM become fully occupied. The equation that describes this curve is summarized in Table 1.

3.2. Au/MEP SERS-active capture matrices

Fig. 4 shows SERS spectra measured for individual samples of Au/MEP capture matrices and chromate solutions that had been sealed in melting point tubes. It can be seen that the intensities of the peaks due to MEP and chromate vary as do the baselines. As discussed vide supra, because of these variabilities between the spectra obtained for the individual samples, it is not possible to do spectral subtractions to obtain the chromate peak area. However, Crane et al. [13] showed that it was possible to use SERS to obtain adsorption isotherms for 4-(2-pyridylazo)resorcinol (PAR) with Pb^{2+}, Cu^{2+}, and Cd^{2+} metal ions that do not exhibit Raman active bands by ratioing the intensities of a PAR Raman peak that varied upon complexation to one that did not. The use of this approach to generate calibration curves for both the Au/MEP conventional substrate and capture matrices was explored.

In Fig. 3a, the MEP band at 1000 cm^{-1} minimally varies as a function of chromate concentration. The MEP peaks at 1196, 1558, and 1600 cm^{-1} increase in intensity with increasing chromate concentration, Fig. 3b. The intensities of the 1196, 1558, and 1600 cm^{-1} MEP peaks were then ratioed to the 1000 cm^{-1} MEP peak. The results of ratioing the 1196 and 1600 cm^{-1} MEP peak to the 1000 cm^{-1} MEP peak for the conventional Au/MEP substrate are

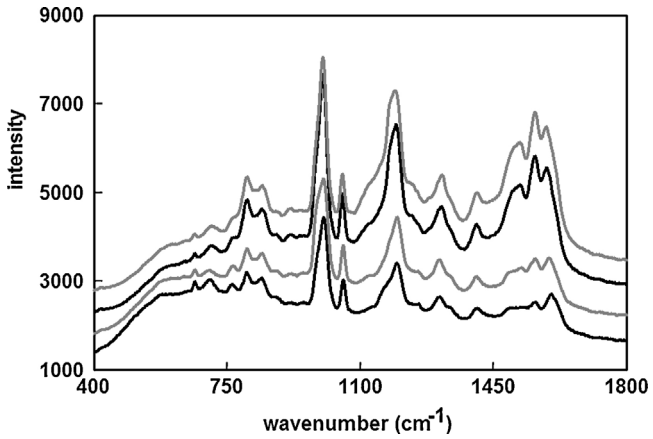

Fig. 4. SERS spectra of Au/MEP capture matrices immersed in solutions of (bottom to top) 0, 5, 50, and 1000 ppm chromate. Capture matrices and solution were sealed in glass melting point tubes. A magnet was used to concentrate the capture matrices in a single spot. SERS spectra were obtained using 785 nm excitation at 21 mW and averaging ten 1 s spectra.

shown in Fig. S3 of the supplementary material. Fig. 5 summarizes the results obtained by ratioing the 1558 cm^{-1} MEP peak to the 1000 cm^{-1} MEP peak. Fig. 5a covers the chromate concentration range 0–10 000 ppm and Fig. 5b covers the chromate concentration range 0–100 ppm. The equation that describes this curve is summarized in Table 1. The calibration plots show that, at low chromate concentrations, the ratio increases with increasing chromate concentration. At higher chromate concentrations (≥100 ppm chromate) the ratio levels off as chromate fully occupies the sites on the MEP coating. The results in Figs. 5 and S3, supplementary material, shows that reasonable calibration curves can be obtained by ratioing MEP peaks that change upon complexation to one that does not.

Supplementary material related to this article can be found, in the online version, at http://dx.doi.org/10.1016/j.aca.2013.09.006.

The ratioing approach to generate calibration curves was then applied to the Au/MEP capture matrices. The results ratioing the 1196 and 1600 cm^{-1} MEP peak to the 1000 cm^{-1} MEP peak for the Au/MEP capture matrices are shown in Fig. S4 of the supplementary material. Fig. 6 summarizes the results obtained by ratioing the 1558 cm^{-1} MEP peak to the 1000 cm^{-1} MEP peak. Fig. 6a covers the concentration range 0–1000 ppm chromate while Fig. 6b covers the 0–50 ppm concentration range. The equation that describes this curve is summarized in Table 1. It can be seen that the results in Fig. 6 obtained for the Au/MEP capture matrices are very similar to what was observed for the Au/MEP conventional SERS substrate, Fig. 5, and shows that the ratioing method can be used to obtain reasonable calibration curves for the capture matrices. For both sets of curves shown in Figs. 5 and 6, the low concentration region shows a nonlinear correlation with concentration. The purpose of showing the signal response at high chromate concentration was to show that the response levels off as the sites on the coating become fully occupied with chromate anions.

Supplementary material related to this article can be found, in the online version, at http://dx.doi.org/10.1016/j.aca.2013.09.006.

In another experiment, a single 50 μL aliquot of the Au/MEP capture matrices was pipetted onto a small spot in the center of the gold foil of the flow through cell shown in Fig. 1b. NdFeB magnets held

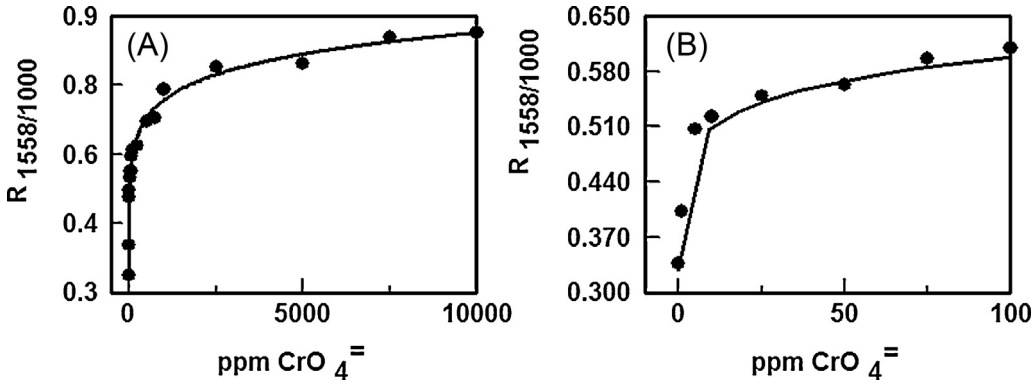

Fig. 5. Plots of the MEP peak intensity at 1558 cm^{-1} ratioed to the 1000 cm^{-1} peak as a function of chromate concentration, for the conventional Au/MEP SERS substrate. Chromate concentration ranges are (a) 0–10 000 ppm and (b) 0–100 ppm. Equation describing the curves is summarized in Table 1.

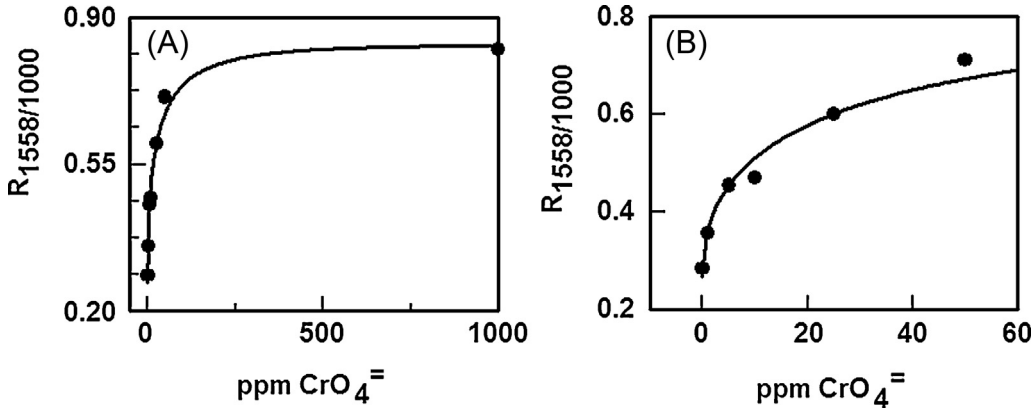

Fig. 6. Plots of MEP peak intensity at 1558 cm^{-1} ratioed to the 1000 cm^{-1} peak as a function of chromate concentration for Au/MEP SERS active capture matrices. Chromate concentration ranges are (a) 0–1000 ppm and (b) 0–50 ppm. Equation describing the curves is summarized in Table 1.

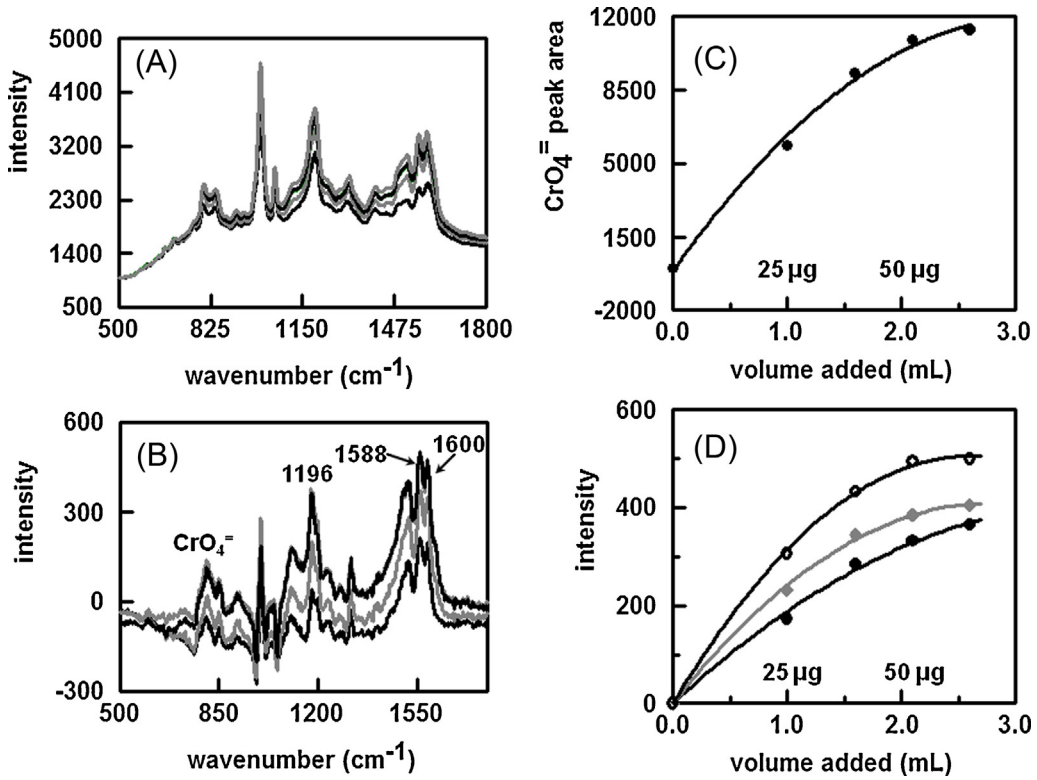

Fig. 7. (a) SERS spectra of Au/MEP capture matrices in the cell shown in Fig. 1b measured as a function of volume of 25 ppm chromate solution flowing through the cell. Spectra were obtained using 785 nm excitation at 30 mW and averaging ten 1 s spectra. (b) Difference spectra obtained by subtracting the 0 ppm spectrum from the 1, 1.6, 2.1, and 2.6 mL of 25 ppm chromate Au/MEP spectra. (c) Plot of chromate peak area as a function of volume of 25 ppm chromate solution. (d) Plot of intensities of MEP peaks at 1196 (●), 1558 (◆), and 1600 (○) cm^{-1} as a function of volume of 25 ppm chromate solution. For both (c) and (d), the mass quantity of chromate that flowed over the capture matrices is indicated. Equations describing the curves are summarized in Table 1.

the capture matrices stationary as a 25 ppm chromate solution was flowed through the cell. Fig. 7a shows SERS spectra of the capture matrices as the chromate solution is flowed through the cell. The chromate peaks between 700 and 900 cm^{-1} were observed to grow in as the chromate solution flowed over the immobilized Au/MEP capture matrices. Likewise increases in the intensities of the MEP peaks at 1196, 1558, and 1600 cm^{-1} were observed. The increase in intensity of these MEP peaks indicates that the MEP is complexing with chromate. These observed responses were instantaneous. Because the capture matrices are held in a fixed spot, the same sample area was interrogated by the laser as the 25 ppm chromate solution was flowed over the Au/MEP capture matrices. It can be seen that the baselines of the spectra are identical and the peaks line up. Under these conditions, spectral subtractions can be done which will give meaningful results. Fig. 7b shows the difference spectra obtained when the spectral contributions of the uncomplexed MEP coating are subtracted out. The results were similar to the difference spectra obtained for the conventional Au/MEP SERS substrate, Fig. 3b. A plot of chromate peak area as a function of chromate solution volume is shown in Fig. 7c. The chromate peak area increased linearly as the capture matrices extracted chromate from the solution and then began to level off as the sites on the MEP SAM are becoming fully occupied. Similar plots were obtained by plotting the intensities of the MEP peaks at 1196, 1588, and 1600 cm^{-1} of the difference spectra, Fig. 7b, as a function of chromate solution volume, Fig. 7d. Also similar plots can be obtained

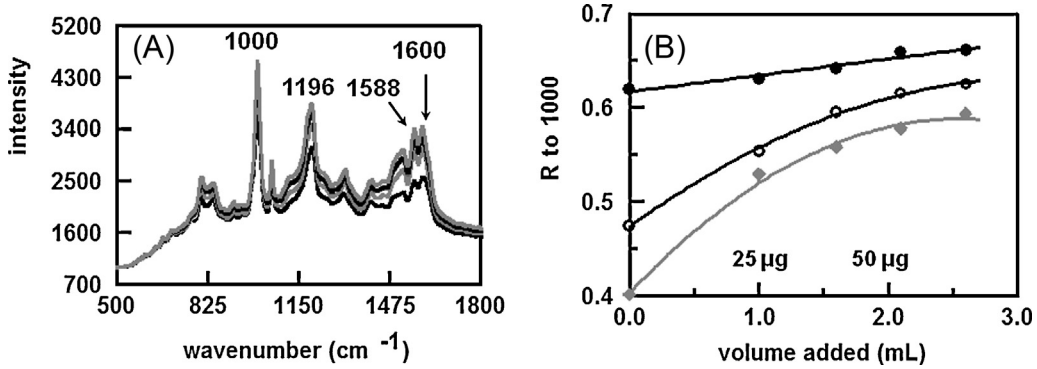

Fig. 8. (a) SERS spectra of Au/MEP capture matrices in the cell shown in Fig. 1b measured as a function of volume of 25 ppm chromate solution flowing through the cell. Spectra were obtained using 785 nm excitation at 30 mW and averaging ten 1 s spectra. (b) Plots of MEP peak intensities at 1196 (●), 1558 (◆), and 1600 (○) ratioed to the 1000 cm^{-1} peak as a function of volume of 25 ppm chromate solution. The mass quantity of chromate that flowed over the capture matrices is indicated in the figure. Equations describing the curves are summarized in Table 1.

by plotting the peak ratios, as described vide infra, as a function of solution volume, Fig. 8b. The equations describing the plots shown in Figs. 7c and d, and 8b are summarized in Table 1.

Using conventional Au/MEP SERS substrates, the limit of detection for chromate was found to be 59 ppb [10]. The results summarized in Figs. 7 and 8 show that the Au/MEP capture matrices are extracting/preconcentrating chromate as the solution flows over them. These capture matrices will continue to extract chromate from solution until the adsorption sites of the MEP coating on the Au colloidal particles become fully occupied. Therefore it is expected that chromate detection limits lower than 59 ppb would be possible using capture matrices. These lower detection limits would be achieved by simply exposing the capture matrices to larger volumes of sample. This has not been demonstrated at this time as we are working on better means of mixing the capture matrices with the sample to improve the extraction efficiency. However, this was demonstrated by both Šafařík and Šafaříková [14] and Shishehbore et al. [15] Šafařík and Šafaříková [14] used copper phthalocyanine modified magnetic microparticles to extract low ppb concentrations of malachite green and crystal violet from 1000 mL water samples prior to their detection by spectrophotometry. Likewise Shishehbore et al. [15] used salicylic acid derivatized magnetic microparticles to extract Cu(II), Cd(II), Ni(II), and Cr(III) ions from up to 800 mL of water prior to detection of these metal ions, in the low ppb concentration range, by flame atomic absorption spectrometry. Both Šafařík and Šafaříková and Shishehbore et al. showed that the efficiency of the analyte extraction was dependent upon the contact time of the sample with the capture matrices. To improve the probability of contact between the analyte and the capture matrices, Shishehbore et al. [15] used ultrasonication for 10 minutes to disperse the capture matrices in the aqueous samples while Šafařík and Šafaříková [14] stirred their samples for 4 h after adding their capture matrices.

4. Conclusions

In this communication, we have shown that capture matrices specific for hexavalent chromium can be fabricated by reacting gold colloidal particles, immobilized on amine-derivatized magnetic microparticles, with 4-(2-mercaptoethyl) pyridinium (MEP) hydrochloride. The resultant capture matrices were SERS active and it was shown that the SERS response obtained for the Au/MEP capture matrices was similar to that observed for conventional Au/MEP SERS substrates. It was shown that calibration curves could be generated by ratioing MEP peaks that increased in intensity upon complexation with chromate with a peak that did not change. The experiment in which the Au/MEP capture matrices were rigidly held in place demonstrated that the capture matrices instantaneously extract chromate from the flowing solution.

The use of derivatized magnetic microparticles in trace chemical analysis is growing [16]. Magnetic particles possess a high surface area which can exhibit higher adsorption capacity for analytes. They also exhibit strong superparamagnetic properties which meets the need of rapid extraction of large volume samples by employing a strong external magnetic field. These derivatized magnetic microparticles can be used in both solutions and suspensions. Since the majority of accompanying impurities in a suspension are diamagnetic, they do not interfere with magnetic particles during the magnetic separation step. These advantages would also apply to the SERS-active Au/MEP capture matrices described in this communication. Another advantage of the SERS-active capture matrices has to do with the fact that the derivatized magnetic particles used by others [14–16] require elution of the analyte off the magnetic particles prior to detection. This elution step is not required for the SERS active capture matrices. In fact elution of the analyte would be counterproductive as the SERS enhancement of both the coating and the analyte is caused by the Au colloidal particles immobilized on the capture matrices.

Acknowledgment

This effort was funded by the SSC Pacific Naval Innovative Science and Engineering (NISE) program.

References

[1] http://www.denix.osd.mil/cmrmd/ECMR/HexChrome/TheBasics.cfm
[2] R.J. Kieber, J.D. Willey, S.D. Zvalaren, Environ. Sci. Technol. 36 (2002) 5321–5327.
[3] A.M. Babyak, Six Emergent Chemicals – Toxicology and Regulatory Issues, in: GRA Symposium, October 9, 2003, 2003.
[4] "EPA Addresses Chromium (VI) in Drinking Water" C&EN 2011, 89(1), 16.
[5] EPA Method 218.7: De67termination of Hexavalent Chromium in Drinking Water by Ion Chromatography with Post-Column Derivatization and UV–Visible Spectroscopic Detection, EPA Document No. EPA 815-R-11-005, November 2011.
[6] S.H. Lieberman, P.A. Boss, J. Cortes, W.T. Elam, Site Characterization and Analysis Penetrometer System (SCAPS) Heavy Metal Sensors Demonstration/Validation: Technology Demonstration Report. ESTCP Technical Report 1868, December 2001.
[7] http://www.cbsnews.com/stories/2010/12/22/politics/main7174717.shtml
[8] P.A. Mosier-Boss, S.H. Lieberman, Anal. Chem. 77 (2005) 1031–1037.
[9] I. Turyan, D. Mandler, Anal. Chem. 69 (1997) 894–897.
[10] P.A. Mosier-Boss, S.H. Lieberman, Appl. Spectrosc. 57 (2003) 1129–1137.
[11] P.A. Mosier-Boss, S.H. Lieberman, Langmuir 19 (2003) 6826–6836.
[12] http://www.kjmagnetics.com/calculator.asp
[13] L.G. Crane, D.X. Wang, L.M. Sears, B. Heyns, K. Carron, Anal. Chem. 67 (1995) 360–364.
[14] I. Šafařík, M. Šafaříková, Water Res. 36 (2002) 196–200.
[15] M.R. Shishehbore, A. Afkhami, H. Bagheri, Chem. Central J. 5 (2011) 41–50.
[16] M. Šafaříková, I. Šafařík, Eur. Cells Mater. 3 (2002) 192–195.

Figure S1. SERS spectra obtained for a conventional Au/MEP SERS substrate as a function of chromate concentration. Chromate concentrations (bottom to top) are 0, 1, 10, 25, 100, 500, and 2500 ppm. Spectra were obtained using 785 nm excitation at 30 mW and averaging ten 2s spectra.

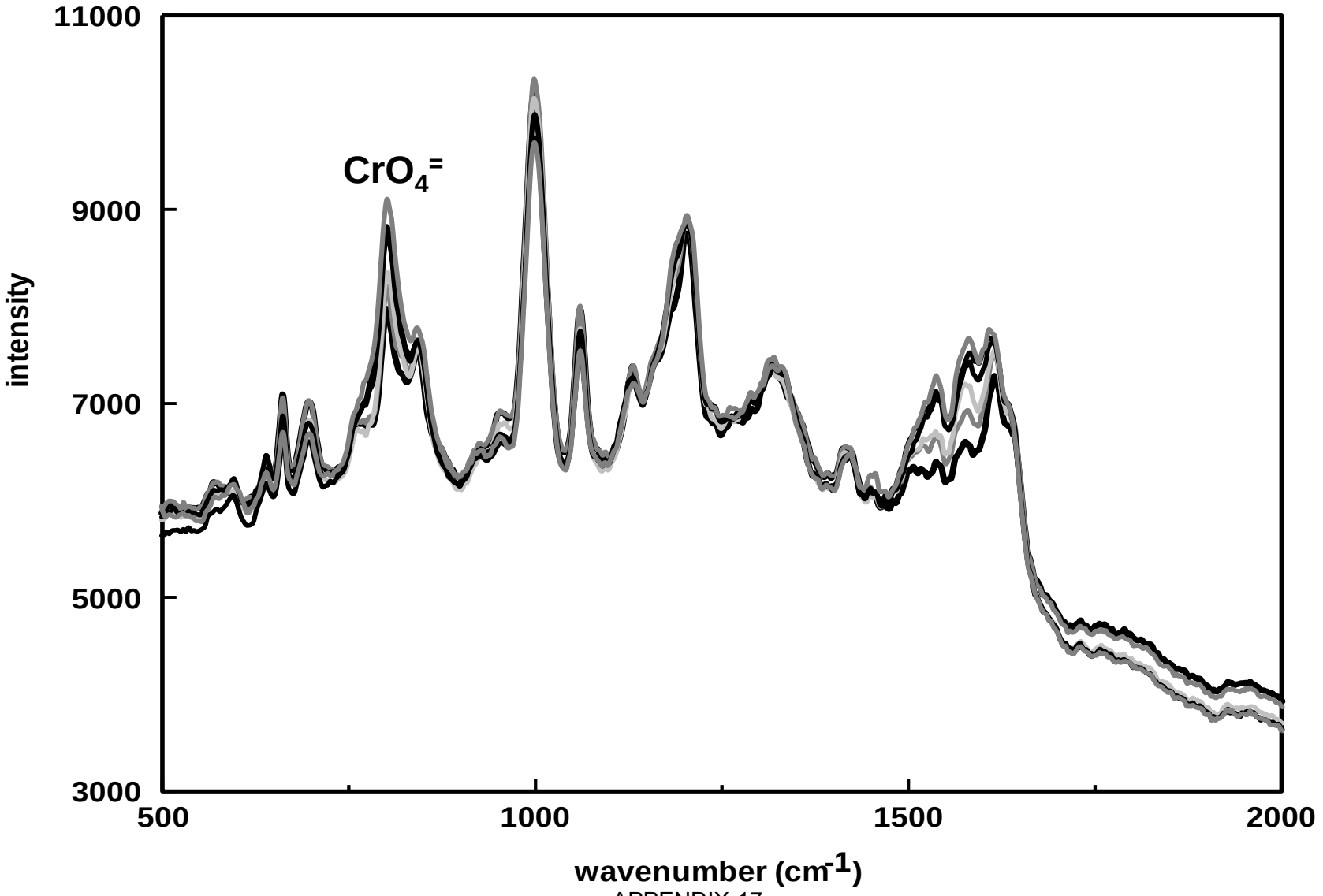

Figure S2. Example of a Au/MEP difference spectrum obtained for a sample that had moved after obtaining the reference spectrum. The position of where the chromate peak should have occurred is indicated.

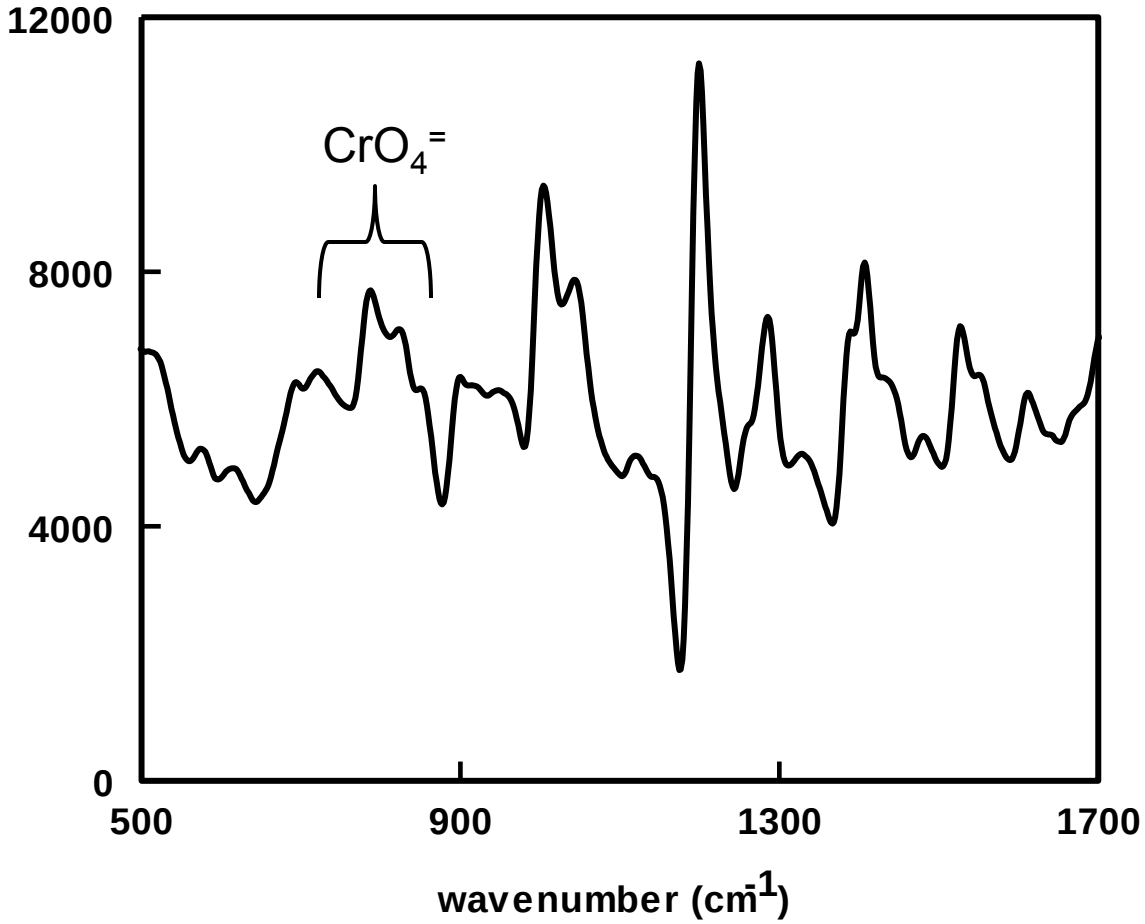

Figure S3. Plots of MEP peak intensities, for the conventional Au/MEP SERS substrate, at 1196 and 1600 cm^{-1} ratioed to the 1000 cm^{-1} peak as a function of chromate concentration Chromate concentration ranges are (a) 0-10000 ppm and (b) 0-100 ppm.

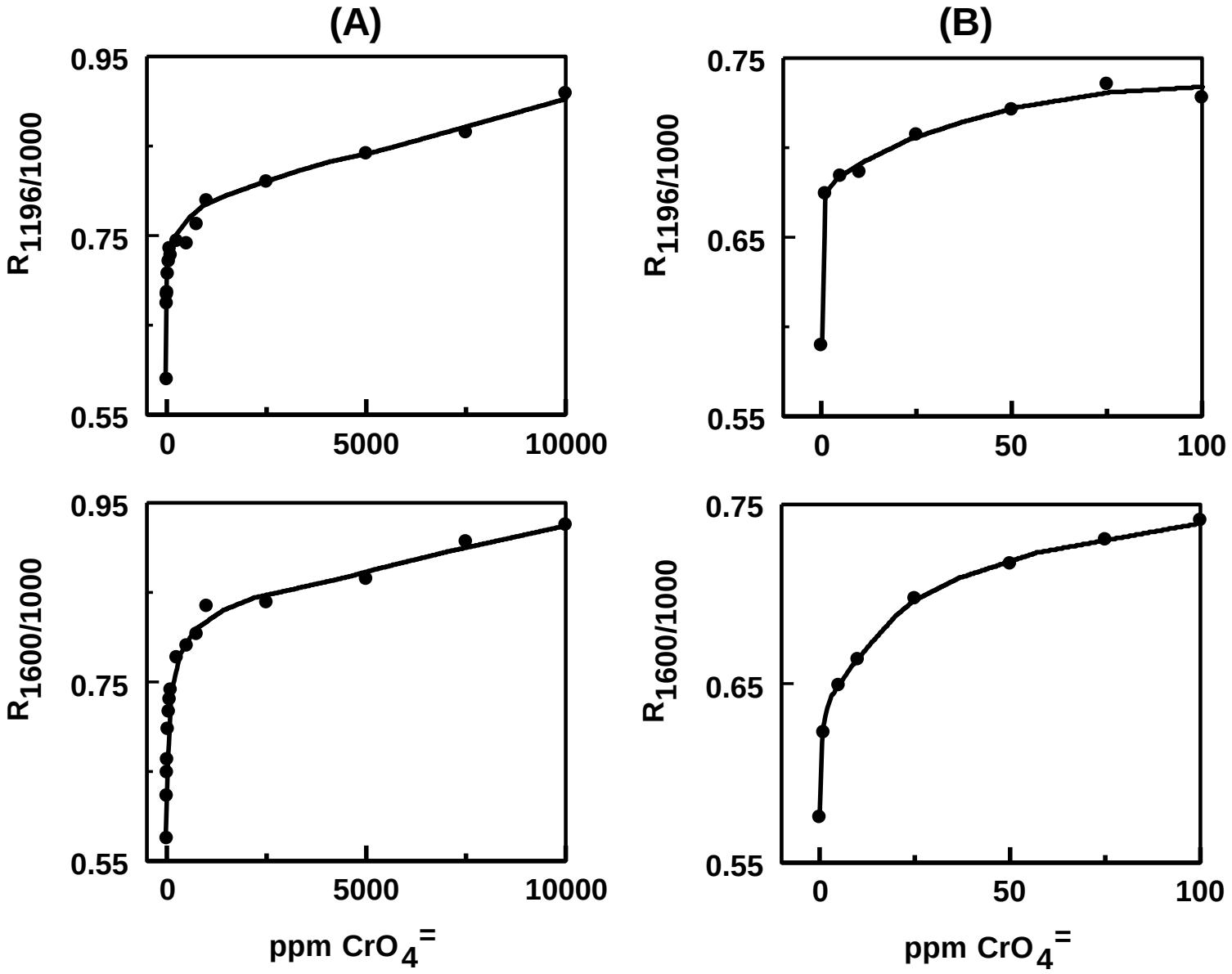

Figure S4. Plots of MEP peak intensities, for the Au/MEP SERS-active capture matrices, at 1196 and 1600 cm^{-1} ratioed to the 1000 cm^{-1} peak as a function of chromate concentration Chromate concentration ranges are (a) 0-10000 ppm and (b) 0-100 ppm.

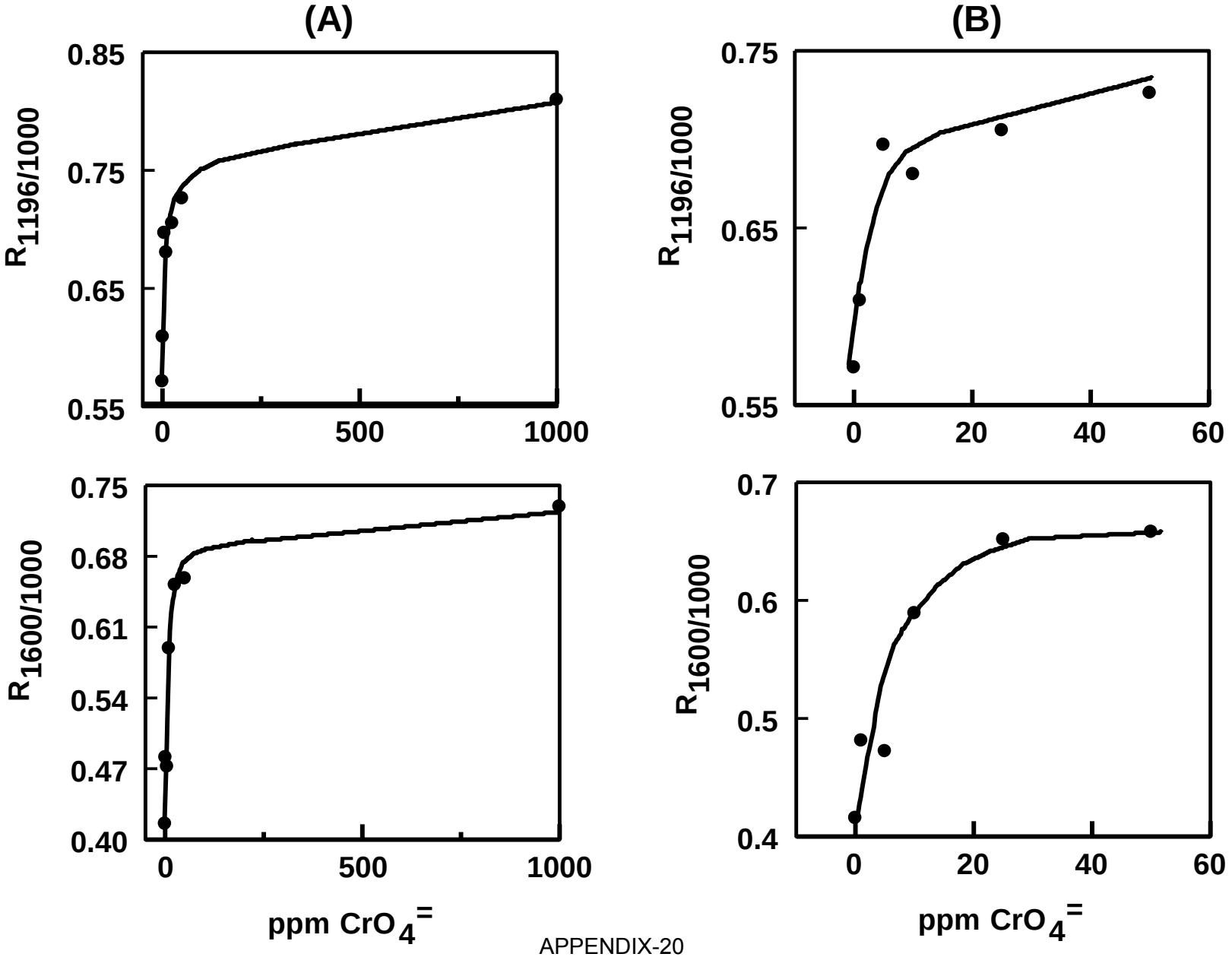

Spectrochimica Acta Part A: Molecular and Biomolecular Spectroscopy 133 (2014) 156–164

Contents lists available at ScienceDirect

Spectrochimica Acta Part A: Molecular and Biomolecular Spectroscopy

journal homepage: www.elsevier.com/locate/saa

Detection of perchlorate using Ag/DMAH$^+$ SERS-active capture matrices

P.A. Mosier-Boss *, M.D. Putnam

SPAWAR Systems Center Pacific, Code 71730, San Diego, CA 92152, United States

HIGHLIGHTS

- Silver colloidal particles were immobilized on amine-derivatized magnetic microparticles.
- The silver colloid was reacted with a thiol to form a self-assembled monolayer (SAM) selective for perchlorate.
- The thiol was dimethylaminoethanethiol hydrochloride.
- The SERS response of the capture matrices were compared to that of conventional SERS substrates.
- The use of solid phase extraction (SPE) to eliminate chloride ion interference was explored.

GRAPHICAL ABSTRACT

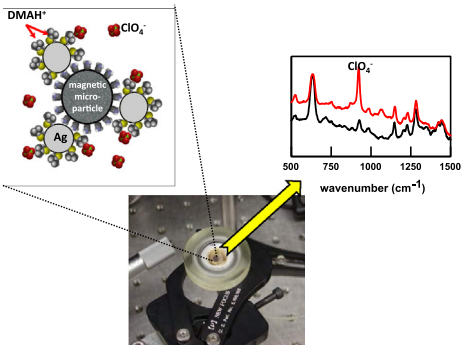

ARTICLE INFO

Article history:
Received 12 February 2014
Received in revised form 11 May 2014
Accepted 18 May 2014
Available online 28 May 2014

Keywords:
Surface enhanced Raman scattering spectroscopy
Perchlorate
Capture matrices

ABSTRACT

In this communication, the fabrication of SERS-active capture matrices for the detection of perchlorate is described. The amine groups of amine-modified magnetic microparticles were used to immobilize silver colloidal particles. Once immobilized, the silver was reacted with dimethylaminoethanethiol hydrochloride (DMAH$^+$Cl$^-$) to form a self-assembled monolayer (SAM). The DMAH$^+$ SAM exhibits reasonably good selectivity for perchlorate. It was shown that calibration curves could be generated by ratioing the perchlorate peak with a DMAH$^+$ peak that did not change upon interaction with the perchlorate ion. Flow experiments, using Ag/DMAH$^+$ capture matrices held in place by a magnet, showed instantaneous response to changes in perchlorate concentration. The use of solid phase extraction (SPE) to eliminate chloride ion interference was explored.

Published by Elsevier B.V.

Introduction

Perchlorate is a contaminant of environmental concern because it greatly impacts human health by interfering with iodide uptake into the thyroid gland [1]. In adults, the thyroid gland helps regulate the metabolism by releasing hormones, while in children, the thyroid helps in proper development [1]. Perchlorate has been used as the oxidizer component and primary ingredient in solid propellant for rockets and missiles [2,3]. Perchlorate is also present in several fertilizers and fertilizer components at levels up to 0.84% [4]. Consequently fertilizers could be a source for perchlorate accumulation in the food chain. Because perchlorate is highly soluble and non-reactive with soil sediments, it is exceedingly mobile in aqueous systems and can persist for many decades under typical ground and surface water conditions. Besides surface and groundwater, perchlorate has been found in food crops, such as lettuce in the southwestern states of the U.S. [5]. The uptake of perchlorate by food crops is attributed to irrigation using perchlorate contaminated water from the Colorado River. In 2003, perchlorate

* Corresponding author. Tel.: +1 (619)553 1603.
E-mail address: pam.boss@navy.mil (P.A. Mosier-Boss).

http://dx.doi.org/10.1016/j.saa.2014.05.036
1386-1425/Published by Elsevier B.V.

was detected in milk samples from Lubbock. TX [6]. The source of this perchlorate was attributed to perchlorate-contaminated alfalfa fed to dairy cows.

Currently monitoring of perchlorate is done by conventional soil and water sampling followed by laboratory analysis using ion chromatography (IC). Of the IC methods developed for perchlorate detection, EPA methods 6850 [7] and 6860 [8] that use IC–MS are preferred because of the specificity of mass spectrometry (MS) in identifying perchlorate in complex sample matrices. The IC methods of monitoring are time consuming, require sample preparation, and are not field deployable.

For long term monitoring purposes, it would be desirable to detect perchlorate in samples on-site and in near real time. Such a capability would minimize sample handling, processing, and overall costs. It would also be desirable to detect perchlorate in the low ppb concentration range with little or no sample preparation and with no interferences. One technology that meets many of these criteria is SERS using chemically modified silver/gold substrates. In the SERS methodology, coatings on the SERS substrate are chosen to attract the analyte of interest. The advantages of SERS using chemically derivatized substrates over other techniques are:

(i) All polyatomic species exhibit a characteristic SERS spectrum.
(ii) The SERS spectral lines are narrow allowing simultaneous detection of multiple polyatomic species.
(iii) Depending upon the dimensions of the nanostructures comprising the substrates, SERS can result in a 10^5–10^{10} enhancement of the Raman signal.
(iv) Water is a very poor Raman scatterer and does not interfere.
(v) The selective coating also exhibits SERS lines that can be used as an internal standard.

The main limitation of the SERS technology has to do with the coating itself. The sensitivity of SERS to detect the desired analyte is dependent upon the selectivity of the coating for that analyte. However, there is a trade-off between selectivity and reversibility. The stronger the interaction between an analyte and a coating, the greater the selectivity of the coating for that analyte and the greater the sensitivity. However, reversibility is often sacrificed. The only practical way around this trade-off is to provide a fresh SERS-active surface between sampling. To address these issues and provide a fresh SERS surface between analyses, we developed SERS-active capture matrices prepared by immobilizing gold/silver colloidal particles on amine-derivatized magnetic microspheres [9]. Afterwards, the immobilized colloidal particles are reacted with a thiol to form a self-assembled monolayer (SAM). To date, the detection of naphthalene [9] using pentachlorothiophenol-derivatized, SERS-active capture matrices and hexavalent chromium [10] using 4-(2-mercaptothyl)pyridinium derivatized, SERS-active capture matrices have been demonstrated. Besides providing a fresh SERS surface between sampling, additional advantages of capture matrices in chemical detection are extraction/concentration of the target analyte from a complex sample matrix, ease of separation, and suitability for automation. In fact the use of derivatized magnetic microparticles for trace chemical analysis is growing [11]. Magnetic particles possess a high surface area which can exhibit higher adsorption capacity for analytes. They also exhibit strong superparamagnetic properties which meets the need of rapid extraction of large volume samples by employing a strong external magnetic field. These derivatized magnetic microparticles can be used in both solutions and suspensions. Since the majority of accompanying impurities in a suspension are diamagnetic, they do not interfere with magnetic particles during the magnetic separation step.

In order to detect perchlorate using SERS-active capture matrices, a coating selective for perchlorate needs to be identified. Earlier Gu et al. [12] demonstrated the use of 2-dimethylaminoethanethiol hydrochloride ($DMAH^+Cl^-$) modified gold nanoparticles to detect perchlorate by SERS in both simulated and contaminated groundwater samples. Using these $DMAH^+$ derivatized-Au nanoparticles, they were able to detect concentrations of perchlorate as low as 0.1 μg/L (or 0.1 ppb). They reported that the presence of higher concentrations of background ionic species (nitrate, sulfate, phosphate, and chloride) did not impact the quantitative analysis of perchlorate. The perchlorate analysis cartridges developed by OndaVia use dimethylaminoethanethiol hydrochloride as the perchlorate selective coating. These cartridges were found it to work pretty well, at least to ~100 ppb, in pH-adjusted (2.5) northern California ground water samples that have (at least) nitrate and sulfate [13]. The interaction of anions with conventional Ag/$DMAH^+$ SERS substrates was reported [14]. It was shown that, when the anion concentration is in M, the measured response of the anion with the $DMAH^+$ coating was described by a Frumkin isotherm. The shape of the Frumkin isotherm was determined by two parameters – *K*, the ion-pair constant between the anion and the coating, and *g*, the Frumkin parameter that takes into account interactions between adsorbed species. The values for *K* and *g* obtained for the $DMAH^+$ coating and anions are tabulated in Table 1. The results in Table 1 indicate that the coating does interact with nitrate, sulfate, and chloride in addition to perchlorate. Mixtures of anions were not examined in this investigation.

Given the results of Gu et al. [12] and OndaVia [13], $DMAH^+$ was chosen to be the perchlorate selective coating. In this communication, we describe the fabrication of SERS-active Ag/$DMAH^+$ capture matrices and discuss their use to detect perchlorate.

Experimental section

Reagents

Silver nitrate (Aldrich), sodium citrate dihydrate (Aldrich), sodium perchlorate (Aldrich), sodium nitrate (Johnson Mathey), sodium sulfate (Aldrich), sodium chloride (Aldrich), potassium chloride (Aldrich), dimethylaminoethanethiol hydrochloride ($DMAH^+$, Aldrich), water (HPLC grade, Aldrich), and ethanol (HPLC grade, Aldrich) were used as received. Aqueous solutions of perchlorate were prepared using deionized water.

A 0.5 mL aliquot of 5 μm diameter, amine-terminated, silica-coated iron oxide microparticles (Bioclone, part no. FA-104) was washed ten times with 1 mL aliquots of HPLC water to remove surfactant. Between washes, a NdFeB magnet is used to separate the magnetic microparticles from the water. After the washes, the volume of the amine-terminated, magnetic microparticles was adjusted to 1.0 mL.

Preparation of conventional Ag/MEP SERS substrates

An insulated copper wire was soldered to a 0.75-cm length of 2 mm diameter silver wire (Aldrich, 99.9%). The silver wire was potted inside a 5-mm outer diameter, borosilicate glass tube using

Table 1
Ion pair constants and Frumkin parameters measured for Ag/$DMAH^+$ interactions with anions [14].

Anion	Ion pair constant (M)	Frumkin parameter
Perchlorate	404 ± 59	−0.64 ± 0.21
Nitrate	301 ± 78	−2.3 ± 1.1
Sulfate	972 ± 85	−1.14 ± 0.13
Chloride	310 ± 180	−2.3 ± 1.1
Hydrogen phosphate	No interaction	No interaction
Dihydrogen phosphate	No interaction	No interaction

a chemically resistant epoxy (Epoxy Patch 1C, Hysol). Prior to use, the silver disk of the electrode was electrochemically roughened in a 0.1 M KCl solution using a PAR 273A potentiostat/galvanostat under computer control. The silver surface was roughened by cycling the electrode potential 25 times between −300 mV (holding 30 s) and 1200 mV (holding 1.3 s) at a sweep rate of 500 mV s^{-1}. Roughened electrode surfaces have been shown to exhibit fractal characteristics [15]. After electrochemical roughening, the silver electrode was rinsed with water (HPLC grade, Aldrich) and then ethanol (HPLC grade, Aldrich). The electrode was immersed in a dilute solution of $DMAH^+$ in ethanol and allowed to react for ~24 h to form a SAM. Before use, the electrode was rinsed thoroughly with ethanol and water.

Preparation of silver colloid

A 250 mL solution containing 45 mg of silver nitrate and a Teflon®-coated stir bar were placed in a two-neck 500 mL, round-bottom flask. A condenser with attached water line was placed on the center neck of the flask. A 25 mL addition funnel, containing 5 mL of 1% sodium citrate dihydrate in water, was placed on the second neck of the flask. Once the silver nitrate solution was brought to boil, the sodium citrate solution was added rapidly with constant stirring. After heating/stirring for one hour, the reaction flask was removed from the heat and allowed to cool to room temperature. The colloidal suspension was yellowish-brown in appearance. The estimated diameter of the colloidal particles is 10–30 nm [16]. The colloidal suspension was concentrated to a final volume of 3 mL by centrifugation.

Preparation of Ag/ $DMAH^+$ capture matrices

A 100 μL aliquot of the washed, amine-terminated, magnetic microparticles was pippetted into a 1.75 mL glass vial containing 1 ml of water (HPLC grade, Aldrich). A 200 μL aliquot of the concentrated silver colloidal suspension was added to the glass vial and the vial was placed on a roller. The rolling action mixes the silver colloid and the magnetic particles. This is preferred over stirring because the glass vials are very small. The amine groups of the magnetic microparticles bind to the silver colloidal particles. After rolling for 2 h, a NdFeB magnet was used to separate the microparticles from the liquid. If the liquid was clear, half the volume was removed and another 200 μL aliquot of the concentrated silver colloidal suspension was added to the glass vial and placed on the roller. The process was repeated until the surface of the magnetic microparticles was completely covered with colloidal silver particles as indicated when the liquid remained yellow-gray in color. The Ag-covered, magnetic microparticles were then washed three times with water (HPLC grade, Aldrich) and then three times with ethanol (HPLC grade, Aldrich). Between washings, a NdFeB magnet is used to separate the Ag-covered magnetic microparticles. Afterwards a dilute ethanolic solution (~0.09 M) of $DMAH^+$ was added to the glass vial. The $DMAH^+$ was allowed to react with the immobilized silver colloidal particles for ~24 h to form a SAM. The Ag/$DMAH^+$ capture matrices were then washed three times in ethanol, as described above. The volume of the Ag/$DMAH^+$ capture matrices was adjusted to 1 mL using ethanol. Capture matrices were refrigerated between uses.

Evaluation of the SERS substrates

SERS measurements of the conventional Ag/$DMAH^+$ substrate and the Ag/$DMAH^+$ capture matrices were made using the Snowy Range Instruments Sierra portable Raman system. The system has a 785 nm laser that can operate at 100 mW and a 3000 element, linear, cooled, NIR enhanced CCD array, dispersive spectrometer (operational range is 200–3200 cm^{-1} and resolution is 10 cm^{-1}). This particular system has three-way sampling for side, bottom, and 'point and shoot' [17]. A knob on the instrument either directs the laser beam into a sample chamber for side and bottom measurements of vials or below and outside the instrument in the 'point and shoot' mode to measure surfaces. To evaluate the conventional SERS substrates and the capture matrices, the instrument was operated in the point and shoot mode.

A schematic of the flow-through cell to evaluate the concentration response of the conventional Ag/$DMAH^+$ SERS substrate to perchlorate is shown in Fig. 1a. The body of the flow-through cell is constructed of Teflon®. A 25 mm diameter, 2 mm thick sapphire disk was used as the optically transparent window. A Kel-F window retainer holds the window in place. An O-ring provides a leak-tight seal between the window and the cell body. A Teflon® bushing holds the SERS substrate in place. A second O-ring provides a leak-tight seal around the glass tube of the SERS substrate. The inlet and outlet consist of 20 gauge stainless steel tubes that have been epoxied in place using a chemically resistant epoxy (Epoxy Patch 1C, Hysol). The volume of the cell is ~0.5 mL. For SERS measurements, the flow-through cell was held in place below the point and shoot optics of the spectrometer with the "Opti-Claw" optical mount (New Focus, part no. 9832) mounted on an *x*,*y*,*z*-translation stage (Newport Corporation, part no. 460A).

To evaluate the perchlorate concentration response of Ag/$DMAH^+$ capture matrices, a 50 μL aliquot of the capture matrices was pipetted into a glass vial. This 50 μL aliquot contains 0.075 mg, or 3.75×10^6, magnetic microparticles. A NdFeB magnet was used to separate the capture matrices from the ethanol. The capture matrices were washed three times with 0.5 mL of water. A NdFeB magnet was used to separate the capture matrices from the liquid between washes. Afterwards a 1 mL aliquot of an aqueous perchlorate solution of a known concentration was added to the vial. The sample was allowed to equilibrate overnight. Afterwards, a pipette was used to transfer the capture matrices and solution to the cell shown in Fig. 1b. The 4.76 mm diameter magnet below the Au foil concentrated the capture matrices in a 17.8 mm^2 area on the surface of Au foil. The sample was then placed below the point and shoot optics of the spectrometer to obtain SERS spectra.

A schematic of the flow-through cell to evaluate the concentration response of Ag/$DMAH^+$ SERS active capture matrices to perchlorate is shown in Fig. 1b. The body of the flow-through cell is constructed of Teflon®. A chemically resistant epoxy (Epoxy Patch 1C, Hysol) was used to epoxy a 0.1 mm thick gold foil on the inside surface of the cell, as shown in Fig. 1b. As shown in Fig. 1b, Loctite Five-Minute Epoxy (Henkel Corporation) was used to pot a NdFeB magnet (part number D32, K&J Magnetics) below the gold-covered sample surface. A 25 mm diameter, 2 mm thick sapphire disk was used as the optically transparent window. A Kel-F window retainer holds the window in place. An O-ring provides a leak-tight seal between the window and the cell body. The inlet and outlet consist of 20 gauge stainless steel tubes that have been epoxied in place using a chemically resistant epoxy (Epoxy Patch 1C, Hysol). The distance between the surface of the magnets and the gold covered sample surface is ~0.1 mm. Fig. 2 shows a plot of the pull force of the magnets calculated as a function of distance [18]. As shown in Fig. 2, the pull force of the magnet decreases as the distance between the capture matrices and the magnet increases. For a distance of 0.1 mm, the pull force of the magnets is 1.22 lb. This pull force was found to be sufficient to hold the capture matrices in place when perchlorate solution was flowed through the cell. For SERS measurements, the flow-through cell was held in place below the point and shoot optics of the spectrometer with the "Opti-Claw" optical mount (New Focus, part no. 9832) mounted on an *x*,*y*,*z*-translation stage (Newport Corporation, part no. 460A).

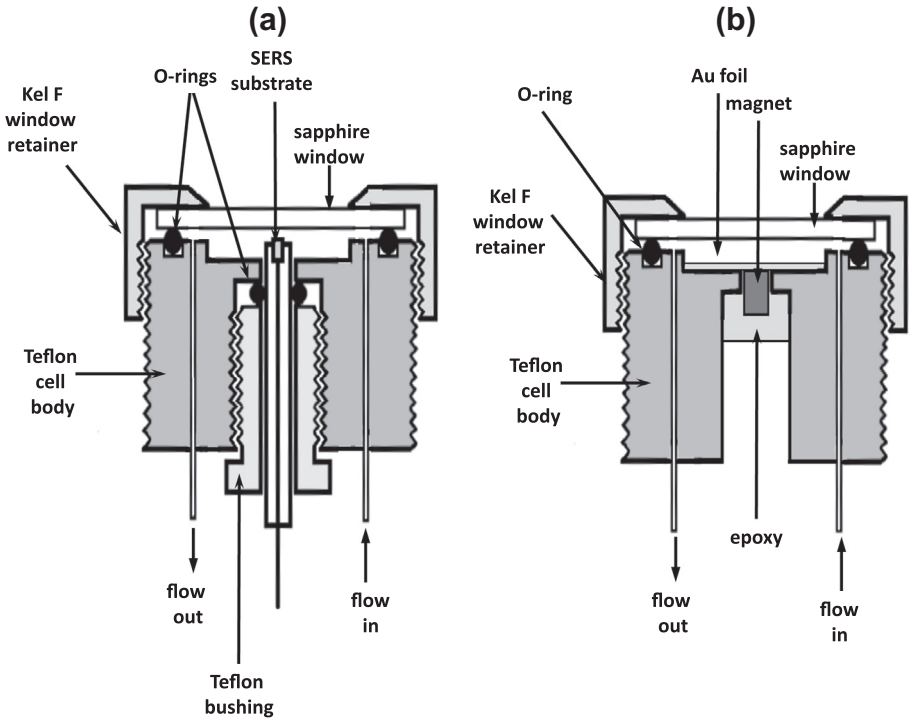

Fig. 1. Schematics of (a) the cell used to measure the concentration response of conventional Ag/DMAH$^+$ SERS substrates to perchlorate and (b) the cell used to evaluate the response of Ag/DMAH$^+$ capture matrices to perchlorate.

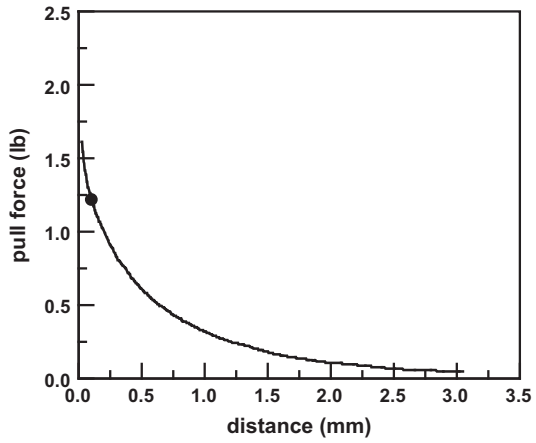

Fig. 2. Magnetic pull force as a function of distance calculated for the NdFeB magnet used in the cell shown in Fig. 1b where ● shows the separation between the magnets and the Au foil surface of the cell.

All manipulations of the spectral data were done using GRAMS/AI7 (Thermogalactic), a software package that can be used to subtract spectra interactively as well as integrate peak areas and measure peak heights.

Sample treatment using solid-phase extraction cartridges

Maxi-Clean IC-Ag Plus cartridges (Alltech) are used to remove chloride ion. These cartridges consist of 1.5 mL of polystyrene-based packing material sandwiched between 20 μm polyethylene frits in a medical-grade polypropylene housing. Each IC-Ag Plus cartridge contains 2 milliequivalents of silver ion. These cartridges remove excess halides through the formation of Ag-halide salts. Maxi-Clean IC-H Plus cartridges (Alltech) are used to remove silver ion that eluted through the IC-Ag Plus cartridge. The IC-H cartridges contain 1.5 mL of sulfonic acid cation exchange resin in the form. Cations from the sample displace the hydronium ion on the resin.

Prior to using the IC-Ag/H cartridge to remove chloride/silver ions in the sample, 10 mL of deionized water was passed through the cartridge to remove interstitial contaminants and to wet the packed bed. The sample was loaded onto the cartridge at a flow rate of 1 mL/min. The first 1 mL of cartridge mobile phase was discarded and the remaining eluate was collected for further analysis. To test for the presence of silver ions, a few drops of sodium chloride solution was added to a few drops of the eluant collected from the IC-Ag cartridge. Formation of a cloudy, white precipitate was indication of the presence of silver ion in the eluant. The pH of the samples, before and after SPE through the IC-Ag and IC-H cartridges, was measured using ColorpHast pH 0–14 indicator strips (EM-reagents).

Results and discussion

Conventional Ag/DMAH$^+$ SERS substrate

SERS spectra were obtained using a conventional Ag/DMAH$^+$ substrate. These spectral results were used to evaluate the performance of the Ag/DMAH$^+$ capture matrices. To obtain the SERS spectra, the conventional Ag/DMAH$^+$ substrate was mounted in the cell shown in Fig. 1a. The cell was filled with water and the substrate was scanned in the *x*, *y*, and *z* directions to optimize the signal. Once optimized, the cell was locked in place and all spectra were obtained at this fixed location on the substrate. A reference spectrum was obtained with the cell filled with water. The water was then sequentially replaced with solutions of varying concentrations of perchlorate, going from the lowest perchlorate concentration to the highest. The response of the DMAH$^+$ coating to perchlorate was instantaneous.

Fig. 3a shows SERS spectra of a conventional Ag substrate coated with DMAH$^+$ at perchlorate concentrations of 0, 500, 1000, 5000, and 10,000 ppm. When exposed to perchlorate, a peak

due to the symmetric Cl–O stretching mode of perchlorate grows in at 923 cm^{-1}. To determine the perchlorate peak area, the spectral contributions of the coating need to be subtracted out. As shown in Fig. 3a, the spectra exhibit similar baselines and the spectral peaks lineup. Under these circumstances, the spectral contributions of the reference spectrum can be subtracted out and the perchlorate peak area measured. A plot of perchlorate peak area as a function of perchlorate concentration is shown in Fig. 3b. This is the calibration curve. At low perchlorate concentration, the perchlorate peak area increases with concentration. At higher perchlorate solution concentrations, the response levels off as the adsorption sites on the $DMAH^+$ SAM become fully occupied. The equation that describes this curve is summarized in Table 2. Determining the equation that describes the curve was an iterative process. In an Excel spreadsheet, the curves were modeled using various combinations of linear and exponential features. When a given combination looked promising, a Marquardt [19] nonlinear least squares fitting routine was used to obtain the values of the parameters and their uncertainties.

Another way to generate calibration curves that does not require spectral subtraction is to ratio the perchlorate peak intensity to a $DMAH^+$ peak that does not change in the presence of perchlorate ion. In Fig. 3a, the peaks at 632 and 711 cm^{-1} are due to the C–S stretching modes of the gauche and trans conformers, respectively [20,21]. With increasing perchlorate concentration, the intensity of the peak due to the gauche conformer increases in intensity. Two $DMAH^+$ peaks that do not vary with perchlorate concentration are at 985 and 1149 cm^{-1}. The 985 and 1149 cm^{-1} peaks are assigned to the ν(C–C) and ν_{asym}(CNC) vibrational modes, respectively [20,21]. The results of ratioing the perchlorate peak to the 985 and 1149 cm^{-1} $DMAH^+$ peaks are shown in Fig. 3c. The concentration responses are very similar to that shown in Fig. 3b. The equations that describe these curves are summarized in Table 2.

Ag/$DMAH^+$ SERS-active capture matrices

Preparation of the capture matrices samples as a function of perchlorate concentration were described *vida supra*. After equilibration, a pipette was used to transfer the capture matrices onto the gold surface of the flow-through cell, Fig. 1b. Fig. 4a shows SERS spectra measured for individual samples of Ag/$DMAH^+$ capture matrices in the absence and presence of perchlorate. It can be seen that the intensities of the peaks due to $DMAH^+$ vary as do the baselines. As discussed *vide supra*, because of these variabilities between the spectra obtained for the individual samples, it is not possible to do spectral subtractions to obtain the perchlorate peak area. To generate calibration curves, the perchlorate peak intensity was ratioed to the 985 and 1149 cm^{-1} $DMAH^+$ peaks. For the conventional SERS substrate, these peaks did not change in the intensity in the presence of perchlorate ion.

Fig. 4b summarizes the results obtained by ratioing the perchlorate peak to the 985 and 1149 cm^{-1} $DMAH^+$ peaks. The equations that describes these curves are summarized in Table 2. It can be seen that the results in Fig. 4b obtained for the Ag/$DMAH^+$ capture matrices are very similar to what was observed for the Ag/$DMAH^+$ conventional SERS substrate, Fig. 3b, and shows that the ratioing method can be used to obtain reasonable calibration curves for the capture matrices. The purpose of showing the signal response at high perchlorate concentration was to show that the response levels off as the sites on the coating become fully occupied with perchlorate anions.

In another experiment, a single 50 μL aliquot of the Ag/$DMAH^+$ capture matrices was pippetted onto a small spot in the center of the gold foil of the flow through cell shown in Fig. 1b. A NdFeB magnet held the capture matrices stationary as a 5 ppm perchlorate solution was flowed through the cell. Fig. 5a shows SERS spectra of the capture matrices as the perchlorate solution is flowed through the cell. Fig. 5b shows the spectra between 850 and 1000 cm^{-1}. This spectral region shows that the $DMAH^+$ SAM on the capture matrices exhibits a peak at 930 cm^{-1}. As the perchlorate solution flows over the immobilized capture matrices, the $DMAH^+$ SAM extracts the perchlorate from solution as demonstrated by the growth of the perchlorate peak at 923 cm^{-1}. Because the capture matrices are held in a fixed spot, the same sample area was interrogated by the laser as the 5 ppm perchlorate solution was flowed over the Ag/$DMAH^+$ capture matrices. It can be seen

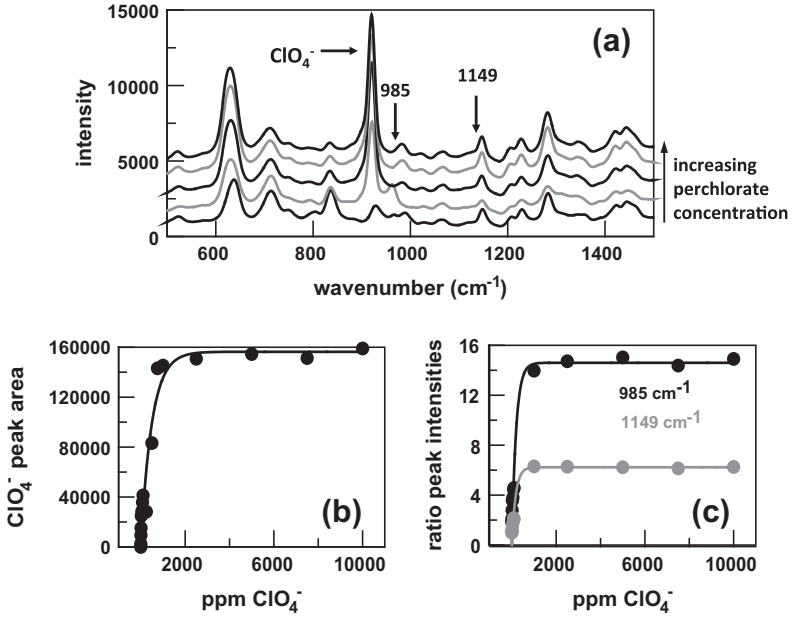

Fig. 3. (a) SERS spectra of a conventional Ag/$DMAH^+$ SERS substrate obtained at perchlorate concentrations of (bottom to top) 0, 500, 1000. 5000, and 10,000 ppm. Spectra were obtained using 785 nm excitation at 30 mW and averaging ten 1s spectra. (b) Plot of perchlorate peak area as a function of perchlorate concentration. Equation describing the curve is summarized in Table 1. (c) Plots of the perchlorate peak intensity at 92 cm^{-1} ratioed to the $DMAH^+$ peaks at 985 and 1149 cm^{-1} as a function of perchlorate concentration. Equations describing the curves are summarized in Table 2.

Table 2
Summary of the equations that describe the observed calibration curves.

Curve	Equation describing curve[a]	R^2	Values of parameters
Fig. 3b	$y = a(1 - \exp(-bx))$	0.9786	$a = 156400 \pm 73{,}000$ $b = 0.00201 \pm 0.00033$
Fig. 3c ratio to 985 cm^{-1} $DMAH^+$ peak	$y = a(1 - \exp(-bx))$	0.9904	$a = 14.60 \pm 0.61$ $b = 0.0051 \pm 0.0010$
Fig. 3c ratio to 1149 cm^{-1} $DMAH^+$ peak	$y = a(1 - \exp(-bx))$	0.9871	$a = 6.23 \pm 0.30$ $b = 0.0058 \pm 0.0013$
Fig. 4b ratio to 985 cm^{-1} $DMAH^+$ peak	$y = a(1 - \exp(-bx))$	0.9738	$a = 7.12 \pm 0.81$ $b = 0.00199 \pm 0.00072$
Fig. 4b ratio to 1149 cm^{-1} $DMAH^+$ peak	$y = a(1 - \exp(-bx))$	0.9723	$a = 2.66 \pm 0.30$ $b = 0.00201 \pm 0.00072$
Fig. 5c	$y = ax^2 + bx$	0.9963	$a = -813 \pm 64$ $b = 6070 \pm 220$

[a] In the equations, y is either the perchlorate peak area or the ratio of peak intensities and x is ppm or mL perchlorate.

that the baselines of the spectra are identical and the peaks line up. Under these conditions, spectral subtractions can be done which will give meaningful results. A plot of perchlorate peak area as a function of perchlorate solution volume is shown in Fig. 5b. The perchlorate peak area increased linearly as the capture matrices extracted perchlorate from the solution and then began to level off as the sites on the $DMAH^+$ SAM are becoming fully occupied. The equation describing the plot shown in Figs. 5b is summarized in Table 2.

Anion interference

The results summarized in Table 1 indicate that the $DMAH^+$ SAM interacts with chloride, nitrate, and sulfate as well as perchlorate [14]. One would therefore expect nitrate, chloride, and sulfate to interfere in the detection of perchlorate. As discussed *vide supra*, Gu et al. [12] had used Au/$DMAH^+$ nanoparticles to detect perchlorate in the presence of nitrate, sulfate, phosphate, and chloride using SERS. The concentrations of the anions used in their simulated groundwater samples are summarized in Table 3. They showed that sulfate and phosphate did not interfere with the detection of perchlorate in simulated groundwater samples containing these concentrations of anions. There was some competition between nitrate and perchlorate for sites on the Au/$DMAH^+$

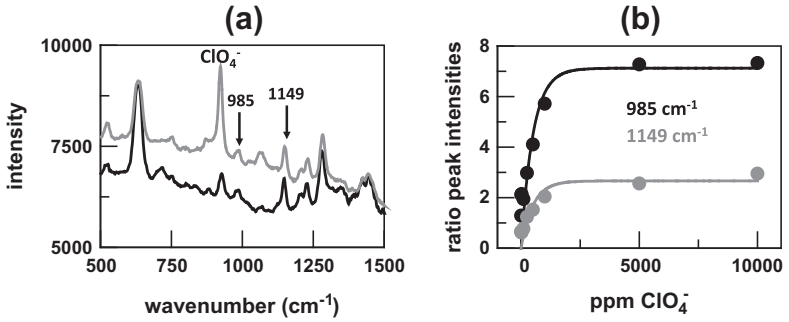

Fig. 4. (a) SERS spectra of Ag/$DMAH^+$ capture matrices immersed in solutions of 0 (bottom) and 10,000 (top) ppm perchlorate. (b) Equations describing the curves are summarized in Table 2.

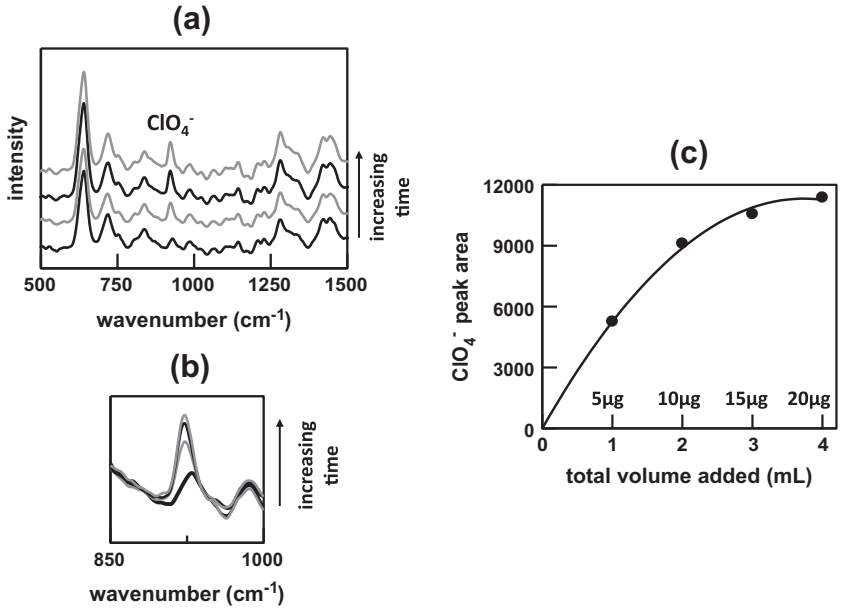

Fig. 5. (a) SERS spectra of Ag/$DMAH^+$ capture matrices in the cell shown in Fig. 1b measured as a function of total volume of 5 ppm perchlorate solution flowing through the cell at a constant rate. Spectra were obtained using 785 nm excitation at 50 mW and averaging ten 1s spectra. (b) Spectra from (a) between 850 and 1000 cm^{-1} showing the peak due to perchlorate (top to bottom, volume of perchlorate through the cell is 0, 2, 3, and 4 mL). (c) Plot of perchlorate peak area as a function of volume of 5 ppm perchlorate solution. The mass quantity of perchlorate that flowed over the capture matrices is indicated. Equation describing the curve is summarized in Table 2.

SAM. Nothing was said about chloride ion interference. For a perchlorate concentration of 0.1 ppm, they saw a 35% decrease in the intensity of the perchlorate peak in the presence of two to three orders magnitude higher concentrations of background ionic species compared with that measured in deionized water.

Concentrations of nitrate, sulfate, phosphate, and chloride in groundwater samples from Pennsylvania, Texas, and northern California are also tabulated in Table 3. The simulated groundwater samples used by Gu et al. [12] are comparable to groundwater samples found in northern California [12] and Pennsylvania [22]. A greater range of background anion concentrations were found in groundwater samples collected in Texas [23]. It was therefore of interest to examine the effect of higher background anion concentrations on the detection of perchlorate using the Ag/DMAH$^+$ capture matrices. A concentration of 250 ppm each chloride, nitrate and sulfate was chosen for these studies as these concentrations were intermediate between anion concentrations found in northern California and Texas.

A 50 μL aliquot of Ag/DMAH$^+$ capture matrices was pippetted onto the gold surface of the flow through cell shown in Fig. 1b. water was flowed over the capture matrices and the resultant spectrum is shown in Fig. 6a(i). Then a solution of 25 ppm perchlorate was flowed through the cell. A peak due to perchlorate can be seen in Fig. 6a(ii). When a solution containing 25 ppm perchlorate and 250 ppm each of nitrate and sulfate, a decrease in the perchlorate peak was observed, Fig. 6a(iii). Also a small peak due to nitrate is seen but no peak due to sulfate. These results are in agreement with the observations of Gu et al. [12]. As both nitrate and perchlorate have peaks in the spectra, it should be possible to determine selectivity coefficients to correct for nitrate interference as is done for ion selective electrodes [24].

When a solution containing 25 ppm perchlorate and 250 ppm each of nitrate, sulfate, and chloride flows through the cell, the nitrate peak disappears and the perchlorate peak practically disappears, Fig. 6a(iv). This suggests that chloride is a significant interferent. To verify this solutions containing only perchlorate and chloride were flowed through the cell containing a fresh 50 μL aliquot of Ag/DMAH$^+$ capture matrices. The results are summarized in Fig. 6b. Fig. 6b(i) shows the SERS spectrum of the DMAH$^+$ SAM in the presence of water. When a 25 ppm solution of perchlorate is flowed through the cell, the DMAH$^+$ SAM extracts perchlorate from the sample as evidenced by the perchlorate peak seen in Fig. 6b(ii). However, when a solution containing 25 ppm perchlorate and 250 ppm chloride flows through the cell, the intensity of the perchlorate peak is greatly reduced, Fig. 6b(iii).

The use of SPE to remove chloride ion interference

The results in Fig. 6 clearly indicate that chloride ion is a significant interferent in the detection of perchlorate by SERS using Ag/DMAH$^+$ capture matrices. In ion chromatography of anions, chloride ion is removed from aqueous solutions using solid phase extraction (SPE) [25]. The SPE cartridges used to remove chloride ion, IC-Ag, contain sulfonic acid cation exchange resin in the Ag$^+$ form. The silver contained on the packing reacts with halides in the sample to form an insoluble salt (silver halide). During the process, cations from the sample are taken up by the resin to replace the silver consumed in the precipitation of the silver halide. The net result is the removal of halides and an equivalent amount of sample cations.

Samples of 25 and 100 ppm perchlorate were prepared in the absence of other anions; in the presence of only 250 ppm chloride; and in the presence of 250 ppm each of nitrate, sulfate, and chloride. SPE was done of the chloride containing solutions using the IC-Ag SPE cartridges.

A 50 μL aliquot of Ag/DMAH$^+$ capture matrices was pippetted onto the gold surface of the flow through cell shown in Fig. 1b. Water was flowed over the capture matrices and the resultant spectrum is shown in Fig. 7a(i). A solution of 25 ppm perchlorate was then flowed over the capture matrices. A peak due to perchlorate grows in as seen in Fig. 7a(ii). Next the eluant obtained after SPE of the 25 ppm perchlorate and 250 ppm chloride solution was flowed through the cell. The resultant spectrum shown in Fig. 7a(iii) shows no decrease in the perchlorate peak indicating that the IC-Ag cartridge removed the chloride ion. However, when the eluant obtained after SPE of the 25 ppm perchlorate and

Table 3
Concentrations of anions in field groundwater samples and a simulated groundwater sample (SGW).

Anion	SGW [12]	Pennsylvania [22]	Texas [23]	Northern California [12]
Nitrate (ppm)	6.2	Up to 10	<5–95	9.9, 32.2
Sulfate (ppm)	9.6	5–50	<50–2660	15.4, 47.1
Phosphate (ppm)	9.5	Not measured	Not measured	0, 0
Chloride (ppm)	35.5	<20	<50–1823	9.9, 106.4

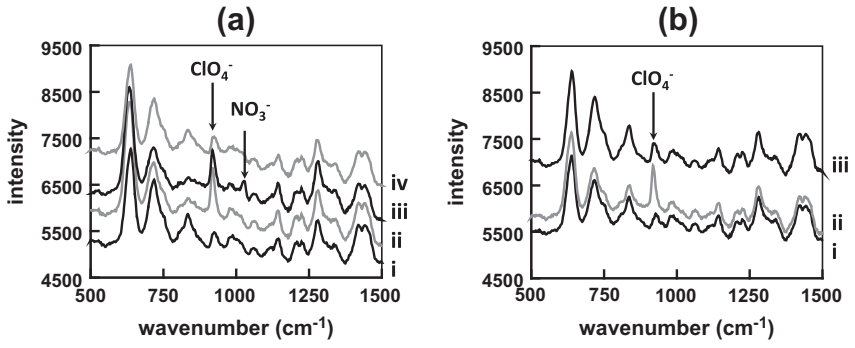

Fig. 6. SERS spectra of Ag/DMAH$^+$ capture matrices obtained using the cell shown in Fig. 1b where (a) i – in water, ii – 25 ppm perchlorate, iii – 25 ppm perchlorate and 250 ppm each nitrate and sulfate, iv – 25 ppm perchlorate and 250 ppm each nitrate, sulfate, and chloride and (b) i – in water, ii – in 25 ppm perchlorate, iii – 25 ppm perchlorate and 250 ppm chloride. In both (a) and (b) the position of the perchlorate peak is indicated.

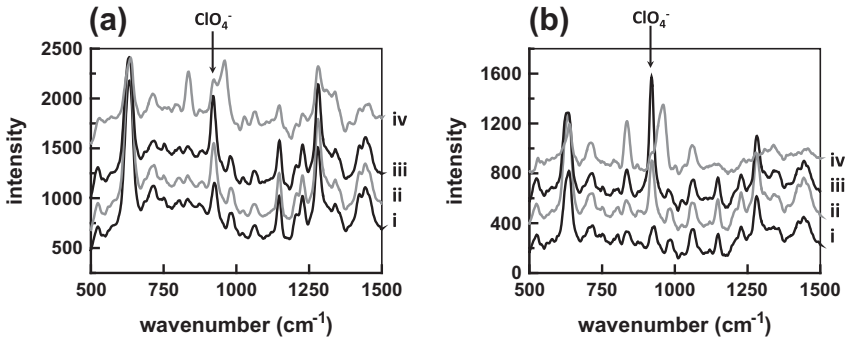

Fig. 7. SERS spectra of Ag/DMAH$^+$ capture matrices obtained using the cell shown in Fig. 1b where (a) i – in water, ii – 25 ppm perchlorate, iii – 25 ppm perchlorate and 250 ppm chloride after SPE through the IC-Ag cartridge, iv – 25 ppm perchlorate and 250 ppm each nitrate, sulfate, and chloride after SPE through the IC-Ag cartridge and (b) i – in water, ii – 100 ppm perchlorate, iii – 100 ppm perchlorate and 250 ppm chloride after SPE through the IC-Ag cartridge, iv – 100 ppm perchlorate and 250 ppm each nitrate, sulfate, and chloride after and SPE through the IC-Ag cartridge. In both (a) and (b) the position of the perchlorate peak is indicated.

Table 4
Summary of silver ion testing and pH before and after SPE.

Sample	Treatment	Ag^+ ion in eluant?	pH
25 ppm ClO_4^- & 250 ppm each of NO_3^-, $SO_4^=$, & Cl^-	None	No	5.5
25 ppm ClO_4^- & 250 ppm each of NO_3^-, $SO_4^=$, & Cl^-	SPE with IC-Ag	Yes	3
25 ppm ClO_4^- & 250 ppm each of NO_3^-, $SO_4^=$, & Cl^-	SPE with IC-Ag & IC-H	No	2
100 ppm ClO_4^- & 250 ppm each of NO_3^-, $SO_4^=$, & Cl^-	None	No	5.5
100 ppm ClO_4^- & 250 ppm each of NO_3^-, $SO_4^=$, & Cl^-	SPE with IC-Ag	Yes	3
100 ppm ClO_4^- & 250 ppm each of NO_3^-, $SO_4^=$, & Cl^-	SPE with IC-Ag & IC-H	No	2

250 ppm each chloride, nitrate, and sulfate solution was flowed through the cell, a decrease in the perchlorate peak was observed and new peaks at 832 and 954 cm^{-1} grew in. Similar results were obtained using a fresh 50 μL aliquot of Ag/DMAH$^+$ capture matrices and the 100 ppm perchlorate solutions. These results are summarized in Fig. 7b.

The pH of the eluants obtained after SPE through the IC-Ag cartridges was measured. The presence of silver ions in the eluants was also measured. These results are summarized in Table 4. For both the 25 and 100 ppm perchlorate solutions in the presence of 250 ppm each of nitrate, sulfate, and chloride, the pH of the eluant decreased compared to the untreated sample and silver ion was present. These results suggest that the nitrate and sulfate ions displace the silver ions present on the sulfonic acid groups present on the packing material inside the IC-Ag cartridges. This supposition is supported by an earlier Raman study that showed that silver ions form ion pairs with nitrate and sulfate ions in aqueous solution [26]. No such interaction was observed to occur between silver ions and perchlorate. The new peaks observed at 832 and 954 cm^{-1} in Figs. 7a(iv) and 7b(iv) are attributed to these silver-nitrate and silver-sulfate complex ions.

To remove the silver ions, the perchlorate/nitrate/sulfate/chloride eluants from the IC-Ag extraction underwent further SPE using the IC-H cartridges. The results summarized in Table 4 indicate that SPE through the IC-H cartridges lowered the pH even more and did remove the silver ions. SERS spectra were obtained of the solutions after SPE through both the IC-Ag and IC-H SPE cartridges. The procedure to obtain these spectra was the same as described *vide infra*. The results, shown in Fig. 8, show that the IC-H extraction did not remove the silver-nitrate and silver-sulfate complex ions.

Conclusions

In this communication, we have shown that capture matrices specific for perchlorate can be fabricated by reacting silver colloidal particles, immobilized on amine-derivatized magnetic microparticles, with dimethylaminoethanethiol (DMAH$^+$) hydrochloride. The resultant capture matrices were SERS active and it was shown that the SERS response obtained for the Ag/DMAH$^+$ capture matrices was similar to that observed for conventional Ag/DMAH$^+$ SERS substrates. It was shown that calibration curves could be generated by ratioing the perchlorate peak with a DMAH$^+$ peak that did not change in the presence of perchlorate. It was also

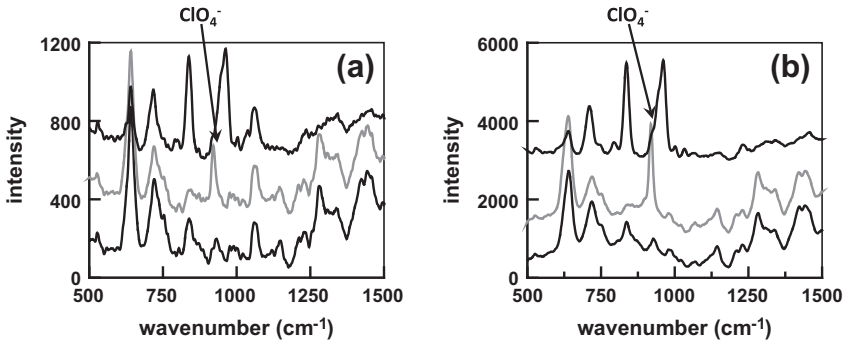

Fig. 8. SERS spectra of Ag/DMAH$^+$ capture matrices obtained using the cell shown in Fig. 1b where (a) in water, 25 ppm perchlorate, 25 ppm perchlorate and 250 ppm each nitrate, sulfate, and chloride after SPE through the IC-Ag cartridge and then the IC-H cartridge and (b) in water, 100 ppm perchlorate, 100 ppm perchlorate and 250 ppm chloride after SPE through the IC-Ag cartridge and then the IC-H cartridge. In both (a) and (b) indicates the position of the perchlorate peak.

shown that nitrate, sulfate, phosphate, hydrogen phosphate, and dihydrogen phosphate minimally interfere in the detection of perchlorate using the Ag/DMAH$^+$ capture matrices. In contrast, chloride ion was shown to be a significant interferent. In the absence of nitrate and sulfate, SPE using IC-Ag cartridges removed the chloride ion from solution thereby mitigating the chloride ion interference. However, the presence of nitrate and sulfate ions displaced silver ions on the sulfonic acid groups of the resin inside the IC-Ag cartridges. The nitrate and sulfate formed complex ions with the silver ions that preferentially interacted with the DMAH$^+$ moieties of the capture matrices. While extraction through IC-H SPE cartridges removes the silver ions from solution, they did not remove the silver-nitrate and silver-sulfate complex ions.

The experiment in which the Ag/DMAH$^+$ capture matrices were rigidly held in place using a NdFeB magnet demonstrated that the capture matrices instantaneously extract perchlorate from the flowing solution. These capture matrices will continue to extract perchlorate from solution until the adsorption sites of the DMAH$^+$ SAM on the Ag colloidal particles become fully occupied. As was discussed *vida supra*, The OndaVia perchlorate cartridges, that use dimethylaminoethanethiol hydrochloride as the perchlorate selective coating, can detect perchlorate down to the 100 ppb level. It is expected that even lower perchlorate detection limits would be possible using Ag/DMAH$^+$ capture matrices. These lower detection limits would be achieved by simply exposing the capture matrices to larger volumes of sample. This has not been demonstrated at this time as we are working on better means of mixing the capture matrices with the sample to improve the extraction efficiency. However, this was demonstrated by both Šafařík and Šafaříková [27] and Shishehbore et al. [28] Both groups of researchers showed that the efficiency of the analyte extraction was dependent upon the contact time of the sample with the capture matrices. To improve the probability of contact between the analyte and the capture matrices, Shishehbore et al. [28] used ultrasonication for 10 min to disperse the capture matrices in the aqueous samples while Šafařík and Šafaříková [27] stirred their samples for 4 h after adding their capture matrices.

Acknowledgement

This effort was funded by the SPAWAR Systems Center Pacific Naval Innovative Science and Engineering (NISE) program.

References

[1] <http://www.dtsc.ca.gov/hazardouswaste/perchlorate/>.
[2] C.J. Koester, H.R. Beller, R.U. Halden, Environ. Sci. Technol. 34 (2000) 1862–1864.
[3] M.L. Magnuson, E.T. Urbansky, C.A. Kelty, Anal. Chem. 72 (2000) 25–29.
[4] S. Susarla, T.W. Collette, A.W. Garrison, N.L. Wolfe, S.C. McCutcheon, Environ. Sci. Technol. 33 (1999) 3469–3472.
[5] C. Hogue, Chem. Eng. News 81 (2003) 37–46.
[6] A.B. Kirk, E.E. Smith, K. Tian, T.A. Anderson, P.K. Dasgupta, Environ. Sci. Technol. 37 (2003) 4979–4981.
[7] <http://www.epa.gov/osw/hazard/testmethods/pdfs/6850.pdf>.
[8] <http://www.epa.gov/osw/hazard/testmethods/pdfs/6860.pdf>.
[9] P.A. Mosier-Boss, S.H. Lieberman, Anal. Chem. 77 (2005) 1031–1037.
[10] P.A. Mosier-Boss, M.D. Putnam, Anal. Chim. Acta 801 (2013) 70–77.
[11] M. Šafaříková, I. Šafařík, Eur. Cells Mater. 3 (2002) 192–195.
[12] B. Gu, C. Ruan, C. Ruan, W. Wang, Appl. Spectrosc. 63 (2009) 98–102.
[13] Mark Peterman of OndaVia, personal communication.
[14] P.A. Mosier-Boss, S.H. Lieberman, Appl. Spectrosc. 57 (2003) 1129–1137.
[15] Y. Yamaguchi, M.K. Weldon, M.D. Morris, Appl. Spectrosc. 53 (1999) 127–132.
[16] R. Stiufiuc, C. Iacovita, C.M. Lucaciu, G. Stiufiuc, A.G. Dutu, C. Braescu, N. Leopold, Nanoscale Res. Lett. 8 (2013) 47.
[17] <http://wysri.com/Sierra/>.
[18] <http://www.kjmagnetics.com/calculator.asp>.
[19] D.W. Marquardt, J. Soc. Ind. Appl. Math. 11 (1963) 431–441.
[20] N.B. Colthup, L.H. Daly, S.E. Wiberley, Introduction to Infrared and Raman Spectroscopy, Academic Press, New York, 1990.
[21] F.R. Dollosh, W.G. Fately, F.F. Bentley, Characteristic Raman Frequencies of Organic Compounds, John Wiley and Sons, New York, 1974.
[22] S.O. Reese, J.J. Lee, Summary of Groundwater Quality Monitoring Data (1985–1997) from Pennsylvania's Ambient and Fixed Station Network (FSN) Monitoring Program, Commonwealth of Pennsylvania Department of Environmental Protection Bureau of Water Supply Management, 1998.
[23] <http://www.beg.utexas.edu/cswr/pdfs/Scanlon%20et%20al.%20HP%20Irrig%20-%20Quality%20Auxiliary.pdf>.
[24] Y. Umezawa, K. Umezawa, H. Sata, Pure Appl. Chem. 67 (1995) 507–518.
[25] I.K. Henderson, R. Sarri-Nordhaus, J.M. Anderson Jr., J. Chromatogr. 546 (1991) 61–71.
[26] R.E. Hester, R.A. Plane, Inorg. Chem. 3 (1964) 769–770.
[27] I. Šafařík, M. Šafaříková, Water Res. 36 (2002) 196–200.
[28] M.R. Shishehbore, A. Afkhami, H. Bagheri, Chem. Cent. J. 5 (2011) 41–50.

REPORT DOCUMENTATION PAGE

Form Approved
OMB No. 0704-01-0188

PLEASE DO NOT RETURN YOUR FORM TO THE ABOVE ADDRESS.

1. REPORT DATE *(DD-MM-YYYY)*	2. REPORT TYPE	3. DATES COVERED *(From - To)*
April 2015	Final	

4. TITLE AND SUBTITLE

Capture Matrices Handbook

5a. CONTRACT NUMBER

5b. GRANT NUMBER

5c. PROGRAM ELEMENT NUMBER

6. AUTHORS

P. A. Boss
M. D. Putnam

5d. PROJECT NUMBER

5e. TASK NUMBER

5f. WORK UNIT NUMBER

7. PERFORMING ORGANIZATION NAME(S) AND ADDRESS(ES)

SSC Pacific, 53560 Hull Street, San Diego, CA 92152–5001

8. PERFORMING ORGANIZATION REPORT NUMBER

TR 2073

9. SPONSORING/MONITORING AGENCY NAME(S) AND ADDRESS(ES)

Naval Innovative Science and Engineering (NISE) Program (Basic Research)
SSC Pacific, 53560 Hull Street, San Diego, CA 92152–5001

10. SPONSOR/MONITOR'S ACRONYM(S)

11. SPONSOR/MONITOR'S REPORT NUMBER(S)

12. DISTRIBUTION/AVAILABILITY STATEMENT

Approved for public release.

13. SUPPLEMENTARY NOTES

14. ABSTRACT

This report describes the fabrication and use of capture matrices for the enhanced detection of harmful chemicals. Capture matrices are composed of affinity ligands grafted onto magnetic microparticles. These capture matrices are essentially preconcentrators/transducers that can be used with either field-deployable sensors or microelectromechanical systems (MEMS) devices. For MEMS, these capture matrices address integrating the device with "real-world" sampling. Depending on the chemical nature of the affinity ligands, capture matrices can be used to enhance the detection of toxic industrial chemicals (TICs), explosive materials, and chemical warfare agents.

The technology developed has relevancy in information dominance. Capture matrices, when used with either MEMs or current field-deployable detectors, will provide the warfighter with information on what chemical species are present in the environment. This will provide the warfighter with enhanced situational awareness and understanding as well as force protection. This technology can also be used for long-term monitoring (LTM) of contaminated U.S. Navy and Department of Defense (DoD) sites. More than 2000 DoD sites have undergone remediation. Long-term monitoring of these sites is required. This LTM cannot be deferred and is a significant part of remediation life-cycle costs for the DoD. The capture matrices technology will benefit the fleet by reducing the costs of LTM. The savings can then be used to procure equipment, vessels, etc. that will directly benefit the warfighter.

15. SUBJECT TERMS

Mission Area: Environmental Science
capture matrices surface-enhanced Raman spectroscopy enhanced chemical detection target analytes affinity ligands

16. SECURITY CLASSIFICATION OF:			17. LIMITATION OF ABSTRACT	18. NUMBER OF PAGES	19a. NAME OF RESPONSIBLE PERSON
a. REPORT	b. ABSTRACT	c. THIS PAGE			Pam Bass
U	U	U	U	102	19B. TELEPHONE NUMBER *(Include area code)* (619) 553-1603

INITIAL DISTRIBUTION

84300	Library	(2)
85300	Archive/Stock	(1)
71730	P. A. Boss	(1)
71750	M. D. Putnam	(1)

Defense Technical Information Center
Fort Belvoir, VA 22060–6218 (1)

Approved for public release.

SSC Pacific
San Diego, CA 92152-5001